

CLARKSON UNIVERSITY

Analysis of Tetramethyldioctyldisiloxane in Sol-Gel Processing

A Thesis

by

Daniel M. Heenan

Department of Chemistry

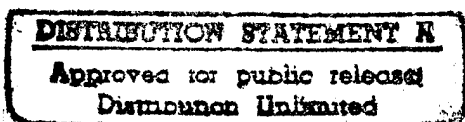
Submitted in partial fulfillment of the requirements

for the degree of

Masters of Science

Chemistry

April 9, 1996



DTIC QUALITY INSPECTED 3

Accepted by the Graduate School

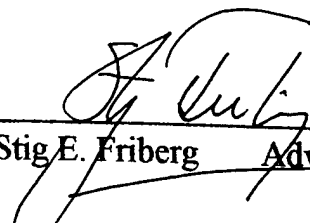
Date

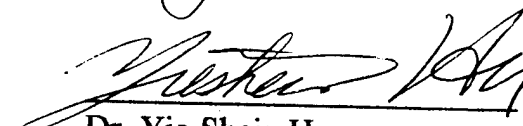
Dean

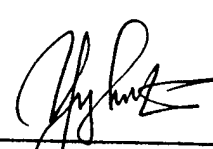
19960508 242

The undersigned have examined the thesis entitled "Analysis of tetramethyldioctyl disiloxane in sol-gel processing" presented by Mr. Daniel M. Heenan, a candidate for the degree of Master of Science, and hereby certify that it is worthy of acceptance.

4/9-96
Date


Dr. Stig E. Friberg Advisor


Dr. Yie-Shein Her


Dr. Yuzhuo Li

Abstract

The hydrolysis and condensation reaction kinetics of methoxydimethyloctylsilane (MDOS) and copper nitrate hydrate were investigated using analytical measurements and Karl Fischer titration. The reaction product was determined to be a dimer of MDOS, tetramethyldioctyldisiloxane (TDDS). The structure of TDDS was confirmed by FTIR, ^{29}Si NMR and ^1H NMR. The initial rates of the hydrolysis and condensation were determined for the half-life of the reaction. The phase separation of TDDS and the reaction mixture was found to be quantitative. The correct stoichiometry reacted all the water and MDOS in solution and resulted in an anhydrous copper nitrate solution in methanol.

In other studies, the phase equilibria of TDDS and various organic components were investigated. The thermodynamic treatment of solubility parameters were used to analysis the phase equilibria qualitatively. The results demonstrated the effects of polarity and hydrogen-bonding dependence on the phase equilibrium. The solubilization of components in solution and colloidal association structures were also revealed. Optical microscopy, refractive index, and x-ray diffraction, were used to analyze the phase equilibria of TDDS.

Dedication

To my mother, father, family, and especially my beloved Carol for their encouragement and support during my studies.

Acknowledgments

I wish to extend my deepest appreciation to Dr. Stig E. Friberg for his guidance and support throughout this investigation. His tireless energy and inquisitive mind inspired me to continue my search for knowledge and understanding of physical science. A special thanks to Dr. Johan E. Sjöblom for the valuable suggestions and friendship he has given me throughout my stay at Clarkson University.

I would like to thank the members of Dr. Fribergs' research group and all of my colleagues in many ways in which they supported me through these past few years.

Finally, thanks are due to the United States Army for the academic scholarship to pursue my studies in Chemistry at Clarkson University and the faculty position to teach these fundamentals to our future leaders at the United States Military Academy, West Point, New York.

Table of Contents

| | |
|---------------------------------|----|
| 1. Introduction | 1 |
| References | 4 |
| 2. The Sol-Gel Method | 7 |
| 2.1 Background | 7 |
| 2.2 Hydrolysis | 10 |
| 2.3 Condensation | 15 |
| 2.4 Growth Models | 17 |
| 2.5 Reaction Kinetics | 19 |
| 2.6 References | 25 |
| 3. Colloidal Systems | 30 |
| 3.1 Surfactants | 30 |
| 3.2 Phase Diagrams | 35 |
| 3.3 Micelles and Microemulsions | 37 |
| 3.4 References | 43 |
| 4. Microemulsion-Gel Method | 44 |
| 4.1 Non Aqueous Systems | 44 |
| 4.2 Microemulsion-Gel Method | 46 |
| 4.3 Hydrated Metal Salts | 48 |
| 4.4 References | 50 |

| | |
|---|----|
| 5. Solubility Parameters | 54 |
| 5.1 Introduction | 54 |
| 5.2 Thermodynamics of Mixing | 54 |
| 5.3 Cohesive Energy and Solubility Parameters | 58 |
| 5.4 Regular Solution Theory | 64 |
| 5.5 References | 66 |
| 6. Article 1: Reaction Between Copper Nitrate Hydrate and Methoxydimethyloctylsilane in Methanol | 67 |
| Abstract | 67 |
| Introduction | 68 |
| Experimental | 69 |
| Results | 70 |
| Discussion | 80 |
| Conclusion | 88 |
| References | 90 |
| 7. Article 2: Phase Equilibria of Methoxydimethyloctylsilane, Tetramethyldioctyldisiloxane in Organic Solvents | 91 |
| Abstract | 91 |
| Introduction | 91 |
| Experimental | 97 |
| Results | 98 |

| | |
|---|-----|
| Discussion | 111 |
| Conclusion | 116 |
| References | 119 |
| 8. Article 3: Phase Equilibria of Tetramethyldioctyldisiloxane, Water and Organic solvents | 121 |
| Abstract | 121 |
| Introduction | 121 |
| Experimental | 123 |
| Results | 125 |
| Discussion | 133 |
| Conclusion | 137 |
| References | 138 |

List of Tables

Chapter 3

| | |
|---|----|
| Table 3.1 - Relation between R and Amphiphilic Association Structures | 33 |
|---|----|

Chapter 7

| | |
|--|-----|
| Table 7.1 - Hansen Solubility Parameters | 112 |
|--|-----|

List of Illustrations and Figures

Chapter 2

- Figure 2.1 - Hydrolysis and Condensation of Silicon at next nearest neighbor level represented in matrix form. 21
- Figure 2.2 - Initial Condensation Rates divided by the Initial Silanol Concentration versus the Initial Silanol Concentration 24

Chapter 3

- Figure 3.1 - Types of Surfactants with Examples 31
- Figure 3.2 - Shapes of Aggregates 34
- Figure 3.3 - Typical Three Component Phase Diagram 36
- Figure 3.4 - Structure of Normal Micelle 39
- Figure 3.5 - The Effect of Surfactant Concentration on Various Properties 40
- Figure 3.6 - Structure of Inverse Micelle 41

Chapter 5

- Figure 5.1 - Gibbs Excess Free Energy of Mixing versus Mole Fraction 57
- Figure 5.2 - Hansen Parameters Represented in Three Dimensional Spacial Sphere 61
- Figure 5.3 - Three Dimensional Display of Solubility Parameter for Polymer, P, Solvent, S, System 63
- Figure 5.4 - Triangular Fractional Cohesion Parameter Solubility Diagram for Parlon P10 resin 65

Chapter 6

| | |
|---|----|
| Figure 1 - ^1H NMR spectra of 5/1 MDOS/ $\text{Cu}(\text{NO}_3)_2 \cdot 2.5 \text{H}_2\text{O}$ mole ratio in methanol. Top: reaction product, Bottom: initial reaction mixture. | 71 |
| Figure 2 - ^{29}Si NMR spectra of 5/1 MDOS/ $\text{Cu}(\text{NO}_3)_2 \cdot 2.5 \text{H}_2\text{O}$ mole ratio in methanol. Top: reaction product, Bottom: initial reaction mixture. | 73 |
| Figure 3 - FTIR spectra of 5/1 MDOS/ $\text{Cu}(\text{NO}_3)_2 \cdot 2.5 \text{H}_2\text{O}$ mole ratio in methanol. Top: reaction product, Bottom: final reaction mixture. | 74 |
| Figure 4a - Dimer Concentration versus Time for reaction 5/1 MDOS/ $\text{Cu}(\text{NO}_3)_2 \cdot 2.5 \text{H}_2\text{O}$ mole ratio in methanol. | 76 |
| Figure 4b - Dimer Concentration versus Time for reaction 2/1 MDOS/ H_2O mole ratio in methanol. | 77 |
| Figure 5 - Water Concentration versus Time for reaction 5/1 MDOS/ $\text{Cu}(\text{NO}_3)_2 \cdot 2.5 \text{H}_2\text{O}$ mole ratio in methanol determined by Karl Fischer titration. | 78 |
| Figure 6 - Phase diagram of MDOS (Q^0), methanol, dimer (Q_1^0) as a weight percentage | 79 |
| Figure 7 - Concentration versus Time for Components: W_1 , W_2 , W_{KF} , Dimer; within the first 24 hours of the reaction. | 85 |
| Figure 8 - Si species Concentration versus Time of reaction between 5/1 MDOS/ $\text{Cu}(\text{NO}_3)_2 \cdot 2.5 \text{H}_2\text{O}$ mole ratio in methanol. | 87 |

Chapter 7

| | |
|--|-----|
| Figure 1 - Phase diagram of MDOS, TDDS, CHCl_3 as a weight percentage | 99 |
| Figure 2 - Phase diagram of MDOS, TDDS, Methanol as a weight percentage | 101 |
| Figure 3 - Phase diagram of MDOS, TDDS, Acetone as a weight percentage | 102 |
| Figure 4 - Phase diagram of MDOS, TDDS, Ethanol as a weight percentage | 103 |

| | |
|---|-----|
| Figure 5 - Phase diagram of MDOS, TDDS, Ethylene glycol as a weight percentage | 105 |
| Figure 6 - Phase diagram of MDOS, TDDS, Propanol as a weight percentage | 106 |
| Figure 7 - Phase diagram of MDOS, TDDS, 1,2 propane diol as a weight percentage | 107 |
| Figure 8 - Phase diagram of MDOS, TDDS, 1,3 propane diol as a weight percentage | 108 |
| Figure 9 - Phase diagram of MDOS, TDDS, Brij 30 as a weight percentage | 109 |
| Figure 10- Phase diagram of MDOS, TDDS, SA9 as a weight percentage | 110 |
| Figure 11- Polar versus H-bonding parameters of Table I | 115 |
| Figure 12- Triangle plot of Table I Hansen solubility parameters | 117 |

Chapter 8

| | |
|--|-----|
| Figure 1 - Phase diagram of Water, TDDS, Methanol as a weight percentage | 126 |
| Figure 2 - Phase diagram of Water, TDDS, Ethanol as a weight percentage | 127 |
| Figure 3 - Phase diagram of Water, TDDS, Propanol as a weight percentage | 129 |
| Figure 4 - Phase diagram of Water, TDDS, Butanol as a weight percentage | 130 |
| Figure 5 - Phase diagram of Water, TDDS, Decanol as a weight percentage | 131 |
| Figure 6 - Phase diagram of Water, TDDS, Brij 30 as a weight percentage | 132 |
| Figure 7 - Phase diagram of Water, TDDS, SA9 as a weight percentage | 134 |

1. Introduction

The work in this thesis concentrates on the preparation, reaction kinetics, and phase equilibria of tetramethyl dioctyldisiloxane using the sol-gel method.

Amphiphilic association structures were introduced by J.W. McBain in 1913 [1], who developed the concept of aqueous micelle dispersions. The association behavior of amphiphilic molecules has been widely studied [2-7] from both theoretical and practical points of view. These studies have established the fundamental understanding in biological systems and in the development of new applications and products. Emulsions in food [8], biomembrane lamellar liquid crystal [9-12], micellar solutions in detergents, catalysis [14], flotation, wetting and lubrication [15] are only a few of the possible avenues these structures have been utilized in. Other recent developments have used microemulsions [16-19] and lyotropic liquid crystals [20] to produce mono-disperse particles and ceramic materials.

In the past thirty years, the sol-gel method [28-30] has received considerable attention to make glasses and ceramics [23-25] ranging from fibers, electrical devices, thin films and monolithic products [26-27]. Several organizations have collected and compiled articles and to provide reviews on the tremendous amount of information available [23-30]. Comparisons of the advantages and disadvantages with conventional methods have also been presented [31].

The success of the sol-gel method has been due to its many advantages [31]. Sol-gelceramic materials can be formed and molecularly mixed without the use of extremely

high temperatures needed in conventional methods. The final material in sol-gel processing will have better homogeneity and purity. However, sol-gel has two distinct disadvantages [31]. The first is the relative high cost of the metal organic precursors, and the second is that mixtures of metal organic and inorganic compounds, as initial materials, have limited solubility in the organic solvents used. These materials have a tendency to crystallize during the evaporation of water [32-36].

There are extensive studies in the literature of tetraalkoxysilane reactions, primarily tetramethylorthosilane (TMOS) and tetraethylorthosilane (TEOS) [26,27]. Although a considerable amount of information is available for these systems, controversy and conflicting experimental data remains unresolved. Hence, direct comparison of reaction rate constants from varying experimental conditions are difficult. The kinetic models currently employed by investigators still dependent on those experimental conditions. In the silicon polymer industry, monoalkoxysilanes are most frequently used to terminate the chain polymerization step in the synthesis of resins and elastamers. Unfortunately, interest in monoalkoxy silanes chemistry has received little attention from the scientific community.

The primary purpose of this research program was to use the sol-gel process in the study of a monoalkoxysilane. The compounds of interest are methoxy dimethyl octyl silane (MDOS) and tetramethyl dioctyl disiloxane (TDDS). The main focus of this research was to establish the phase equilibria of MDOS, TDDS in various organic solvents, follow the reaction kinetics, and provide a comparison to similar systems, which

contain TEOS and TMOS, to elucidate the affect of a monoalkoxy precursor to that of a tetraalkoxy precursor.

The background literature for this research is reviewed in chapters 2 through 5. The evolution of the sol-gel process is reviewed in chapter 2. The surfactants ability to form association structures and their geometrical considerations for colloidal formation in aqueous media are described in chapter 3. Chapter 3 also covers the basic concepts of amphiphilic association structures and their relationships within the phase diagram. Chapter 4 reviews the use of non-aqueous systems in forming microemulsions and their application in the sol-gel process. Solubility parameters are introduced in chapter 5; these fundamental principles and thermodynamic treatment are presented for the prediction of component solubility in various aqueous/non-aqueous systems.

The main results and conclusions are presented in chapters 6, 7 and 8, which contain three articles currently in press. The first article reports the reaction kinetics of copper nitrate hydrate and MDOS, submitted to the Journal of Solution Chemistry. Articles 2 & 3 are presented in chapters 7 and 8, respectively, on the phase equilibria of TDDS with various organic components; both of these articles will be published in the Journal of Dispersion Science and Technology (in press).

References

- [1] McBain, J.M., Trans. Farad. Soc., 9, 99, 1913.
- [2] Winsor, P.A. "Solvent Properties of Amphiphilic Components." Butterworth, London 1954
- [3] Wennerstrom, H., and Lindman, B., Phys. Rep. 52, 2, 1979.
- [4] Ekwall, P., in "Advances in Liquid Crystals." Vol 1, (G.H. Brown, ed), Academic Press, NY, p.1, 1975.
- [5] Mitchell, D.J. , Nimham, B.W., J. Chem. Soc. Faraday Trans. II, 77, 601, 1981.
- [6] Degennes, P.G. Taupin, C., J. Phys. Chem. 86, 2294, 1982.
- [7] Lindman, B., Stilbs, P., "surfactants in Solution". Vol 3, (Mittal, K.L and Lindman B. eds) Plenum Press, NY p. 1651, 1951.
- [8] Friberg, S.E., Ed. "Food Emulsions", Marcel Dekker, NY 1976.
- [9] Friberg, S.E., Ed., "Lyotropic Liquid Crystals and the Structures of Biomembranes", Advances in Chemistry Series 152, American Chemical Society, Washington DC 1976.
- [10] Fendler, J.H. "Membrane Mimetic Chemistry", John Wiley & Sons, NY 1982.
- [11] Elias, P.Mp., J. Invest. Dermatol., 80, 445, 1983.
- [12] Osborne, D.W., Friberg, S.E., Tombridge, T.L., J. Soc. Cosmet. Chem., 36, 349, 1985.
- [13] Shah, D.O., Ed., "Surface Phenomena in Enhanced Oil Recovery", Plenum Press, NY 1981.

- [14] Fendler, J.H., Fendler, E.J., "Catalysis in Micellar and Macromolecular Systems", Academic Press, NY 1975.
- [15] Adamson, A.W. "Physical Chemistry of Surface", 4th Ed., John Wiley & Sons, NY 1982.
- [16] Boutonnet, M., Kizling, J., Stenius, P., Maire, G., Colloids Surfaces 5, 209, 1982.
- [17] Kurhara, K., Kizling, J., Stenius, P., Fendler, J.H., J. Am. Chem. Soc. 105, 2574, 1983.
- [18] Gobel, M., Kon-no, K., Kandori, K., Kitahara, A., J. Colloid Interface Sci., 93, 293, 1987.
- [19] Kandori, K., Kon-no, K., Kitahara, A., J. Colloid Interface Sci., 115, 579, 1987.
- [20] Friberg, S.E., Worn, C.S., Coll. Polymer Sci., 263, 156, 1985
- [21] Matijevic, E., Acc. Chem. Res., 14, 22, 1981.
- [22] Stinson, S.C., Chem. Eng. News, 26, 9, 1982.
- [23] Ulrich, D.R., J Non-Crystalline Solids, 100, 74, 1988.
- [24] Hench, L.L. and Ulrich, D.R., Eds., "Ultrastructure Processing of Ceramics, Glasses and Composites", Wiley-Intersciences, NY 1984.
- [25] Hench, L.L. and Ulrich, D.R., Eds., "Science of Ceramics Chemical Processing", Wiley-Intersciences, NY 1986.
- [26] Klien, L.C., Ed., "Sol-Gel Technology for Thin Films, Fibers, Preforms, Electronics and Specialty Shapes", Noyes Publications, NY 1988.
- [27] Brinker, C.J., Clark, D.E., Ulrich, D.R., Eds., "Better Ceramics through Chemistry", MRS, Vol 32, Elsevier Science Publishing, 1984.

- [28] Roy, R. Science 238, 1664, 1987.
- [29] Mehrotra, R.C., J Non-Crystalline Solids, 100, 1, 1988.
- [30] Schmidt, H., J Non-Crystalline Solids, 100, 51, 1988.
- [31] Mackenzie, J.D. J Non-Crystalline Solids, 48, 1, 1982.
- [32] Roy, R, J. Amer. Ceram. Soc., 52, 344, 1969.
- [33] McCarthy, G.J., Roy, R., J. Amer. Ceram. Soc., 54, 639, 1971.
- [34] Hayashi, A., Saito, H., J. Mater. Sci., 15, 1971, 1980.
- [35] Brinker, C.J., Mukerjee, S.P., J. Mater. Sci., 16, 1980, 1981.
- [36] Holand, W., Plumet, E.R., Duvigucand, P.H., J Non-Crystalline Solids, 48, 205, 1982.
- [37] Ma, Z. Friberg, S.E., Noegi, P., Colloids & Surfaces, 33, 249, 1988.

2.0 The Sol-Gel Method

2.1 Background

The sol-gel method is a generalized term used for many kinds of metal oxide reactions in solution. The first stage of such reactions is the formation of a sol. A sol is a suspension of colloidally dispersed material in a liquid medium [1, 2]. Gels can be formed from particulate sols where aggregation results from the collapse of the repulsive double layer in the charged particles. Such an aggregation causes primary particles to link together and form a network. When the colloidal particles in a sol are interconnected by bonds, the structure of the sol will transform into a rigid network. This process is called the sol-gel transition.

The history of sol-gel processing dates back to 1845, where Ebelman [3] reported the formation of a gel from a metal alkoxide and water when tetraethylorthosilane (TEOS) was mixed with water. These materials remained relatively unnoticed in the literature for almost a century. Early researchers [4, 5] explored the growth of crystals in gels which arose from periodic precipitation phenomena. Geffcken [6] recognized alkoxide precursors could be used in the preparation of oxide films and subsequently developed a process to prepare these inorganic films.

Although inorganic gels from aqueous gels were studied for some time, Graham [7] demonstrated that the water in the silica gel could be exchanged for other organic solvents. This discovery supported the theory that the gel consisted of a solid network

with continuous porosity. Rival theories of the 1930's argued the gel structure as: emulsions, particles surrounding by bound water and coagulated sol composites [1, 2].

The network structure of silica gels gained wide acceptance after the work Hurd [8], who showed that these gels must consist of a polymeric skeleton of silicic acid enclosing a continuous liquid phase. The process of supercritical drying to produce aerogels reported by Kistler [9] demonstrated the existence of solid skeletal network contained in gels and validated the Hurd theorem.

However, the real interest in the sol-gel process did not develop until Yoldas [10, 11] and Yamano [12] demonstrated that monoliths could be produced by carefully drying the gels. The allure of a room-temperature process for the preparation of glasses and ceramics presented irresistible possibilities to adapt the system to more industrial applications.

The ceramics industry became interested in a large number of novel ceramic compositions in the early seventies [13-16]. Ceramic fibers were also made from organometallic precursors on a commercial basis by several companies[17-19]. Countless ceramic and powder compositions involving silicon, titanium, zirconium, etc., were produced [20].

While the ceramic industry was interested in the production of composite materials, other investigators turned their attention towards more fundamental aspects of the process. Investigations on the experimental influences on the reaction rate, controlling the size and morphology of particles, the development of reaction mechanisms, and the

reaction kinetics under a wide range of experimental conditions were published. In the past five years alone, over 2100 individual journal/article publications are listed in the Science Citation Index to date, this does not include other significant research distributed in workshops, books, industrial research, or pending patents. Despite the wealth of information available, the reaction mechanisms involved and the effect of various experimental parameters are still not completely understood.

The advantages of sol-gel processing of glasses/ceramics [1, 2] over classical glass/ceramic processing methods are; (1) lower temperatures of preparation; (2) Better homogeneity in mixing at the molecular level; (3) purity from raw materials and products. The disadvantages are: (1) the high cost of the precursor alkoxy compounds; (2) large amount of shrinkage during processing; and (3) residual unreacted/unbonded species remaining in the monolith.

The emphasis on preparation of sol-gel materials relies on the precursor chemistry and the desired properties of the system. Sol-gel monoliths can be prepared by three general methods: (1) gelation of a solution of colloidal powders; (2) hydrolysis and condensation of alkoxide precursors followed by supercritical drying of gel; (3) hydrolysis and condensation of alkoxide precursors followed by aging and drying under ambient temperatures. In methods 1 and 3, the core liquid is removed at ambient pressure by thermal evaporation and results in shrinkage, the monolith is called a xerogel.

As mentioned earlier, the materials formed by the sol-gel method are dependent on the individual processes involved. The alkoxy chemistry of virtually every element has

been investigated to some extent. Alkoxy compounds are exceedingly reactive and form oligomers quite readily, which provides an exceptional basis to form inorganic oxide compounds. A variety of metal alkoxide precursors have been used in the sol-gel method [21, 22]. The electronegativity of the alkoxy groups influences the reactivity on the central metal atom, thus making it susceptible to nucleophilic attack by acids, esters, aldehydes, water, silanols, and other organic electronegative species. Guglielmi [23] has reported the hydrolysis of various metal alkoxides and their respective reactivities with other compounds.

2.2 Hydrolysis

The basis of the sol-gel method is the hydrolysis of metal alkoxides and their resultant condensation of hydrolyzed monomers into a gel. The production of silane gels have utilized a variety of metal alkoxides, usually, tetraethylorthosilane (TEOS) or tetramethylorthosilane (TMOS). However, other alkoxides and mixed sols have also been used to make composite gels, such as: zirconium SiO_2 [24], SiO_2 - TiO_2 [25], and lithium-aluminosilane [26].

The research presented here is focused on the reactions of monoalkoxide precursors, thus a review of similar systems of TEOS and TMOS are used for a basis of comparison. Three reactions are generally used to describe the sol-gel method [1]

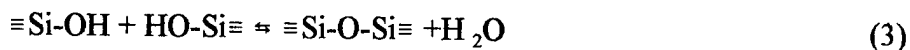
Hydrolysis



Alcohol Condensation



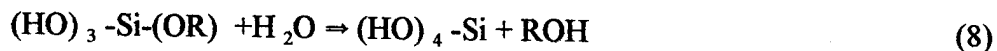
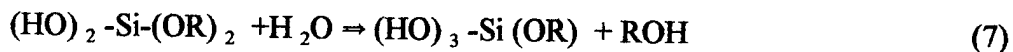
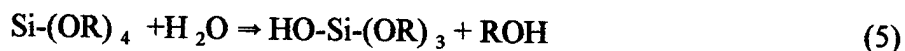
Water Condensation



where R is an alkyl group, $\text{C}_x\text{H}_{2x+1}$, in most cases ethanol or methanol. In the water condensation, Eq. 3, water is produced as a by-product. When the stoichiometry of equations 1, 2, & 3 are balanced to a molar ratio of water to alkoxide of 2, then all the water is consumed in the reaction and is sufficient to complete the process resulting in



The hydrolysis, in Eq. 1, for a tetra functional precursor like TMOS undergoes four separate hydrolysis steps:

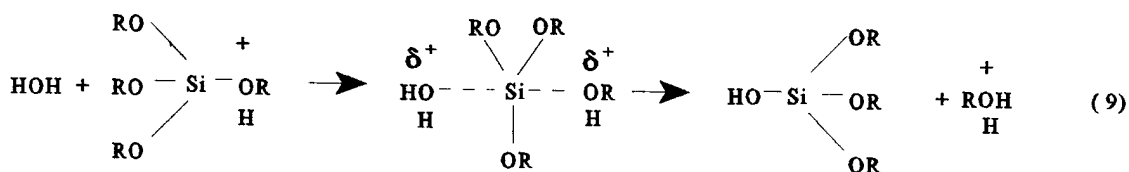


The hydrolysis of alkoxides is sensitive to experimental conditions being used: pH [27], catalysts [28,29], temperature [30], pressure [31], chain length of alkoxide [32], alkoxide concentration [32], the solvent used [33], the molar ratio of water to alkoxide [33-35].

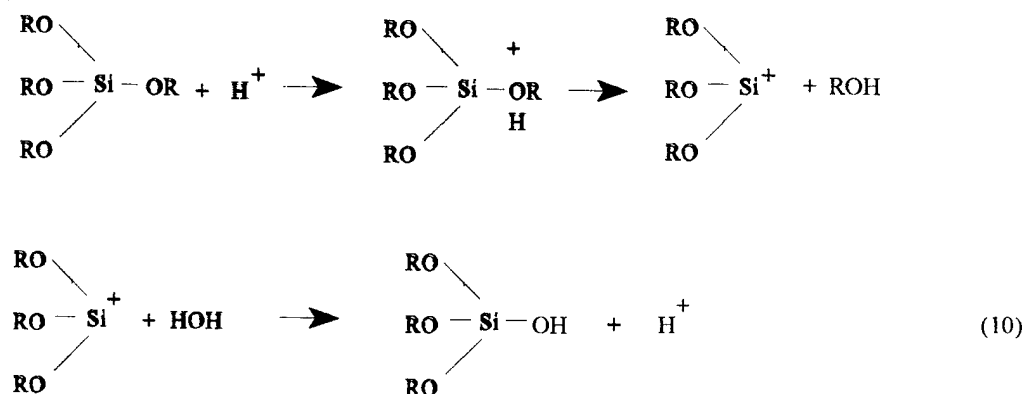
The hydrolysis is generally catalyzed with either an acid or a base. Typical acids used in the hydrolysis reaction are HCl, HNO_3 , and HF. The most common base used is NH_4OH . The results to be presented in chapter 6 are concerned with acid catalyzed

hydrolysis, although both types of mechanisms will be discussed in the present chapter.

For acid catalyzed hydrolysis, the most likely mechanism is a bimolecular nucleophilic substitution, i.e. S_N2 reaction. In this scheme, the alkoxide is rapidly protonated before the approach of water. The electron density is withdrawn from the silicon, thus making it electrophilic and susceptible to attack by water. The following mechanism is illustrative to this type of reaction



The nucleophilic attack of water is 180 degrees from the leaving ligand, which acquires an additional positive charge from the penta-coordinated intermediate, as reported by McNeil [36], and Zerda [31]. However, an alternate mechanism has been proposed by Tims [37]:



Schimdt [32] reported that the reaction rate was zero order with respect to the concentration of water, using the assumption that the overall reaction rate is one [38] and thus follows that the reaction rate with TEOS concentration is first order.

Chemical modifications of the alkoxy groups, like increasing its chain length, will decrease the hydrolysis rate[38-40]. Steric (spatial) factors and inductive effects play a central role in the reactivity of the silica species. Substitution of an alkyl group on the silicon atom will increase the electron density on the silicon atom. Substitutions of more electronegative groups, such as -OH or -O-Si will reduce the electron density on the silicon atom. The effect of these experimental factors that will influence the hydrolysis rate are summarized [1,2]:

Low pH (7 to 0) --> Increase hydrolysis rate

High pH (7 to 14) --> Increase hydrolysis rate

Increasing alkoxide chain length --> Decrease hydrolysis rate

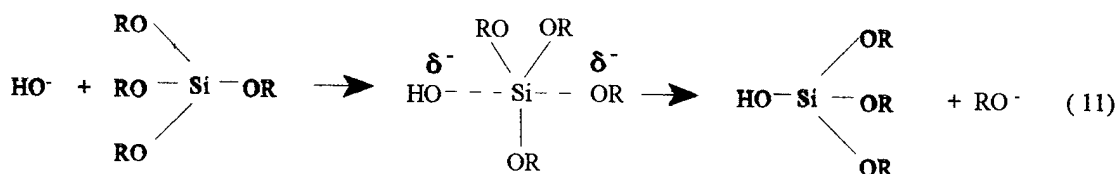
Increasing TEOS concentration --> Increase hydrolysis rate

Increasing alkyl group length --> Increase hydrolysis rate

Brinker [41] found that each successive hydrolysis step occurs more rapidly than the preceding one in acid catalyzed systems. Yang [27] later confirmed this observation and determined the rate constants for the successive hydrolysis reactions; $k_0 = 1.43 \times 10^{-2}$ /min, $k_1 = 6.4 \times 10^{-2}$ /min, $k_2 = 0.29$ /min, and $k_3 = 1.3$ /min. Pouxiviel [35] et. al. collaborated these findings and found that measurable quantities of unhydrolyzed

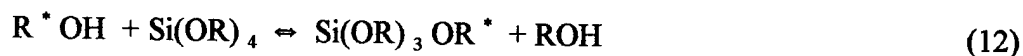
monomers were present four hours after hydrolysis was initiated.

Base catalyzed hydrolysis usually proceeds in alkaline solutions where water dissociates into hydroxyl anions which attacks the silicon atom [1, 2]



This S_N2 mechanism will again be influenced by steric and inductive effects as mentioned earlier for the acid catalyzed hydrolysis. Here the steric effect is more important than the inductive effects, where the pentacoordinate intermediate acquires an additional negative charge.

The hydrolysis rate of both base and acid catalyzed system will also be affected by transesterification, i.e. an exchange of alkoxide group with an alcohol



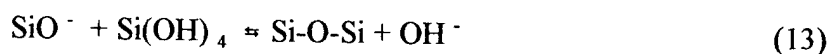
This process will occur when an alkoxide is hydrolyzed in an alcohol consisting of different alkyl groups. The inductive characteristics of the exchanged alkoxide will then influence the kinetics after transesterification [42]. If the alcohol medium is of longer chain length than the precursor alkoxide, then the hydrolysis rate will decrease after transesterification.

2.3 Condensation

Polymerization to form silanol and siloxane bonds occurs either by alcohol producing, Eq. 2, and by water producing condensation, Eq. 3. Alcohol condensation occurs if water to alkoxide molar ratio (R) is less than two, while water condensation is the preferred path if R is equal to or greater than two [2]. These two reactions can occur between very different species such as monomers, oligomers, etc., which have undergone different hydrolysis steps. Dimers are formed in Eq. 2, which then undergo subsequent condensations to form trimers and tetramers. It has also been reported [35,44] that the evolution of tetramers from monomers may take place in the first ten minutes of the reaction. It is therefore important to understand the steric and inductive effect for tetraalkoxy metals precursors, which are not well documented [1, 2, 51, 80].

Voronkov [39] reported that the condensation rate of triorganosilanols was decreased with increasing chain length or branching of the alkyl group. It was further investigated that the condensation rate increased with increasing number of silanol groups on the silicon atom, thereby increasing the acidity. Hence, the condensation was influenced by inductive and steric effects, although the inductive effects resulting from longer alkyl chain substituents are probably of minor importance [39].

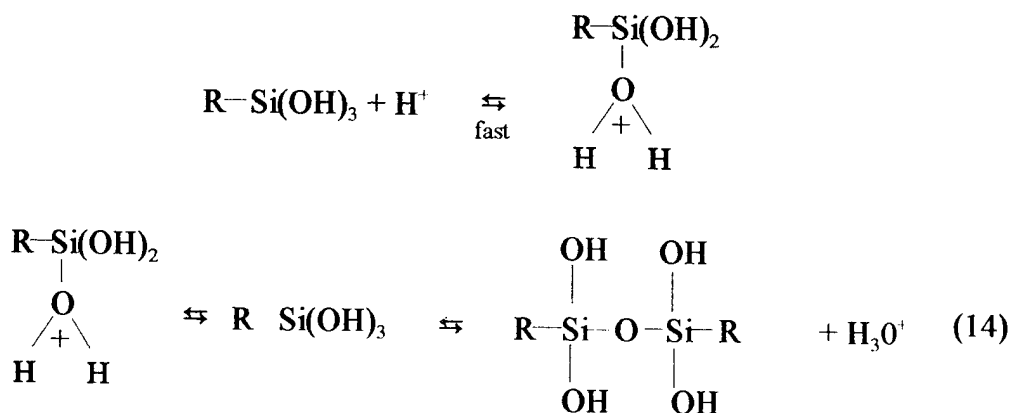
The most widely accepted mechanism for the condensation reaction involves the attack of a nucleophilic deprotonated silanol on a neutral silane species as proposed by Iler [1] to explain condensation in aqueous silane systems:



This reaction pertains above the isoelectric point of silica (>pH 2-2.45) where the surface silanols may be deprotonated depending on their acidity. The acidity of a silanol depends on the other substituents on the silicon atom. When basic OR and OH are replaced with OSi, the reduced electron density on Si increases the acidity of the protons on the remaining silanols [45]. Hence, Iler's mechanism favors reactions between larger, higher condensed species containing acidic silanols and smaller, less branched species. The condensation rate is maximized near neutral pH where significant concentrations of both protonated and deprotonated silanols exist.

The gelation time decreases below pH 2 for acid condensation. It is reasonable to assume that the acid mechanism involves a protonated silanol species. The monomer or weakly branched oligomer silanol are most likely to be protonated. Thus making the silicon atom more electrophilic and therefore susceptible to nucleophilic attack. This means that the condensation will occur between neutral species and protonated silanol on monomers or end groups on chains.

Pohl and Osterholz [50] proposed a mechanism involving a protonated silanol



Johnson recently proposed an alternate condensation mechanism involving a hydrogen bonded intermediate that contains a five coordinate $\text{Si}(\text{OH})_5^-$ - anionic species [46,47,48]. Liebau [48] found a gradual change from tetrahedrally bonded Si to trigonal bipyramidal while studying the crystal structures of various ligands attached to Si.

Both acid and base catalyzed condensation involves pentacoordinate transition states, hence steric and inductive effects will influence the condensation kinetics. In acid catalyzed condensation, extensive hydrolysis and condensation will destabilize the positive charge and thus reduce the condensation rate. In base catalyzed condensation, exchange of more electron providing alkoxy groups with more electron withdrawing groups as hydroxyl or OSi will stabilize the charge and enhance the kinetics in this transition nucleophile. Substituents on the silicon atom reduces the crowding in the transition state and will enhance the condensation kinetics of groups attached to the central atom.

The hydrolysis and condensation reactions can not be separated completely since the latter depends upon the former. However, under certain conditions, e.g., medium or high water content, the hydrolysis rate is much faster than the condensation rate thus the two are essentially separate [27, 35,43].

2.4 Growth Models

The first condensation reaction products are dimers, although these undergo further condensation to form tetramers and trimers. Kelts [51] found the initial condensation products were actually trimers and tetramers. Campostrini [52] reported that monomers and dimers were consumed within six minutes of the condensation process.

The hydrolysis and condensations reactions lead to the growth of clusters that eventually collide and link together to form a gel. The colloidal particles and the condensed silica link together to form a three dimensional network. At the gelation point, the viscosity increases sharply, and a solid matrix results in the shape of a mold. The elasticity of sols to support such a stress marks the turning point into a gel. This is defined as the gelation point [44].

Several models have been developed to describe the gelation and growth of polymeric sol-gel species: classical theory, percolation theory, kinetic models, and experimental studies.

The classical theory or equilibrium model was proposed by Flory [53,54] and Stockmayer[55], whose basic concept to describe the gel as a system consisting of spanning clusters. This gel model neglects the initial formation of clusters and their geometrical considerations.

The percolation theory requires that fractal aggregates grow until they coalesce with each other and reach the gel point [57-59]. Gelation begins with the formation of these aggregates. This theory predicts the structure and size distribution of growing polymers, however it is limited to static and dynamic properties of the kinetic models used[1].

Since the classical and percolation theory are both equilibrium theories, they do not describe the kinetics of cluster growth. Due to the deficiencies in the classical and percolation theories on describing cluster growth, kinetic models were introduced to

bridge the gap [58,59]. The initial kinetic models assumed irreversible reactions, equal and independent reactivities of Si-OR groups. These models are used to predict the kinetics of growth and fractal structure of the resulting clusters. The evolution of the size, distribution and shape can be accounted for with computer simulations which are in reasonable agreement to experimental results.

The most common experimental technique used in the study of gelation is ^{29}Si NMR, which is used to examine the relative amounts of the different silane species present at a given point during the hydrolysis and condensation. Combination techniques frequently employed in gelation studies are: ^{29}Si NMR and Raman spectroscopy [68,69,70], FTIR and size exclusion chromatography [71], FTIR and Raman spectroscopy [72]. Other experimental techniques include: gas-liquid chromatography [73], mass spectroscopy [67], wide-angle x-ray scattering (WAXS) and small angle x-ray scattering (SAXS)[24], and viscosity [74,75].

Gelation is also influenced by such variables as: the container size [1], pH [61], solvent [62], water concentration [63], type of alkoxide [62], catalyst [64-66], and temperature [62].

2.5 Reaction Kinetics

Thus far the discussion of hydrolysis and condensation reactions have been presented at a rudimentary level which ignored how the various functional groups, OR, OH, OSi, are distributed on the silicon atom. There are three reactions and three rate constants of importance when describing the kinetics of the functional groups from

equations 1 through 3.



where 1 is hydrolysis, 2 is water producing condensation, 3 is alcohol producing condensation. Recall that hydrolysis and condensation occur concurrently, and at the nearest functional group level there are 15 distinguishing local chemical environments. Kay and Assink [43, 78-80] have represented the 15 silcate species in matrix form as shown in figure 2.1

The triplet (X, Y, Z) represent the number of -OR, -OH, -OSi groups attached to the central silicon atom, $\text{Si}(\text{OR})_X (\text{OH})_Y (\text{OSi})_Z$ and $X + Y + Z = 4 =$ coordination of silicon.

Assink and Kay [76-80] have used ^1H and ^{29}Si NMR to determine the values of k_1 , k_2 , and k_3 during the initial stages of the acid catalyzed hydrolysis of TMOS and have considered several kinetic models to explain the temporal evolution of functional groups surrounding silicon.

A review of equations 14-16 provides a reasonable approach to the functional groups rates of reaction. Proton NMR is used to measure the relative amounts of methoxy functional groups and methanol molecules as a function of time. There are two limiting cases.

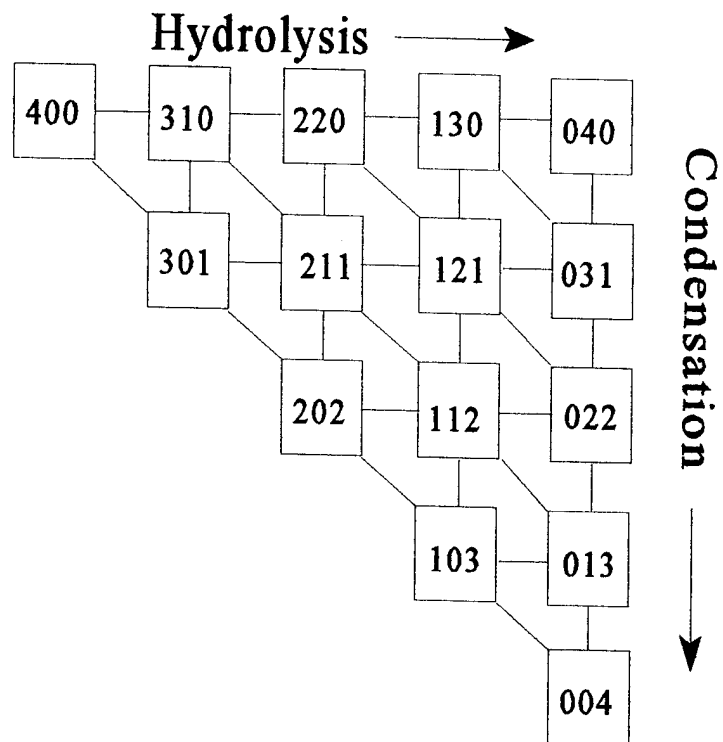


Figure 2.1 Hydrolysis and Condensation of Silicon at next nearest neighbor level represented in matrix form [43, 78-80].

If the hydrolysis rate is much larger than either condensation rate, then the methoxy group concentration will quickly be reduced to the value corresponding to complete hydrolysis without condensation (reduction in methoxy functional group concentration equals the concentration of added water). Further reduction in the methoxy group concentration occurs at a lower rate commensurate with the overall rate of the condensation reactions. If hydrolysis rate is much smaller than either condensation rate, hydrolysis will be followed by immediate condensation. In this case, the reduction in methoxy functional group concentration will occur at a rate proportional to the hydrolysis rate.

²⁹ Si NMR may be used to determine the rate of formation of Si-O-Si bonds.

Again, two limiting cases may be considered based on the equation:

$$d[(\text{SiO})\text{Si}]/dt = k_2 [\text{SiOH}]^2 + k_3 [\text{SiOH}][\text{SiOR}] \quad [17]$$

If k_2 is much greater than k_3 , the condensation rate will be proportional to $[\text{SiOH}]^2$. If k_2 is much smaller than k_3 , then the condensation rate will be proportional to $[\text{SiOH}][\text{SiOR}]$. By measuring the initial overall condensation rate as a function of the initial water concentration, it is possible to determine if either of these limiting cases apply.

In the case where the initial overall condensation reaction is negligible with respect to the initial hydrolysis rate and the initial hydrolysis reaction is complete, equation 17 may be expressed as:

$$\frac{d[(\text{SiO})\text{Si}]/dt}{[\text{SiOH}]} = (k_2 - k_3)[\text{SiOH}] + k_3 [\text{SiOR}]_0 \quad [18]$$

This expression is valid at early times when the concentration of Si-O-Si is small compared

to the initial methoxy functional group concentration. According to this equation, the condensation rates are determined from a plot of the initial condensation rate divided by the $[\text{SiOH}]$ versus $[\text{SiOH}]$ where $[\text{SiOH}]$ is the average value of the silanol group concentration over the measurement window. Figure 2.2 shows the results from Assink data [76]

The reaction rates analyzed by Kay and Assink [78] used a statistical model assuming equal and independent reactivities of polyalkoxysilanes. As a consequence, the consecutive hydrolysis steps were assumed to be linear, decreasing the respective rate constants. However, linearly increasing rate constants in hydrolysis was shown by Yang [27] and Pouxvil [35], which contradicted the earlier trend reported by Assink [78]. McCormick and coworkers [81, 82], resolved this issue by showing that the consecutive hydrolysis steps were in fact less thermodynamically favorable and counteracted the increasing rate constant trend.

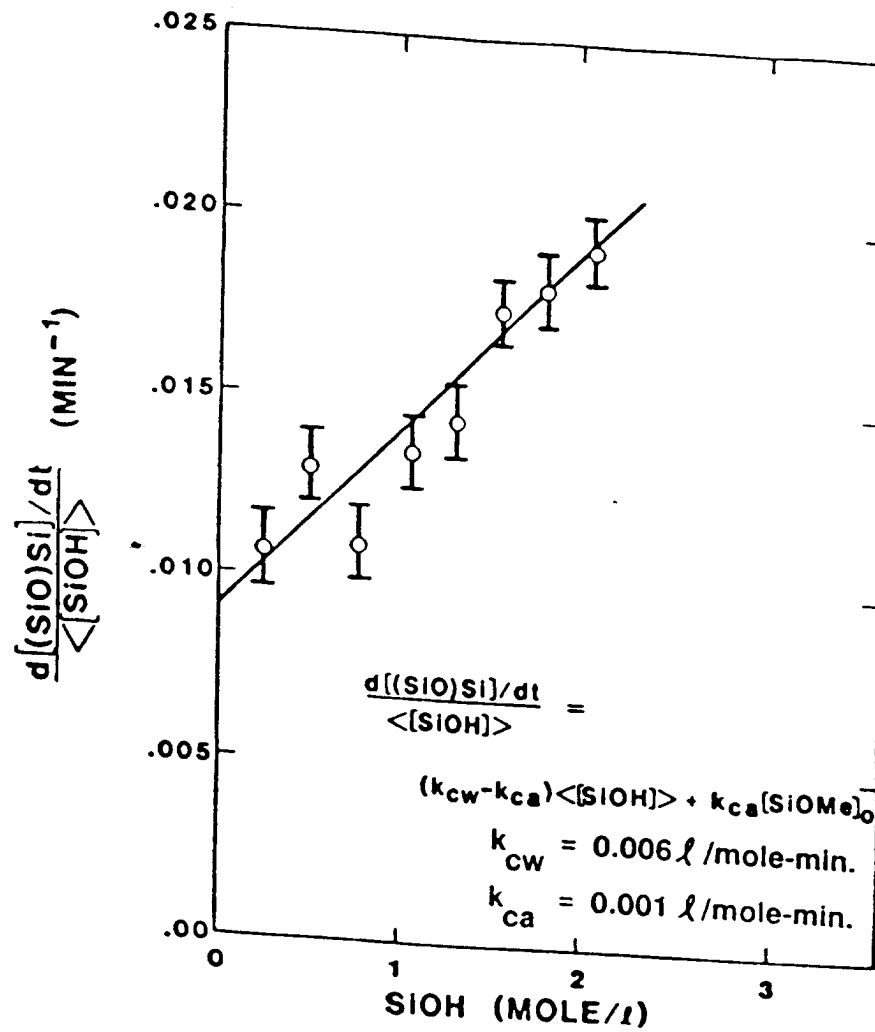


Fig 2.2 Initial Condensation Rates divided by the Initial Silanol Concentration versus the Initial Silanol Concentration. [43].

2.6 References

- [1] C.J. Brinker and G.W. Scherer, Sol-Gel Science, The Physics and Chemistry of Sol-Gel Processing, Academic Press, NY 1990
- [2] I.M. Thomas, "Sol-Gel Technology of Thin Films, Fibers, Preforms, Electronics and Specialty Shapes", Noyes Publications, NJ 1988
- [3] J.J. Ebelman, Ann., 57, 331, 1846
- [4] W.Z. Otwald, J. Phys. Chem., 27, 386, 1897.
- [5] L. Rayleigh, Philos. Mag. 38, 738, 1919
- [6] W. Geffcken, E. Berger, German Patent 736 411, May 1939
- [7] T. Graham, J. Chem. Soc., 17,87, 1864.
- [8] C.B. Hurd, Chem. Rev., 22, 403, 1938.
- [9] S.S. Kistler, J. Phys. Chem., 36,52, 1932.
- [10] B.E. Yoldas, J. Mater. Sci., 10, 1856, 1975.
- [11] B.E. Yoldas, J. Mater. Sci., 12, 1203, 1977.
- [12] M. Yamano, A. Shinji, T. Sakaino, J. Mater. Sci., 13, 865, 1978.
- [13] L. Levene, I.M. Thomas, US patent 3,640,093 1972
- [14] H. Dislich, Angewandte Chemie, 10, 6, 363, 1971
- [15] R. Roy, J. Am Ceram. Soc. 52, 344, 1969
- [16] G.J. McCarthy, R. Roy, J.M. McKay, Am. Ceram. Soc. 54, 637, 1971
- [17] E. Wainer, German Patent 1,249,832 1968

- [18] H.G. Sowman, US Patent 3,795,524 1974
- [19] S. Horikuri, K. Tssuji, Y. Abe, A. Fukui, E. Ichiki, Japanese Patent 49-108325 1974
- [20] Advances in Ceramics, Vol 21: ceramic-powder Science, eds. G.L. Messings, K.S. Mazdiyasni, J.W. McCauley, R.A. Haber, Am. Ceram. Soc., Westerville, OH 1987.
- [21] R.C. Mehtotra, J. Non Crystalline Solids, 100, 1, 1988
- [22] R.C. Mehtotra, J. Non Crystalline Solids, 121, 1, 1990
- [23] M. Guglielmi, G. Carturan, J. Non Crystalline Solids, 100, 16, 1988
- [24] M. Naogami, K. Nagasaka, J. Non Crystalline Solids, 109, 79, 1989
- [25] Y. Abe, N. Sugimoto, Y. Nagao, T. Misons, J. Non Cryst. Solids, 104, 164, 1988
- [26] G. S. Lee, G.L. Messing, F.G.Delaat, J. Non Crystalline Solids, 116, 125, 1990
- [27] H. Yang, Z. Ding, X.Xu, J. Non Crystalline Solids, 112, 449, 1989
- [28] E.J.A. Boonstra, J.M. E. Baker, J. Non Crystalline Solids, 122, 171, 1990
- [29] J-B. Chan, D-W. Hua, R. Winter, J.Jonas, J. Mat. Res, 4,693, 1989
- [30] A.H. Boonstra, T.N.M. Bernards, J. Non Crystalline Solids, 105, 207, 1988
- [31] T.W. Zerda, G.Hoang, J. Non Crystalline Solids, 109, 9, 1989
- [32] H. Schimdt, H. Scholze, A.Kaiser, J. Non Crystalline Solids, 63, 1, 1984
- [33] C.J. Brinker, J. Non Crystalline Solids, 100, 31, 1988
- [34] I. Strawbridge, A.F. Craievich, P.F. James, J. Non Crystalline Solids, 72, 139, 1985.
- [35] J-C. Pouxvil, J.P. Bailot, J.Y. Lallemand, J. Non Crystalline Solids, 89, 345, 1987.
- [36] K.J. McNeil, J.A. DiCaprio, D.A. Walsh, R.F. Pratt, J.Am.Chem.Soc,102, 1859,1980
- [37] R.E. Tims, J. Am. Chem. Soc., A, 1969, 1971.

- [38] R. Aldion, A. Loebel, E. Eirich, J. Am. Chem. Soc., 72, 5702, 1950.
- [39] M.G. Voronkov, V.P. Mileshevich, Y.A. Yuzhekevski, The siloxane Bond, Consultants Bureau, NY 1978.
- [40] W. Noll, Chemie und Technologies der silicone, 2nd ed. Verlag Chemie, Weinheim, F.R. Germany, 1968.
- [41] C.J. Brinker, K.D. Keefer, R.A. Schaefer, Assink, B.D. Kay, J. Non Crystalline Solids 63, 45, 1989.
- [42] C.J. Brinker, K.D. Keefer, R.A. Schaefer, Assink, B.D. Kay, C.S. Ashley, J. Non Crystalline Solids 62, 45, 1984.
- [43] R.A. Assink, B.D. Kay, J. Non Crystalline Solids 99, 359, 1988.
- [44] C.J. Brinker, J. Scherer, J. Non Crystalline Solids, 70, 301, 1985.
- [45] R.T. Morrison and Boyd, Organic Chemistry, Allyn & Bacon 1984.
- [46] S.E. Johnson, J. Am. Chem. Soc. 111, 3250, 1989.
- [47] R.R. Holmes, Chem. Rev., 90, 17, 1990.
- [48] L.W. Burggarf, L.P. Davis, Mat. Res. Soc. Symp. Proc, Vol. 73, C.J. Brinker, D.E. Clark, D.R. Ulrich (eds), Mat. Res. Soc., Pittsburg, PA., 1986.
- [49] F. Liebau, Inorg. Chem. Acta., 89, 1, 1989.
- [50] E.R. Pohl, F.D. Osterholtz, "Molecular Characterization of Composite Interfaces" H. Ishida, G. Kumar (eds), Plenum, NY 1984.
- [51] L.W. Kelts, N.J. Armstrong, C.J. Brinker, D.E. Clark, D.R. Ulrich (eds), Better Ceramics through Chemistry Mat. Res. Soc., Pittsburg, PA., 1988.

- [52] R. Campostrini, G. Carturan, G. Soranu, P. Traldi, J. Non Crystalline Solids, 108, 315, 1988.
- [53] P.J. Flory, J. Phys. Chem., 46, 132, 1942.
- [54] P.J. Flory, J. Am. Chem. Soc., 63, 3083, 1941.
- [55] W.H. Stockmayer, J. Phys. Chem., 11, 45, 1943.
- [56] J.M. Fletcher, C. Hardy, J. Chem. and Ind., 18, 48, 1968.
- [57] B.E. Yoldas, Appl. Chem. Biotechnol., 23, 803, 1973.
- [58] B.E. Yoldas, J. Mater. Sci., 10, 1856, 1975.
- [59] J. Pawlaczyk, Z. Kokot, A. Borkowski, J. Pharmacol. Pharm., 32, 409, 1980.
- [60] W.G. Klemperer, V. Mainz, S.D. Ramamurthi, F. Rosenberg, Mat. Res. Soc. Sym., Vol. 121, MRS, 1988 p.15.
- [61] M. Yamano, S. Inoue, A. Yasumori, J. Non Crystalline Solids, 63, 13, 1984.
- [62] J.D. McKenzie, Science of Ceramic Chemical Processing, (Hench, Ulrich eds), Wiley, NY 1986 p.113.
- [63] M.W. Colby, A. Osako, J.D. McKenzie, J. Non Crystalline Solids, 81, 365, 1986.
- [64] S. Sakka, K. Kamiya, J. Non Crystalline Solids, 42, 403, 1980.
- [65] J.C. Debsikdar, Adv. Ceram. Mater., 1, 93, 1986.
- [66] S. Wallace, L.L. Hench, Better Ceramics Through Chemistry II, MRS, 1984.
- [67] R. Campostrini, G. Carturan, B. Pelli, P. Traldi, J. Non Crystalline Solids, 108, 143, 1989.
- [68] I. Artaki, M. Bradley, T.W. Zerda, J. Jonas, J. Phys. Chem., 89, 4399, 1985.

- [69] T.W. Zerda, I. Artaki, J. Jonas, J. Non Crystalline Solids, 81, 365, 1986
- [70] C.A.M. Mulder, A.A.J.M. Damen, J. Non Crystalline Solids, 93, 169, 1987.
- [71] C.C. Lin, J.D. Basil, ibid ref., 51, p. 585.
- [72] C.A. Balfe, K.J. Ward, D.R. Tallant, S.L. Martinez, ibid ref 51, p.619.
- [73] J. Chojnowski, M. Cypriak, K. Kazwierski, J. Non Crystalline Solids, 125, 40, 1990.
- [74] J.C. Ro., I.J. Chang, J. Non Crystalline Solids, 126, 259, 1990.
- [75] S. Kozawa, H. Kuroki, S. Sakka, J. Non Crystalline Solids, 95-96, 1181, 1987.
- [76] R.A. Assink, and B.D. Kay, Non Crystalline Solids, 99, 359, 1988.
- [77] B.D. Kay, R.A. Assink, Non Crystalline Solids, 104, 112, 1989.
- [78] R.A. Assink, and B.D. Kay, Non Crystalline Solids, 107, 35, 1988.
- [79] R.A. Assink, and B.D. Kay, Better Ceramics Through Chemistry, C.J. Brinker, D.E. Clark, D.R. Ulrich eds., MRS 1984, p.301-306.
- [80] Assink, and B.D. Kay, Better Ceramics Through Chemistry IV, C.J. Brinker, D.E. Clark, D.R. Ulrich eds., MRS 1989.
- [81] J. Sanchez, M.Reise, A. McCormick, Better Ceramics Through Chemistry IV, C.J. Brinker, D.E. Clark, D.R. Ulrich eds., MRS 1989.
- [82] J. Sanchez, A. McCormick, J. Phys. Chem. 96, 8973, 1992.

3. Colloidal Systems

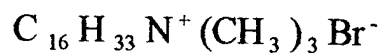
Colloidal systems consist of two immiscible phases, one dispersed as small domains in the continuous phase. The phases can be gases, liquids or solids or combinations of the three for mentioned. The size of the dispersed material can be characterized to the size range of 1×10^{-8} to 2×10^{-6} meters. Colloidal systems are usually stabilized by surfactants.

3.1 Surfactants

Surfactants are molecules that possess both an oil soluble (hydrophobic) and water soluble (hydrophilic) components. Because of this unique structure, surfactants are capable of modifying an existing interface by adsorbing at the interface/surfaces and associate into aggregates in bulk solutions. Therefore they are ideal emulsifiers, which must have this amphiphilic structure.

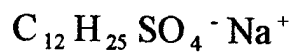
The hydrophobic region of the surfactant is often a long-chain hydrocarbon or fluorocarbon (C_8 - C_{16}). Figure 3.1 shows different surfactant structures with examples. The hydrophilic region (often referred to as the head group) is usually either ionic or polar moiety. Ionic surfactants dissociate when dissolved in an aqueous medium. Factors affecting the behavior of ionic surfactants include electrolyte concentration and pH. In the case of the ionic head groups, they can be broken down into anionic (e.g. sodium dodecylsulfate), cationic (e.g. hexadecyl trimethylammonium bromide), or zwitterionic (e.g. phospholipid, which contain both cationic and anionic moieties).

Cationic Surfactants



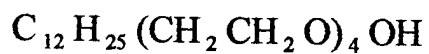
Cetyltrimethylammonium bromide
(CTAB)

Anionic Surfactants

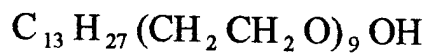


Sodium dodecylsulfate (SDS)

Nonionic Surfactants



Brij 30



SA9 Synperonic A-9

Figure 3.1. Types of Surfactants with examples.

The nonionic surfactants often have an ethylene oxide head group, where the number of ethylene oxide chains can vary from two up to one hundred. The greater the number of ethylene oxide units, the greater the water solubility of the surfactant.

Nonionics are very temperature dependent, and the degree to which they will dissolve in water is dependent on the hydrophobic-lipophilic balance (HLB). This balance is the tendency of the surfactant to dissolve in water versus a non-polar medium (low HLB, insoluble in water).

Surfactants are well known for their applications as detergents, stabilizing agents for emulsions and foams, and cosmetic formulation. The role of surfactants in such systems uses their unique structural effects, which are of decisive importance in their application.

Surfactants form amphiphilic association structures such as micelles, vesicles, microemulsions, and lyotropic liquid crystals when combined with each other and with water. There are two principle kinds of amphiphilic association structures. The predominant *colloidal* structure is the micelle. Micelles are formed as separate micro droplets that move freely in a liquid. Their appearance is isotropic and transparent to the naked eye. The other predominate structure is the *lyotropic liquid crystal*, which will precipitate out of a colloidal dispersion, forming separate phases with gel-like properties. The relationship between these two predominate structures can easily be understood from their geometry and thermodynamic properties.

The characteristics implied in surfactant behavior can be summed up in the

associative properties of these molecules. Whether surfactants are adsorbed at the interface/surface or aggregated in bulk solution, they organize into simple geometrical shapes of spheres, cylinders and lamellar sheets. These geometrical considerations were introduced by Ninham and Israelachvili (1, 2) as the surfactant packing parameter R.

$$R = \frac{V}{A \cdot L} \quad (3.1)$$

where V is the real volume of the hydrocarbon chain, A is the cross sectional area of the surfactant in the structure and L is the length of a fully extended hydrocarbon chain. The value of A in equation 3.1 is not the geometrical cross-section of the polar part of the surfactant *per se* but the area including one half of the distance to the closest neighbor. The ratio R is the ratio between the hydrocarbon chain real volume and the volume calculated by multiplying the area A by the length L. The relationship between the packing parameter and the association structures are listed in Table 3.1.

| Surfactant Packing Parameter, R | Association Structure |
|---------------------------------|-------------------------------|
| < 1/3 | spherical micelles |
| 1/3 - 1/2 | rod shaped micelles, cylinder |
| 1/2-1 | Lamellar sheet |
| >1 | inverse micelle or cylinder |

Table 3.1 Relation between R and Amphiphilic Association Structures

It is easily recognized by inspection of equation 3.1 that when the two volumes are equal, the molecules tend to pack in a lamellar or parallel arrangement. However, this packing is retained for all R values in the range 1-0.5. Reducing the value below $R=0.5$, a new packing is obtained: a cylinder. If R is reduced further to less than $1/3$ then spherical packing will be obtained. To illustrate this point, an ionic single chain surfactant volume of hydrocarbon chain, V , will be small and normal micelles will form, Fig 3.2a. The large value of A is due primarily from electrostatic repulsion between head groups. By reducing the repulsion between head groups, the A term is thus reduced and, hence, R values will increase to cylindrical micelles Fig. 3.2b. Lamellar sheets will form when the calculated volume is proportional to the real volume of the hydrocarbon chain Fig. 3.2c. When the area covered by the head groups becomes too small compared to the volume of the hydrocarbon chains inverse micelle form Fig 3.2d.

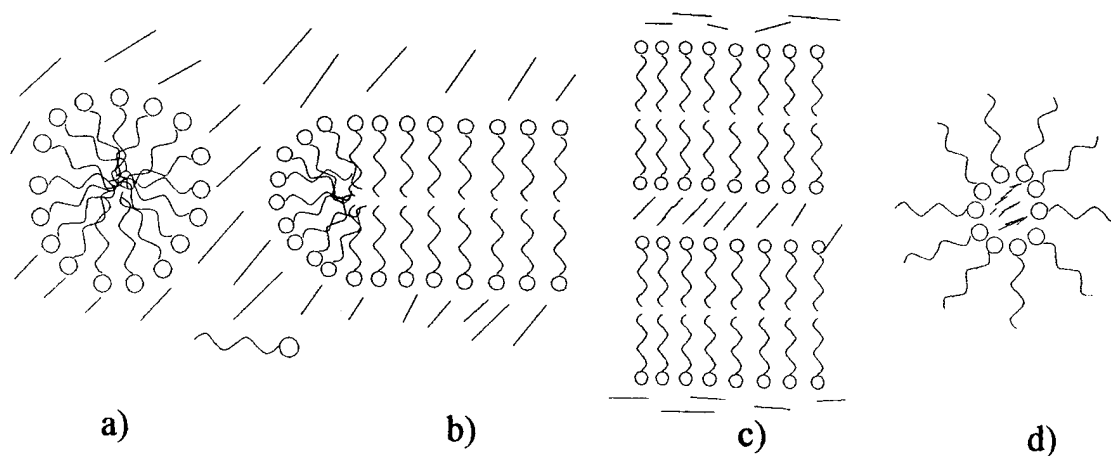


Figure 3.2 Shapes of the aggregates

3.2 Phase Diagrams

The use of binary and ternary phase diagram provides a closer examination of the relationship between the different surfactant association structures. In Fig. 3.3 a typical three component phase diagram is displayed.[10].

The system of interest contains water, ionic surfactant, and a long or medium chain alcohol. The combination of these three components results in the formation of four structures. At first, the ionic surfactant forms spherical micelles in the aqueous solution, L1 (bottom left). This structure is expected because the polar groups of an ionic surfactant give repulsive forces between them, and as a consequence, a huge apparent value of A in equation 3.1. Hence, spherical micelles are expected structures in aqueous solutions and they are the ones formed. The spherical micelles are able to solubilize a long chain alcohol to a maximum of approximately 10%.

Addition of more ionic surfactant to the L1 phase leads to turbidity and forms an E phase of cylindrical micelles. In the E phase (center bottom), the A value in equation 3.1 is extremely large due to the repulsion between ionic groups and thus extends the micelles in to the form shown in Figure 3.2b.

Addition of more Alcohol to the L1 phase results in turbidity; the solubility limit has been reached and a new phase, D, appears. With a long chain alcohol and ionic surfactant, a lamellar packing is favored and thus separates from the dilute aqueous solution (center left). The structure of the D phase is a result of the combination of the OH groups of the alcohol and the charged polar group of the surfactant. The alcohol

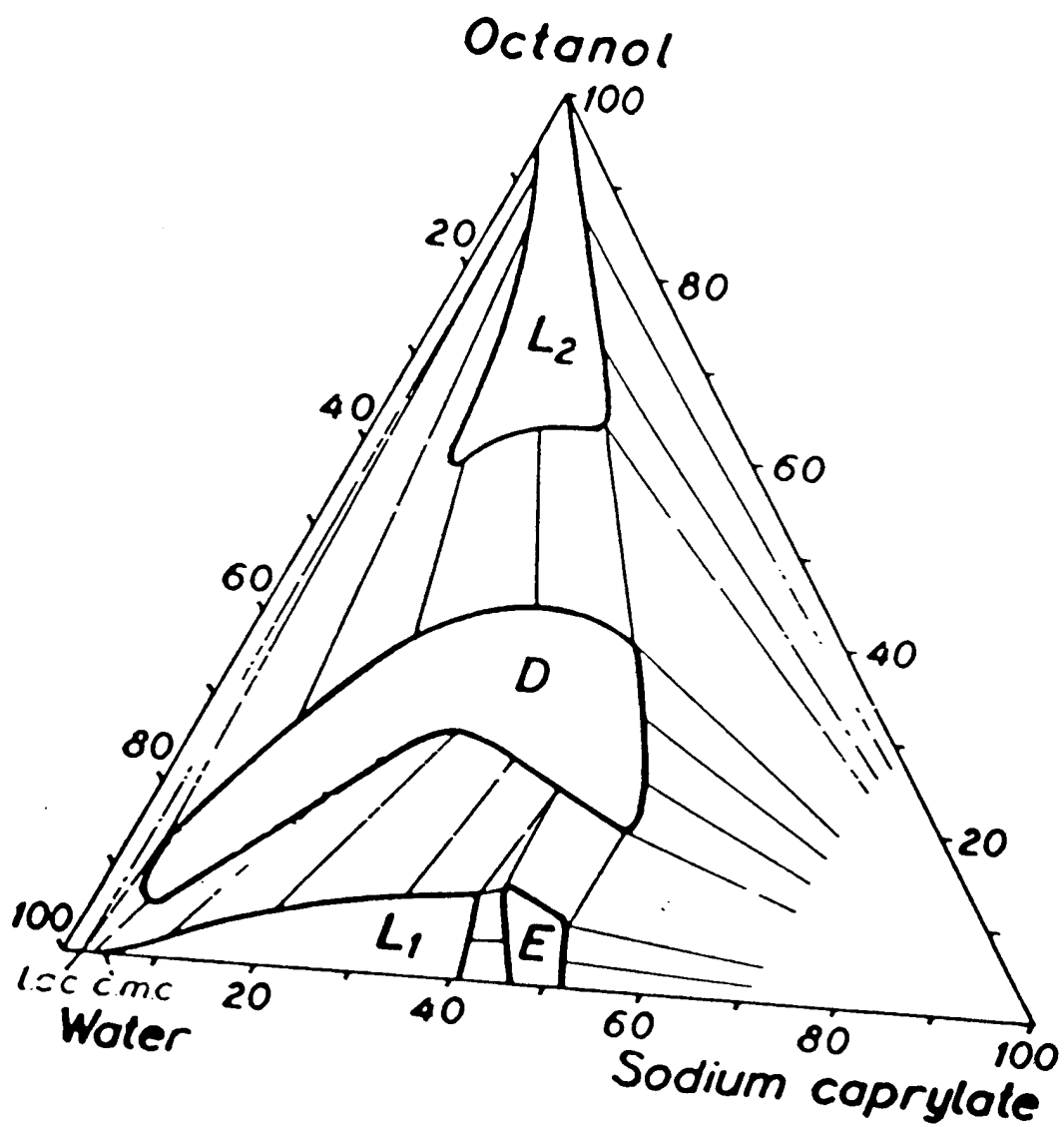


Figure 3.3 Ternary Phase Diagram for Water/Octanol/Sodium Caprylate[10].

group has no repulsion to the charged groups of the surfactant and will fit into the space between them, giving a strong reduction of the average A value in equation 3.1. There is no reduction in the V value, which results in R values exceeding 0.5 limit and a lamellar structure forms.

The lamellar structure has two properties of importance. It has a viscous gel-like consistency, which is easily identified with a simple tap test. It is also easy to detect due to its birefringence between crossed polarizers.

When the alcohol/surfactant ratios in excess of those in the lamellar liquid crystal result in a continued reduction of the A value (equation 3.1). The R value in equation 3.1 now exceeds 1.0, and inverse micelles are formed in the L2 alcohol solution. The structure of the inverse micelle with their central water pool surrounded by the surfactant and alcohol chains pointing outward, makes them suitable for solubilization of water or aqueous solutions into hydrocarbons. This solubilization is obtained in the microemulsion.

3.3. Micelles and Microemulsions

Microemulsions are transparent, thermodynamically stable liquid in liquid dispersions. The droplets are sufficiently small (0.0015×10^{-6} m to 0.15×10^{-6} m radius) and form spontaneously with agitation needed to obtain gross mixing. These systems contain relatively large amounts of water and oil, stabilized by a surfactant, ionic or nonionic, and often a co-surfactant [3-6]. However, in order to discuss microemulsions, the subject of micelles should be addressed first.

Recalling the fact that surfactants are surface active, when added to an aqueous

continuous system, they adsorb to the water-air or water-oil interface, thus causing a reduction in the interfacial tension. As the surfactant concentration is increased, the interfacial tension continues to decrease until a saturated solution concentration is reached. After this certain concentration point, the interfacial tension will remain relatively constant even with significant increases of surfactant is added. The rational for this behavior is that the surfactant molecules above this concentration begin to associate into spherical aggregates called micelles, Figure 3.4. The concentration which "micellization" occurs is referred to as the "critical micellization concentration" or CMC. Any additional surfactant added beyond the CMC exists in the form of micelles [7].

The interfacial tension is only one of the physical properties that is dramatically changed as the CMC is reached. Turbidity, osmotic pressure, and conductivity plotted versus the surfactant concentration also demonstrate a change in their curves at CMC, Figure 3.5 [8]. Micellization is dependent on the temperature. The solubility of the surfactant will increase at a well defined temperature. At this temperature, CMC is reached and micelles start to form. This temperature is called the Krafft point [11].

One of the main advantages for using surfactant systems is the solubilization of compounds that are usually insoluble in water (e.g. oils). In micellar systems, oils can be solubilized to a limited extent (up to 10%). Through various methods, the solubilization of oils can be dramatically increased, and microemulsions can be prepared. There are various starting points in the preparation of microemulsions. They derive from micellar solutions, liquid crystalline phases or from surfactant emulsions [9].

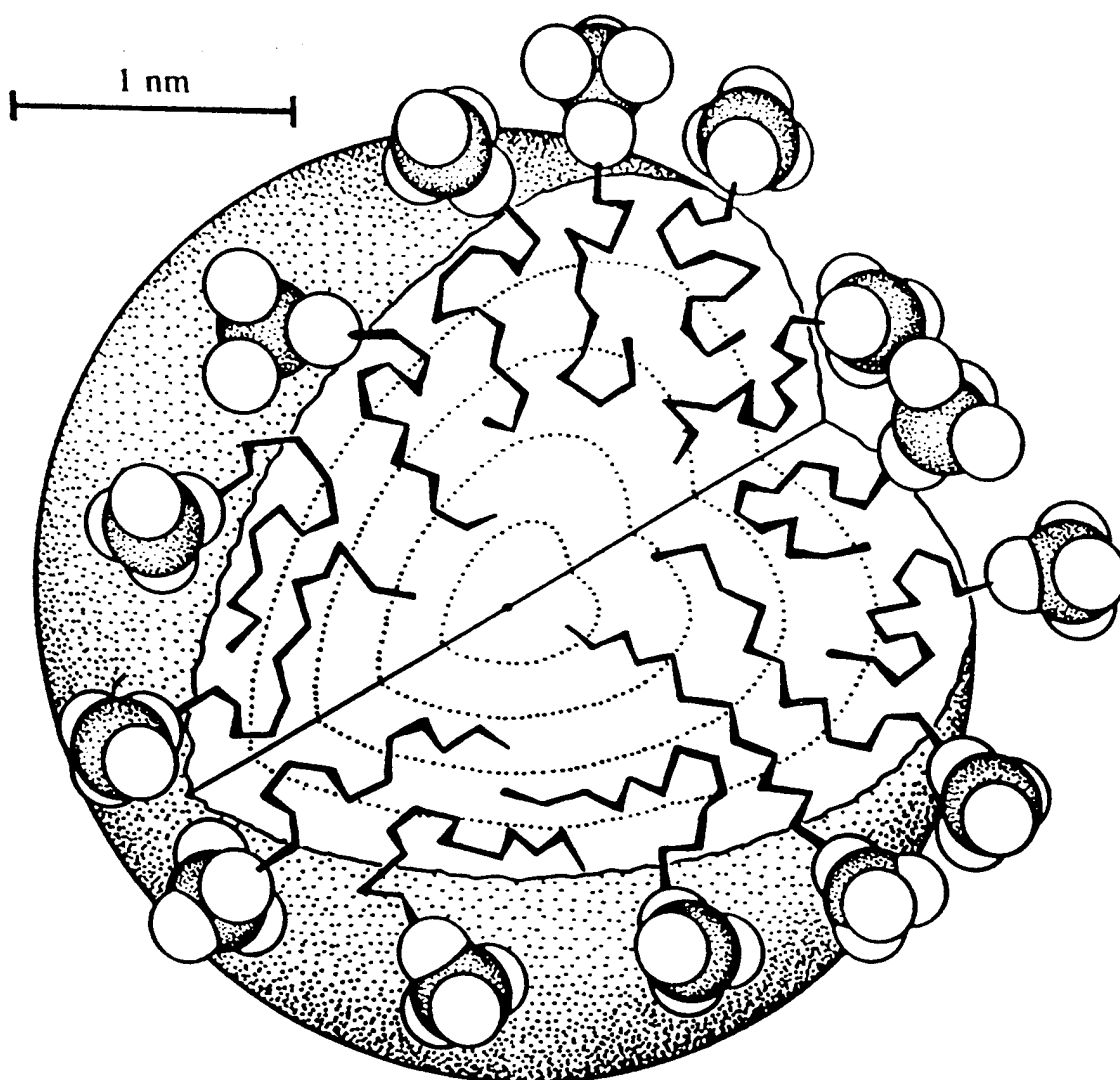


Figure 3.4 The Structure of a Normal Micelle.

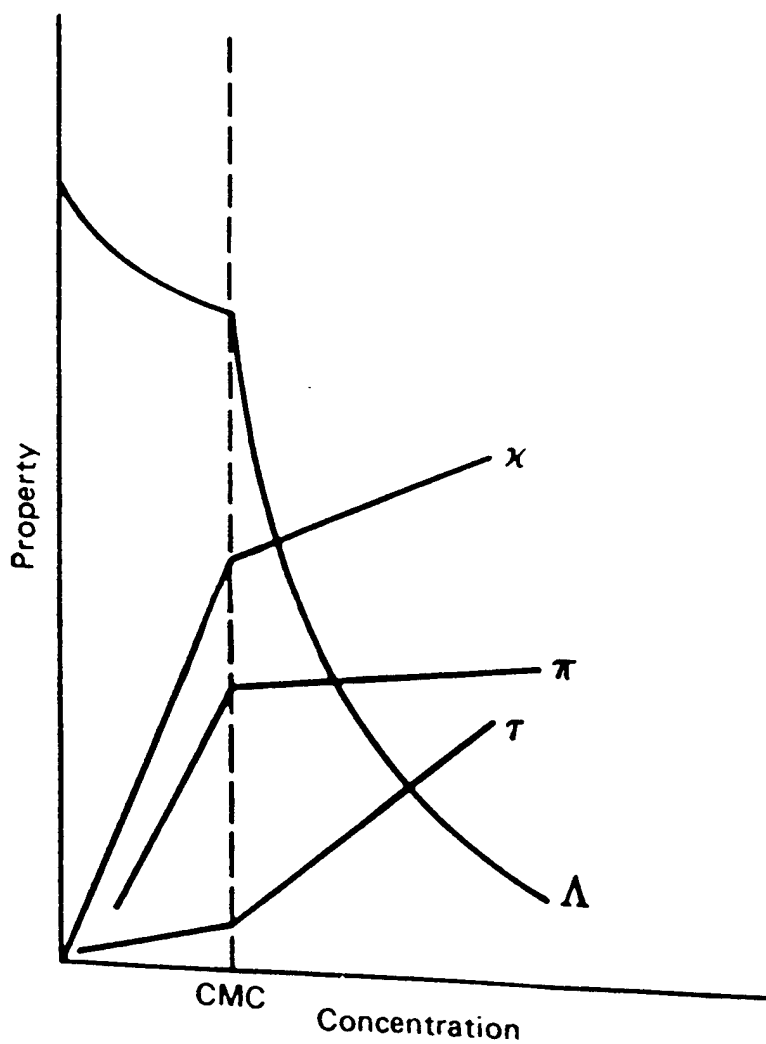


Figure 3.5 The Effect of Surfactant Concentration on Various Properties.

Conductivity, κ , turbidity, τ , equivalent conductivity, Λ , osmotic pressure, π .

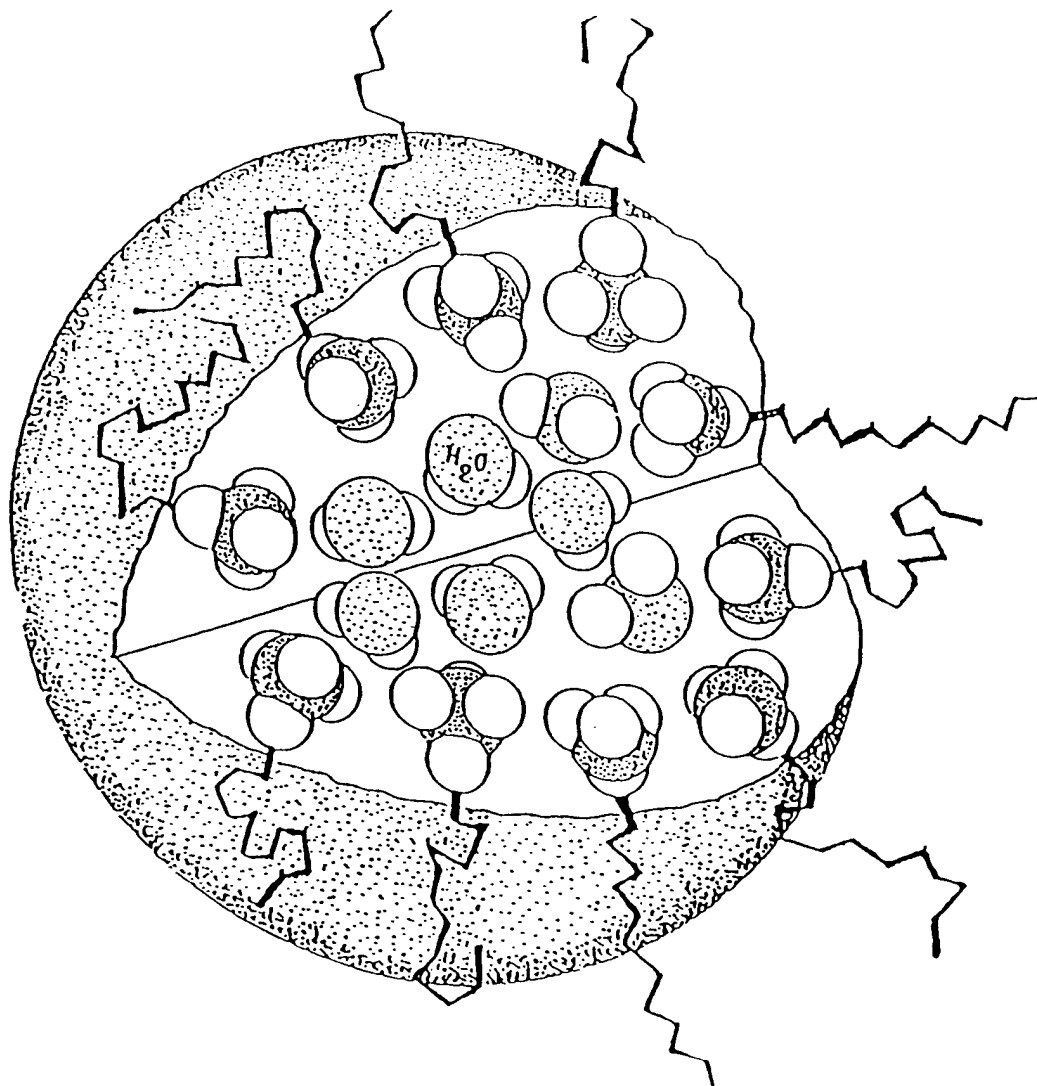


Figure 3.6 The Structure of an Inverse Micelle.

In addition to normal micelles, the oil phase can be the continuous phase, and at a certain concentration of surfactant, inverse micelles can form as represented in Figure 3.6. The polar groups of the surfactant in an inverse micelle are oriented towards the aqueous core.

There are two possible structures of microemulsions, depending on the which component is dispersed in the other. The microemulsion may be oil or water continuous or, for some systems, even bicontinuous. They may be stabilized by a single nonionic surfactant [12, 13], or by a combination of an ionic surfactant and a cosurfactant (e.g., a medium chain length alcohol) [14, 15].

Water in oil (W/O) microemulsions are formed when the amount of surfactant is increased in the inverse micelle. Oil in water (O/W) microemulsions are formed when the amount of oil is increased in a normal micells or the water content is increased in the lamellar liquid crystal.

3.4 References

- [1] J.N. Isrealachvili, D.J. Michell and B.W. Ninham, J. Chem. Soc. Faraday Trans. 2, 72, 1525, 1976
- [2] J.N. Isrealachvili, Intermolecular and Surface Forces, Academic Press, 1985.
- [3] I. Danielsson and B. Lindman, Colloids & Surfaces 3, 391, 1981.
- [4] K. Shinoda and S.E. Friberg, Emulsions and Solubilization, Wiley-Interscience 1986
- [5] K. Shinoda and Y. Shibata, Colloids & Surfaces 19, 185, 1986.
- [6] K. Shinoda and B. Lindman, Langmuir 3, 135, 1987.
- [7] Friberg, S.E. "Vesicles, Liposomes and Liquid Crystals", Struktur, Loslighet och Upplosningshastighet, Kompendium, Apotekarnas Kurverksanhet
- [8] Heimenz, P.C. Principles of Colloid and Surface Chemistry, 2nd ed. Marcel Dekker, 1986.
- [9] Myers, D. Surfactant Science and Technology VCH Publishers, NY 1988.
- [10] P. Ekwall, Advances in Liquid Crystals, Vol. 1 G.H. Brown, Academic Press 1975.
- [11] F. Krafft and H. Wiglow, Ber, 28, 2566, 1895
- [12] J. Sjöblom, P. Stenius, I. Danielson, "Nonionic Surfactants, Physical Chemistry", M.J. Schick ed. Marcel Dekker.
- [13] A.J. I. Ward, H. Ku, M.A. Phillippi, C. Marie, Mol. Cryst. Liq. Cryst. 154, 55, 1988
- [14] S.E. Friberg, A.J. I Ward, D W Larsen, Langmuir 3, 735, 1987
- [15] S.E. Friberg, G. Rong, J. Phys. Chem. 92, 7247, 1988

4. The Microemulsion-Gel Method

4.1 Non-Aqueous Microemulsions

A microemulsion is a combination of water, oil, and surfactant, which spontaneously form a transparent system. A medium chain length alcohol is often included to facilitate the solubility of different components. Schulman[1] was first to report these systems. The combination of immiscible compounds into a single phase by the addition of a surfactant does not imply thermodynamic stability. In comparison to solutions which form no discrete structures, microemulsions do form association structures due to the behavior of surfactants added. The surfactant forms an interface between components, forming discrete droplet structures. Since microemulsion droplets are less than 0.15×10^{-6} m in diameter, they do not interact with visible light and therefore appear transparent to the naked eye. Friberg [2] proposed that microemulsions are a direct extension of the micellar solutions, built on the pioneering investigations by Ekwall [3]. At the same time, theoretical studies were published by Ruckenstein [4] and Friberg and Venable [5] which summarized the stability, phase equilibria, and applications of microemulsions.

This field of study expanded into new avenues when it was discovered independently by Friberg [6], Lattes[7,8], and Robinson[9] that microemulsions could be formed using polar solvents rather than water. Friberg and Podzimek reported forming microemulsions using ethylene glycol, lecithin, and decane. The solubility region of approximately 10% lecithin and 20-70% ethylene glycol was reported. Lattes produced

microemulsions composed of formamide, cyclohexane, butanol, and cetyltrimethylammonium bromide and others of formamide, perfluorinated surfactants, co-surfactants, and oils. Robinson combined glycerol, heptane, and Aerosol OT to form non-aqueous microemulsions. Non-aqueous microemulsions as well as non aqueous liquid crystals [10-14], have been reported using various compositions of surfactants, co-surfactants, polar solvents, and oils.

The thermodynamics of non-aqueous microemulsions has been studied for many years by Evans [15-17]. At low temperatures the formation of micelles has been considered to be the result of a large positive entropic change caused by the release of three-dimensionally ordered water from around the hydrocarbon chains, which is not completely balanced by the introduction of surfactant and the subsequent micelle formation [18]. At high temperatures the ordered structure of water is absent, yet enthalpy change is negative, and thus becomes the driving force for formation. A negative enthalpy change is considered to be the deciding factor for systems with hydrazine replacing water, since even at low temperatures it does not form ordered structures in pure form. Evans studied the thermodynamics and hydrocarbon transfer in water-surfactant systems and hydrazine-surfactant systems, in an attempt to isolate the distinct features of water that cause certain "hydrophobic processes" [16,19, 20].

The earliest reports describing the interaction of polar solvents and surfactants discussed the possible formation of micelles of indeterminate size[21-24]. Numerous articles thereafter described the apparent presence of a critical micelle concentration

employing NMR, fluorescence spectroscopy, surface tension measurements, and viscosity. However, the conclusions were based upon those already reached for aqueous systems and were not definitively proven. Almgren[25] reported that a break point in conductance concentration plots does not necessarily indicate the presence of a critical micelle concentration. It was then shown by this group that self-diffusion, surface tension, and fluorescence quenching results did indicate the presence of micellar aggregates.

The results obtained from glycerol, SDS, hexanol, and decane combinations, Friberg concluded that these systems are critical solutions and not microemulsions. The absence of detectable droplets from light scattering results [26,27] confirmed this conclusion. The correlation length maximum that was observed to be a result of the change from one solvent system to another at the critical point, these critical solutions were further verified by several subsequent studies [28-31]. The existence of micelles in non-aqueous microemulsions has continued to be questioned and they are believed to be present only in systems incorporating non-ionic surfactants such as Aerosol OT.

Based upon the results of previous gelation studies [3] and the above discussion done using microemulsions of formamide, cetyltrimethylammonium bromide, decanol, decane, it is firmly believed that these systems do not form discrete droplet structures. They are in fact critical solutions. It will be shown in the next section that this has a direct consequence on the formation of gels from these microemulsions.

4.1 Microemulsion-Gel method for non-aqueous systems

In the sol-gel method an alcohol is typically used as a solvent. However, it has

been shown that a microemulsion can be used as the precursor solvent. The gelation of microemulsions by a metal alkoxide was first achieved by Friberg and Yang [32]. In one study, Water in oil microemulsions were prepared by combining water, SDS, and pentanol, to which TEOS was added. In another study, LA4, hexane, and water were used to form the precursor microemulsion. The hydrolysis and condensation observed were similar to those which occur when gelation takes place in organic solvents. The formation of transparent gels was found to depend on the minimum water requirements of the alkoxide added. Specifically, the area of the phase diagram for transparent gels shifted toward higher water content when more TEOS was included. It was decided that part of the water requirement was due to the need for water to solubilize the silicic polymers formed.

A subsequent investigation [33] studied the effect of water consumption during hydrolysis and liberation of ethanol during condensation on the amphiphilic association structures present. The phase diagrams were changed markedly by these changes in composition. The results indicated that an R value of 4 was required, however, ^{29}Si NMR results showed that condensation began shortly after hydrolysis had begun and the processes occurred concurrently. It was concluded that only two water molecules were needed in the hydrolysis reaction for each molecule of TEOS. The addition of surfactant resulted in the formation of transparent gels at lower water concentrations. This in turn, produced gels from which little water had to be evaporated, reducing shrinkage while drying and lowering the surface tension of the interstitial liquid.

4.3 Hydrated Metal Salts

The mechanism of gel formation after hydrolysis and condensation of alkoxysilanes has recently been investigated in more complex systems. Friberg and co-workers have demonstrated the use of microemulsions as reaction media [32-34] thereby allowing metal salts to be included, in colloidal form, within a gel. Sjöblom and co-workers have introduced systems in which the reaction takes place between the water in hydrated metal salts dissolved in alcohols and tetraethoxysilane (TEOS) [35]. Hydrated metal salts have, in contrast to the nonhydrated ones, a high solubility in low molecular weight alcohols [36]. Depending on the solvent, the hydrated salts will either form ion pairs or dissociate completely. In a series of articles, Friberg et al. [50-52] has investigated reactions between TEOS and different hydrated metal salts in ethanol and methanol, without any added water. ^{29}Si NMR was used to follow the kinetics. When TEOS is introduced to such a nonaqueous electrolyte solution, the hydration water will readily react with TEOS and initiate the hydrolysis step. The reaction kinetics are very dependent on the hydrated metal salt and its molecular state in the alcohol [35, 37]. The final condensation will result in a colloidal dispersion of a metal in a silica matrix. Selle and coworker [53] used fourier-transform infrared spectroscopy to compare the earlier results of Friberg [50-52] and concluded that the hydrolysis rate depended on the dissolution of hydration water into the alcohol medium.

Other recent developments have shown that alkoxy silanes also react directly with aluminum halogenides in alcoholic solution [45]. This reaction has found an application in

in the new non-hydrolytic condensation reaction between metal halides and alkoxide [46]. These investigations used aluminum chloride to extract sodium from sodium salt of silanol in the synthesis of aluminum siloxide compound [47, 48]. Friberg *et al.* [49] utilized the reaction of aluminum chloride with methoxydimethyloctyl silane to deduce the structure of this reaction product to contain two silicon atoms and two aluminum atoms.

These extensions combined with the introduction of nonporous silica materials by Kresge *et al.* [38] have centered the interest on the interactions between silicates and long range amphiphilic association structures [39, 40]. The reactions in such systems do not follow the complex reactions in homogeneous solution [41]. Lyotropic liquid crystals of lecithin and ethylene glycol have been gelled with TEOS and water [42]. The TEOS and water were shown by x-ray diffraction to be compartmentalized in the non-polar and polar regions, respectively. ^{29}NMR results [42] have shown the hydrolysis and condensation reactions were influenced by the separation. However as TEOS underwent hydrolysis, it became more polar and moved to the interface, thus the monomers proceeded immediately to the tetrahydroxysilanes and that condensation when initiated, results in the formation of high molecular weight SiO_2 . The subsequent release of ethanol gradually disrupted the association structure and thus broke down the barrier separating the different regions. No intermediate compounds were found.

With these results at hand, further investigations on the hydrolysis of monomolecular layers of trimethoxysilanes at the air/water interface [43] and later investigated inside a lamellar liquid crystalline phase [44] were conducted.

4.4 References

- [1] J.P.Hoar, J.H. Schulman, *Nature*, 152, 102, 1943.
- [2] S.E.Friberg, I Buraczewska, *Prog. Coll. Polm. Sci.*, 63, 1, 1978.
- [3] P. Ekwall, in G.H. Brown(Ed.), *Advances in Liquid Crystals*, Academic Press, NY 1975,p1.
- [4] E. Ruckenstein, in K.L. Mittal(Ed.), *Micellization, Solubilization, and Micoremulsions*, Plenum, NY 1977, p.755.
- [5] S.E. Friberg, R.L. Venable, in P. Becher (Ed.), *Encyclopedia of Emulsion Technology*, Marcel Dekkar, NY, 1980, p.287.
- [6] S.E. Friberg, M. Podimek, *Colloids Surf.*, 262, 252, 1984.
- [7] B. Escoula, N. Hajjaji, I. Rico, A. Lattes, *J. Chem. Sci. Chem. Comm.*, 12, 33, 1984
- [8] N. Rico, A. Lattes, *J. Coll. Interface Sci.*, 102, 1 1984.
- [9] P.D. I. Fletcher, M.F. Galal, B.H. Robinson, *J. CHem. Soc. Faraday Trans. I*, 80, 3307, 1984.
- [10] S.E. Friberg, C.S. Wohn, *Coll. Polmer Sci.*, 263, 156, 1985.
- [11] N. Moucharafich, S.E. Friberg, *Mol. Cryst. Liq. Crst.*, 49, 231, 1979.
- [12] D.W.Larsen, S.E. Friberg, H. Christenson, *J. Am. Chem. Soc.*, 102, 6565,1980.
- [13] M.A. El Nokaly, S.E. Friberg, D.W. Larsen, *J. COLL, Interface Sci.*, 84, 228, 1981.
- [14] L. Ganzuo, M.A. El Nokaly, S.E. Friberg, *Mol. Cryst. Liq. Cryst.* 72, 183, 1982.
- [15] D.F. Evans, E.Z.Yamauchi, R.Ronan, E.Casassa, *J. Coll. Interface Sci.*, 88, 89, 1982.

- [16] D.F.Evans, S.Chen, G.W.Schrive, E.M. Arnett, J. Am. Chem. Soc, 103, 481, 1981.
- [17] D.F.Evans, B.W. Ninham, J. Phys. Chem., 87, 5025, 1983.
- [18] H.S. Frank, D.F.Evans, J. Chem. Phys., 13, 507, 1945.
- [19] M.S. Ramadan, D.F.Evans, R.Lumry, J. Phys. Chem., 87, 4538, 1983.
- [20] M.S. Ramadan, D.F.Evans, R.Lumry, S. Philson, J. Phys. Chem., 89, 3405, 1985.
- [21] A.Ray, J. Am. Chem. Soc., 91, 6511, 1969.
- [22] A. Ray, Nature, 231, 313, 1971.
- [23] H.N. Singh, S.Saleem, R.P. Singh, K.S. Birdi, J. Phys. Chem., 84, 2191, 1980.
- [24] I. Rico, A.Lattes, J. Phys. Chem., 90, 5870, 1986.
- [25] M.Almgren, S.Swarup, J.E.Lofroth, J. Phys. Chem., 89, 4621, 1985.
- [26] S.E. Friberg, Y-C. Liang, in S.E. Friberg and P. Bothorel (Eds.), Microemulsions: Structure and Dynamics 1985.
- [27] S.E. Friberg, Y-C. Liang, Coll. and Surf., 24, 325, 1987.
- [28] S.E. Friberg, Y-C. Liang, in S. Martecalli and A.N. Chester (Eds.), "Progress in Microemulsions" Plenum, NY, 1989, p.73.
- [29] S.E. Friberg, G. Rong, Langmuir, 4, 796, 1988.
- [30] S.E. Friberg, G. Rong, A.J.I. Ward, J. Phys. Chem., 92, 7247, 1988.
- [31] S.E. Friberg, W.M.Sun, Coll. Polym. Sci., 268, 755, 1990.
- [32] S.E. Friberg, C.C. Yang, in F.M.Doyle, S. Raghaven, P. Somasundaran and G.W. Warrens (eds), Innovations in Materials Processing Using Aqueous, Colloid and Surface Chemistry, The Minerals, Metals and Materials Society, Wanendale, PA p. 181 1988.

- [33] S.E. Friberg, C.C. Yang, J. Sjöblom, *Langmuir*, 8, 372, 1988
- [34] M.H. Selle, J. Sjöblom, S.E. Friberg, T. Young, C.C. Yang, *Prog. Colloid Polym. Sci.*, 88, 42, 1992.
- [35] J. Sjöblom, T. Skodvin, M.H. Selle, J.O. Saeton, S.E. Friberg, *J. Phys. Chem.*, 96, 8578, 1992.
- [36] B. Gestblom, S.C. Mehrotra and J. Sjöblom, *J. Solution Chem.*, 15, 55, 1986.
- [37] A. Amran, S.E. Friberg, J. Sjöblom, *J. Dispersion Sci. Technol.*, in press
- [38] C.T. Kresge, M.E. Leonowicz, W.J. Roth, J.C. Vartuli, J.S. Beck, *Nature*, 359, 710, 1992.
- [39] M. Dubois, Th. Gulik-Krzywicki, B. Cabane, *Langmuir*, 9, 3, 1992.
- [40] A. Monnier, F. Schmith, Q. Huo, D. Kumar, D. Margol, R.S. Maxwell, G.D. Stucky, M. Krsnamurthy, D. Pertolt, A. Firouzi, M. Janicke, B.F. Chmelka, *Science*, 261, 1299, 1993
- [41] J. Sanchez, A. McCormick, *J. Phys. Chem.*, 96, 8973, 1992.
- [42] S.E. Friberg, Z. Ma, *J. Non-Cryst. Solids*, 147&148, 30, 1992.
- [43] J. Sjöblom, H. Ebeltoft, A. Bjorseth, S.E. Friberg, C. Brancewicz, *J. Dispersion Sci. Technol.*, 15, 21, 1994.
- [44] J. Sjöblom, M.H. Selle, S.E. Friberg, T. Moaddel, C. Brancewicz, *Colloids and Surfaces*, 88, 235, 1994.
- [45] S.E. Friberg, in preparation

- [46] S. Acosta, R. Corrier, D. Leclery, P.H. Mutin and A. Viouk, *J. Sol-Gel Sci. Technol.* 2, 25, 1994.
- [47] A.W. Apblett and A.R. Barron, *Organo-metallics*, 9, 2137, 1990.
- [48] H. Schidbaur and M. Schnuat, *J. AM. Chem. Soc.*, 84, 1069, 1962.
- [49] S.E. Friberg, A. Al-Bawaab, J. Sjöblom, G. Farrington, W. Nie, *Colloids and Surfaces*, 105, 251, 1995.
- [50] J. Sjöblom, S.E. Friberg, A. Amran, *J. Dispersion Sci. Technol.*, 16, 31, 1995
- [51] S.E. Friberg, A. Amran, J. Sjöblom, *J. Dispersion Sci. Technol.*, 15, 621, 1994
- [52] S.E. Friberg, J. Yang, A. Amran, J. Sjöblom, G. Farrington, *J. Phys. Chem.*, 98, 13528, 1994.
- [53] M. Selle, F. Fredriksen, J. Sjöblom, A. Christy, S.E. Friberg, *Acta Chemica Scandinavia*, 50, 12, 1996.

5. Solubility Parameters

5.1 Introduction

In order to acquire a better understanding of the stability and mixing behavior of different components, investigators quite often use thermodynamic relationships to interpret experimental results. Colligative properties of a system are used to establish the deviations from ideal solution behavior. Gibbs [11] is often referred to as the father of modern thermodynamics for establishing fundamental relationships for the chemical potential, free energies and defining the standard state of these quantities.

5.2 Thermodynamics of Mixing

For mixing to be possible, the molar Gibbs free energy of mixing at constant pressure must be negative:

$$\Delta G_m = \Delta H_m - T\Delta S_m \leq 0 \quad (1)$$

The entropy change of a mixing process is usually positive, therefore it is necessary to evaluate the enthalpy term in equation 1. When ΔH_m is negative, or positive and less than the $T\Delta S_m$ mixing can occur. The aim of cohesion parameter is to predict the magnitude of this enthalpy term. Spontaneous "unmixing" or phase separation may occur if the temperature of a mixture is decreased. This is due primarily to the temperature dependence of the entropy term however, metastable homogeneous systems may also occur under these conditions.

Differentiation of the Gibbs free energy of mixing with respect to the amount of substance i provides the chemical potential μ_i of component i relative to its chemical

potential μ_i^0 in the pure liquid. The chemical potential is also known as the relative partial molar Gibbs free energy, or the Gibbs free energy of dilution and can be subdivided into enthalpy of dilution and entropy of dilution terms. The activity a_i of component i follows from

$$RT \ln a_i = \mu_i - \mu_i^0 \quad (2)$$

For an ideal mixture there is no volume change during the formation, $\Delta V_m = 0$, no enthalpy change at constant pressure, $\Delta H_m = 0$, and an entropy change equal to that of an ideal gas mixture as a result in the extra degrees of freedom created by the mixing.

$$\Delta S_m = -R \sum_i X_i \ln X_i \quad (3)$$

where X_i is the mole fraction of component i .

The resulting molar Gibbs free energy change in the formation of an ideal mixture is therefore provided by the entropy increase of each component. Substitution of equation 3 into equation 1

$$\Delta G_m = \Delta H_m - T\Delta S_m = RT \sum_i X_i \ln X_i \quad (4)$$

The components form an ideal mixture are always completely miscible in all proportions.

Another way to look at an ideal mixture is on the molecule level; an ideal mixture is one in which the different types of molecules, i and j for example, behave exactly as if they are surrounded by molecules of their own kind; that is all molecular interactions are equivalent.

In non ideal systems, the Gibbs free energy change is not equal to the ideal value, and the excess Gibbs free energy change on mixing is

$$\Delta G_E = \Delta G_m - RT \sum_i X_i \ln X_i \quad (5)$$

Similarly the excess entropy of mixing is defined

$$\Delta S_E = \Delta S_m + R \sum_i X_i \ln X_i \quad (6)$$

An ideal mixture follows Raoult's Law, which states that the partial pressure, P_i , of any component i is given by

$$P_i = X_i P_i^0 \quad (7)$$

where X is the mole fraction and P_i^0 is the vapor pressure of the pure component.

Negative deviations from Raoult's law occur when interactions between unlike molecules are markedly stronger than like pair interactions. Moderate positive deviation are usual, and occur when there is little or no specific interactions between any of the molecules. Strong positive deviations result from situations where molecules of one or more components undergo strong self interactions as in alcohol-hydrocarbon mixes. Very strong positive deviations from Raoult's law leads to liquid-liquid immiscibility. This type of behavior can be investigated by means of a vapor pressure versus composition curve.

Liquid - liquid immiscibility can also be analyzed by plotting the excess Gibbs free energy of mixing against the mole fraction of the mixture. If this curve has no point of inflection and is concave upward, the mixture is stable at all compositions, Figure 5.1a, and no phase separation occurs. If the curve has two upward facing concavities by a convex section and two points of inflection, Figure 5.1c, there is a region of total immiscibility, two meta stable regions, and at either end of the composition range - two regions of mixture stability. Figure 5.1b illustrates the case where the inflection point is not

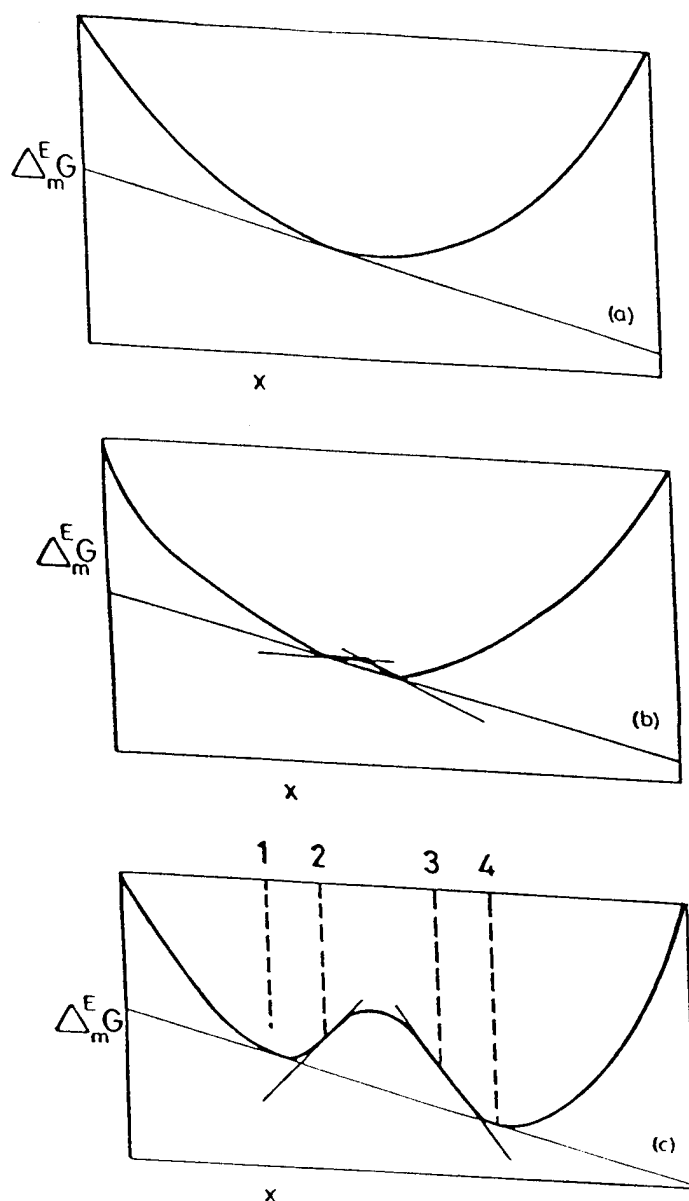


Figure 5.1 Gibbs Excess Free Energy of a binary mixture as a function of mole fraction, x . (a) miscibility in all proportions; (b) Onset of Demixing; (c) Existence of Two Regions of Stability (2, 4) and metastability (1, 3), one region of instability. [14].

high enough to produce measurable phase separation.

5.3 Cohesive Energy and Solubility Parameters

Hildebrand [1] was the first to utilize the Gibbs functions and propose a fundamental thermodynamic relationship between solubility, of solvents and solutes, to the molar internal “cohesive” energy of individual components. The cohesive energy, ΔE , of a liquid is the energy required to separate its molecules into a infinitely dilute vapor at constant temperature. The theory considers the events in a mixing process: the molecules of each component in a mixture are separated from one another by an infinite distance, comparable in many respects to the phase transition of a liquid to a gas in the vaporization process. Although ΔE is temperature dependent, at pressures below atmospheric pressure and temperatures below the normal boiling point of the liquid, the cohesive energy is routinely calculated from the molar heat of vaporization ΔH_{vap} as

$$\Delta E = \Delta H_{\text{vap}} - RT \quad (8)$$

where R is the gas constant, T is kelvin temperature and the term RT accounts for the volume work done during the isothermal expansion. Equation 8 is a good approximation when the saturated vapor is considered an ideal gas under low pressure. However this is not a valid argument when a component approaches the critical point, ΔH_{vap} becomes zero, which leads to negative values in equation 1 for the cohesive energy.

The cohesive energy density (CED) is defined as the ratio of the internal energy per molar volume $\Delta E/V$. By definition, the solubility parameter is the square root of the

CED value

$$\delta = (\text{CED})^{1/2} = [\Delta E/V]^{1/2} = [(\Delta H_{\text{vap}} - RT)/V]^{1/2} \quad (9)$$

The δ values have the unit SI dimensions of $\text{MPa}^{1/2}$. Molar volume and enthalpy information is easily obtained in standard references [2-5]. However, for many materials, especially polymers, solids and surfaces it is necessary to use indirect empirical relationships to estimate the cohesion parameters. The group contribution theory is one such method which uses the chemical structure of a material to estimate the cohesion parameters.

The Hildebrand solubility parameter is often referred to as the "total cohesion parameter, δ_t ", due to the variety of "partial" cohesion parameters developed by other researchers. In a pioneering effort to characterize the total cohesion parameter into partial contributing terms, Hansen [2] proposed an extension of the Hildebrand parameter to include polar and hydrogen bonding systems [6, 7]. The total cohesion parameter, δ_t , is a function of dispersion δ_d , polar δ_p , and hydrogen bonding δ_h partial parameters. The three partial parameters are related to the total cohesion parameter by

$$\delta_t^2 = \delta_d^2 + \delta_p^2 + \delta_h^2 \quad (10)$$

The Hansen total cohesion parameter, δ_t , corresponds to the Hildebrand non-polar parameter, however the two quantities are determined by different methods and should not be expected to be identical. The advantage of the partial parameters over the Hildebrand parameter seems self evident. The Hansen partial cohesion parameters for a material can be represented as a vector in three dimensional space as illustrated in

Figure 5.2. This feature allows both visual and numerical comparisons in the relative strength of each partial parameter coordinate.

Similar to the forementioned Group Contribution theory, the Group molar contribution or F-method provides a useful estimation of the Hansen parameters δ_d , δ_p , and δ_h directly from structural contributions of each functional group's energy to the chemical structure of interest. The dispersion contribution is defined as:

$$\delta_d = (\sum_i F(i)_d) / V \quad (11)$$

where the sum of all structural group energies $F(i)_d$ ($J^{1/2} \text{ cm}^{3/2} \text{ mol}^{-1}$) per molar volume ($\text{cm}^3 \text{ mol}^{-1}$) are listed on several tables in Bartons book [2,3]. The polar group contribution is similarly defined

$$\delta_p = (\sum_i F(i)_p^2)^{1/2} / V \quad (12)$$

The treatment of the polar contribution energies is slightly different than the dispersion, where polarity must be reduced by multiplying δ_p by an asymmetry factor if two identical polar groups are present in symmetrical positions;

0.5 for one plane of symmetry

0.25 for two planes of symmetry

0.0 for more planes of symmetry

The reduction for symmetrical contributions is a good approximation when one considers the reduced dipoles of symmetrical molecules such as acetone.

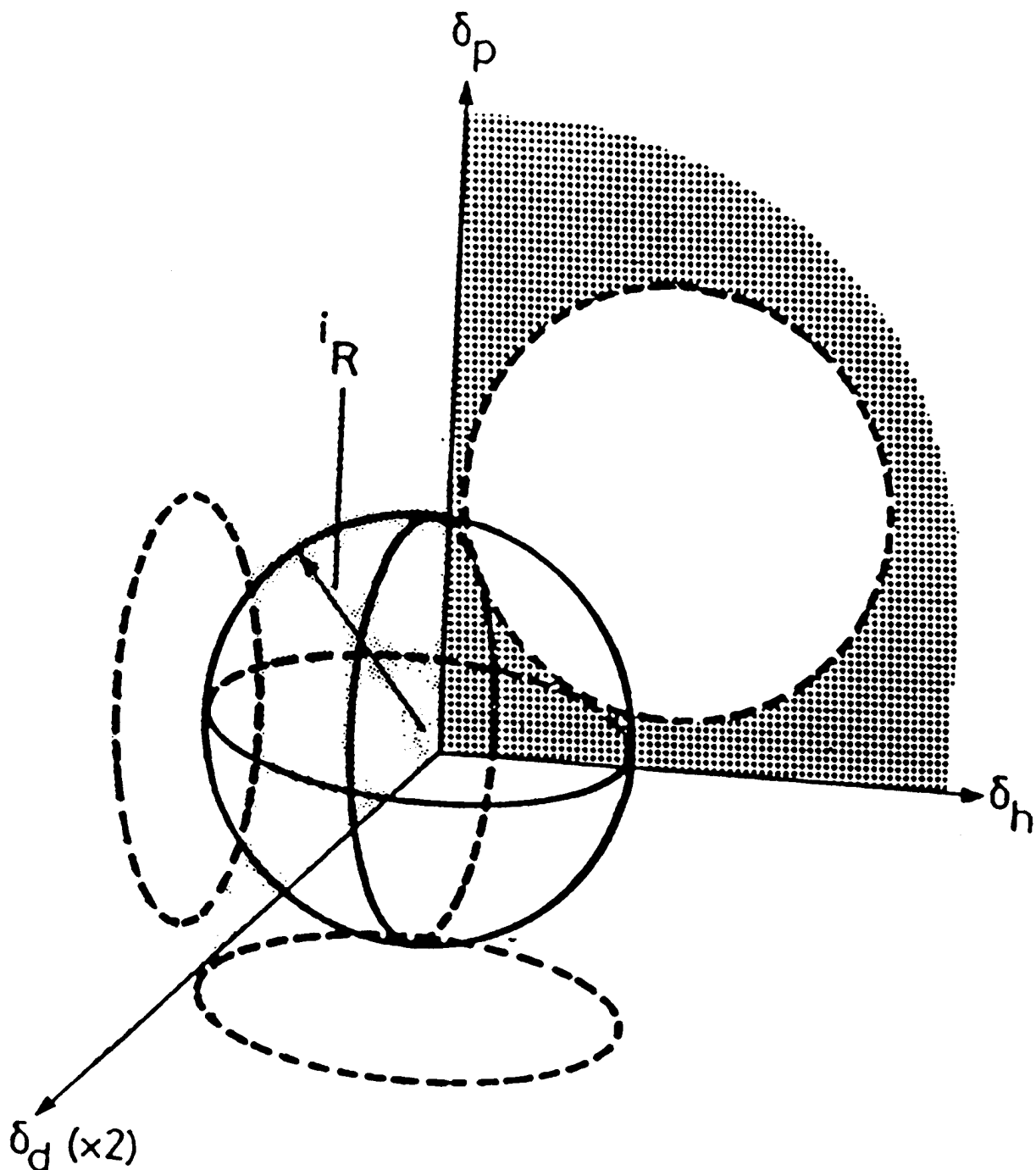


Figure 5.2 Representation of a Hansen Parameter Solubility Sphere with Radius of Interaction i_R and Projections on Three Axial Plane [13].

The hydrogen bonding cohesive energy is assumed to be additive in the F-method, leading to

$$\delta_h = (-\Sigma_i U_h / V)^{1/2} \quad (13)$$

the internal energy, U_h , of the hydrogen bonding contributonal groups should be used with extreme caution, as noted by the author [1,2], where this parameter interaction really requires both donor and acceptor component. The total cohesive parameter is calculated using equation 10 and substituting the values obtained by the F-method partial parameters in equations 11, 12, and 13.

The most exact determination of solubility behavior is in a series of solvent mixtures with varying degrees of hydrogen bonding ability and polarity. The distance of solvent coordinates $(\delta_d^i, \delta_p^i, \delta_h^i)$ from the center point $(\delta_d^j, \delta_p^j, \delta_h^j)$ of a solute determines the degree of interaction and solubility of the solvent i and the solute j is

$${}^iR = [4(\delta_d^i - \delta_d^j)^2 + (\delta_p^i - \delta_p^j)^2 + (\delta_h^i - \delta_h^j)^2]^{1/2} \quad (14)$$

where iR is the radius of interaction of the solute sphere. When this difference in iR is less than the radius of jR alone, the probability of the solvent to dissolve the solute is high. Figure 5.3 illustrates this principle for a solvent /polymer system [10].

The Hansen parameters were extended further by Teas[8] in the development of fractional cohesion parameters. These were defined as

$$f_d = \frac{\delta_d}{(\delta_d + \delta_p + \delta_h)} \quad f_p = \frac{\delta_p}{(\delta_d + \delta_p + \delta_h)} \quad f_h = \frac{\delta_h}{(\delta_d + \delta_p + \delta_h)} \quad (15)$$

The fraction parameters defined in equation 15 are strictly an empirical relationship, but they have the advantage of spreading data points more uniformly over a triangular chart.

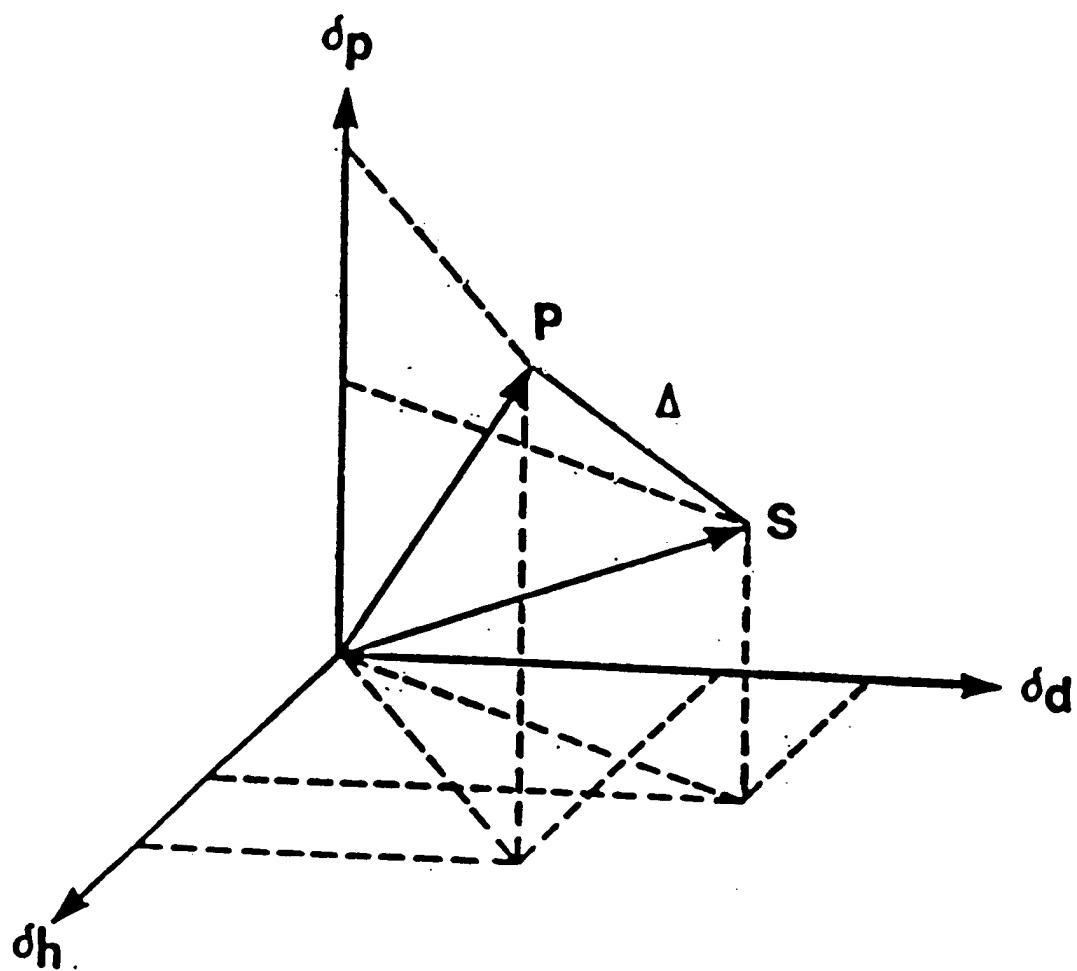


Figure 5.3 Three-Dimensional Display of Solubility Parameter for a Polymer, P, and a Solvent, S, system. [10].

Figure 5.4 illustrates the fractional parameters of a polymer system. The determination of Hansen solubility parameters has gained considerable interest in solvent extraction and polymer miscibility systems [8-10].

5.4 Regular Solution Theory

Hildebrand's regular solution theory [1] provides a basis for evaluating the excess energy terms of mixing under the conditions of constant pressure and temperature. The theory states that under constant temperature and pressure the entropy excess of mixing is vanishes and no volume change occurs. With $\Delta S_E = \Delta V_E = 0$ results in a binary mixture as

$$\Delta G_{E12} = \Delta H_{E12} = \Delta E_{E12} = \phi_1 \phi_2 (X_1 V_1 + X_2 V_2) (\delta_1 - \delta_2)^2 \quad (15)$$

the corresponding activity coefficients are

$$RT \ln \gamma_1 = V_1 \phi_2^2 (\delta_1 - \delta_2)^2 \quad (16)$$

$$RT \ln \gamma_2 = V_2 \phi_1^2 (\delta_1 - \delta_2)^2 \quad (17)$$

where ϕ_1 , X_1 , V_1 are the volume fraction, mole fraction, molar volume of each component respectively. The expression in equation 15 can be expanded to three component mixture

$$\Delta E_{E123} = (X_1 V_1 + X_2 V_2 + X_3 V_3) [\phi_1 \phi_2 (\delta_1 - \delta_2)^2 + \phi_1 \phi_3 (\delta_1 - \delta_3)^2 + \phi_2 \phi_3 (\delta_2 - \delta_3)^2] \quad (18)$$

where $\phi_1 = (X_1 V_1) / (X_1 V_1 + X_2 V_2 + X_3 V_3)$. By inspection of equation 18, it follows that excess energy should not prevent mixing if $(\delta_1 - \delta_2)$ is small or equal to zero. Insolubility occurs when $(\delta_1 - \delta_2)$ difference is considerable large for components i and j .

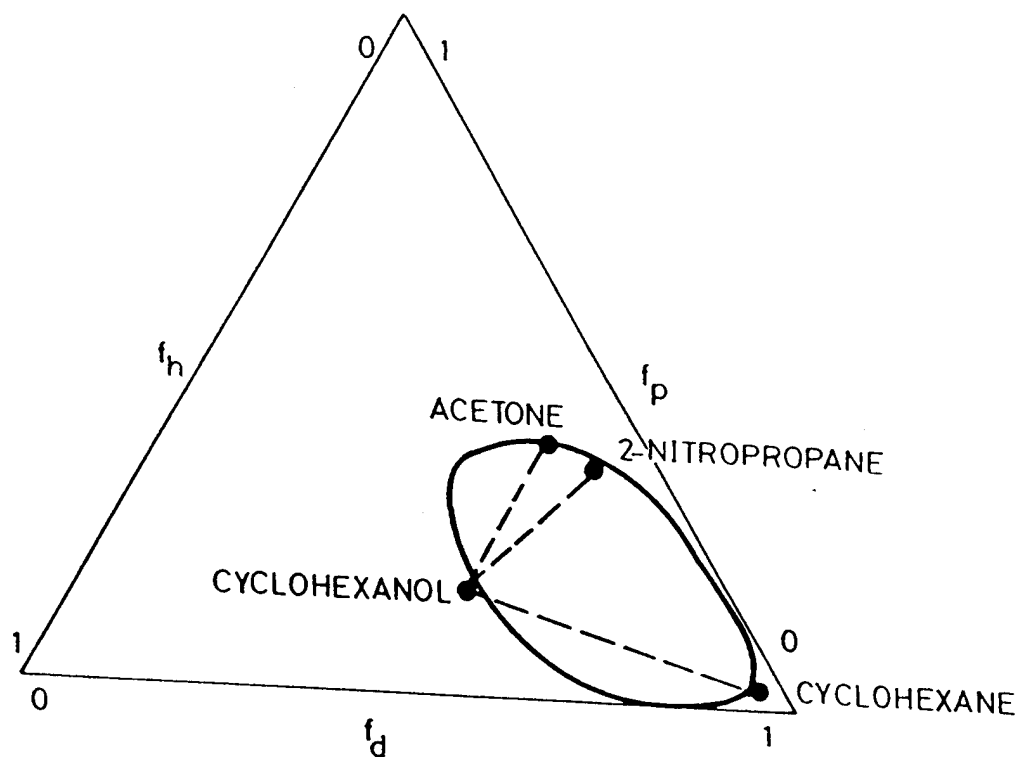


Figure 5.4 Triangular Fractional Cohesion Parameter Solubility Diagram for Parlon P10 resin (Hercules Inc.) indicating suitable mixtures of nonsolvents [8].

5.5 References

- [1] Hildebrand J.H., Scott, R.L., *Regular and Related Solutions*; Van Nostrand Reinhold Company, NY, NY 1970
- [2] Barton, A.F. M. *Handbook of Solubility Parameters and Other Cohesion Parameters*; CRC Press; Boca Raton, FL, 1983.
- [3] Barton, A.F. M. *Handbook of Polymer-Liquid Interaction Parameters and Solubility Parameters*; CRC Press; Boca Raton, FL, 1983.
- [4] CRC Handbook of Chem. and Physics; CRC Press, Boca Raton, FL, 1982
- [5] Perrys Chemical Engineering Handbook; McGraw Hill Pub., NY 1984.
- [6] Hansen, C.M. J. Paint Technol., 39, 505, 104-117, 1967
- [7] Hansen, C.M., Ind Eng Chem Prod Res Dev., 8, 1, 2-11, 1969
- [8] Teas, J.P., J. Paint Technol., 40, 516, 19, 1968
- [9] Hansen, C.M., Anderson, B.H., Am Hyg. Assoc J., 49, 6, 1988
- [10] Archer, W. L., Ind Eng Chem Prod Res., 30, 2292, 1991
- [11] Acree, W.E., Thermodynamic Properties of Nonelectrolyte Solutions, Academic Press, 1984.
- [12] Van Krevelen, D.W., Hoftyzer, P.J., Properties of Polymers: Their Estimation and Correlation with Chemical Structure, 1976.
- [13] A. Beerbower, J.R. Dickey, AM. Soc. Lubric. Eng Trans., 12, 1, 1969.
- [14] Dayantis, J. Plast. Mod. Elastomers, 29 (2), 58, 1977.

6. Article 1: Reaction Between Copper Nitrate Hydrate and
 Methoxydimethyloctylsilane in Methanol

Daniel M. Heenan, Stig E. Friberg

Center for Advanced Materials Processing, Clarkson University,

Potsdam, New York 13699-5814

Johan Sjöblom

Department of Chemistry, University of Bergen,

N-5007 Bergen, Norway

and Gregory C. Farrington

Department of Engineering, University of Pennsylvania

Philadelphia, Pennsylvania 19104-6391

Abstract

The reaction rate was determined for copper nitrate hydrate with methoxydimethyloctylsilane (MDOS) in methanol. The rate constants of hydrolysis and condensation were established by quantitative measurement of the product and Karl Fischer water determination. The reaction with the hydrated copper salt resulted in the phase separation of an insoluble product from the reaction mixture. The structure of the product was determined, by FTIR and NMR, to be a dimer of the MDOS. The results showed the alcohol producing condensation reaction was negligible in the formation of the dimer, contrary to the case for the well known reaction by trialkoxysilanes and tetraalkoxysilanes.

Introduction

The application of the sol/gel method [1] has led to extensive research efforts into the development of glasses, gels, ceramics and polymers, based on the hydrolysis of polyalkoxysilanes with water at low pH. The reactions of these polyalkoxy structures have been extensively investigated [2] using different experimental methods.

The reaction rates analyzed early on by Kay and Assink [3] used a statistical model assuming equal and independent reactivities for the polyalkoxysilane. As a consequence, consecutive hydrolysis steps assumed to linearly decrease their respective rate constants. However, the opposite trend, linearly increasing rate constants in the hydrolysis, was shown by the results of Yang [4] and Pouxvil [5]. The issue was resolved by Sanchez and McCormick [6], who showed that the consecutive hydrolysis steps were in fact less thermodynamically favorable and counteracted the increasing rate constant trend.

The reaction between hydrated metal salts and polymethoxysilanes was introduced into the sol/gel method by Sjöblom [8] utilizing the fact that a large number of hydrated metal salts are alcohol soluble. A significant number of investigations into tetraalkoxysilanes with metal hydrates have been reported [9-11] and the reaction rate constants compared to reactions with dissolved water.

We found the reaction between hydrated copper nitrate and a trialkylsilane compound to be of interest because of the more attainable differential equations resulting from the reaction rates. This method may elucidate the reaction rate of the monovalent site with that of hydrated metal salts and the results may provide a useful comparison to

similar systems with polyvalent methoxysilane rates.

Experimental

Materials

The methoxydimethyloctyl silane (MDOS 98%), methanol (Absolute 99+%), and tetramethylsilane (TMS, analytical grade) were obtained from Aldrich Chemical Company, Milwaukee, WI. Deuterated methyl alcohol (d_4 99.8% atom %D) from Isotec Inc., Miamisburg, OH was used as solvent for NMR studies. The $\text{Cu}(\text{NO}_3)_2 \cdot 2.5 \text{H}_2\text{O}$ (98.4%), Karl Fischer reagent, and pH 1 & 4 aqueous standards used were purchased from Fischer Scientific Co., Fair lawn, NJ. The water used was deionized and doubly distilled. Nitric acid, analytical grade, from J.T. Baker Chemical Co., Phillisburg, NJ was used as an acid medium to adjust the water pH to 2.5.

Preparation of Samples

Samples were mixed by dissolving the metal salt hydrate, water, and MDOS in separate solutions of 50%, 50%, and 25% respectively by weight in methanol. Mole ratios of two MDOS to one H_2O were combined and mixed for 10 seconds until one continuous phase appeared. The 50% w/w H_2O in methanol was pH adjusted with nitric acid to correspond to copper nitrate in methanol solution of pH 2.5.

As the reaction proceeded, the solutions became turbid after three hours and gradually separated into two distinct phases. Each phase was processed for FTIR and NMR spectra. Product phase was measured by weight. The separated reaction mixture was measured by BD & Co. volumetric syringe and injected into Karl Fischer vessel for

water determination over time.

Once the product phase was determined, the volume change in a 10 ml graduated cylinder was observed over time at STP. All cylinders were capped to prevent the evaporation of methanol. All samples were centrifuged for one minute prior to removal of product and reaction mixture water reading.

Determination of pH: A Pope Model 1502 pH meter, Radiation Laboratory, Copenhagen, Denmark, Model PM, used after calibration with pH one and four standard aqueous solutions.

NMR: ^{29}Si , ^1H spectra were obtained by GF AF-250 NMR equipped with data acquisition on an IBM NR. Relaxation delay was equal to zero.

FTIR: Spectra were obtained on a Mattson Galaxy 2000 Fourier Transform Infrared Spectrometer, controlled by a Packard Bell AT compatible computer, using First software from Mattson. The spectral resolution was set at 2 cm^{-1} .

Karl Fischer: Trace water determination was obtained by Fischer Model 391 K-F Titrimeter. Both phases were analyzed for water content.

Plotting: Smooth curve fit plotting of data points was generated by TableCurve software from Jandel Scientific Co.. Experimental data at each point were corrected to curve values at the corresponding time for rate constant calculations.

Results

The ^1H NMR spectra of the product and MDOS are shown in Figure 1. The spectra illustrate two features of interest. First, the product shows no characteristic

FIGURE 1

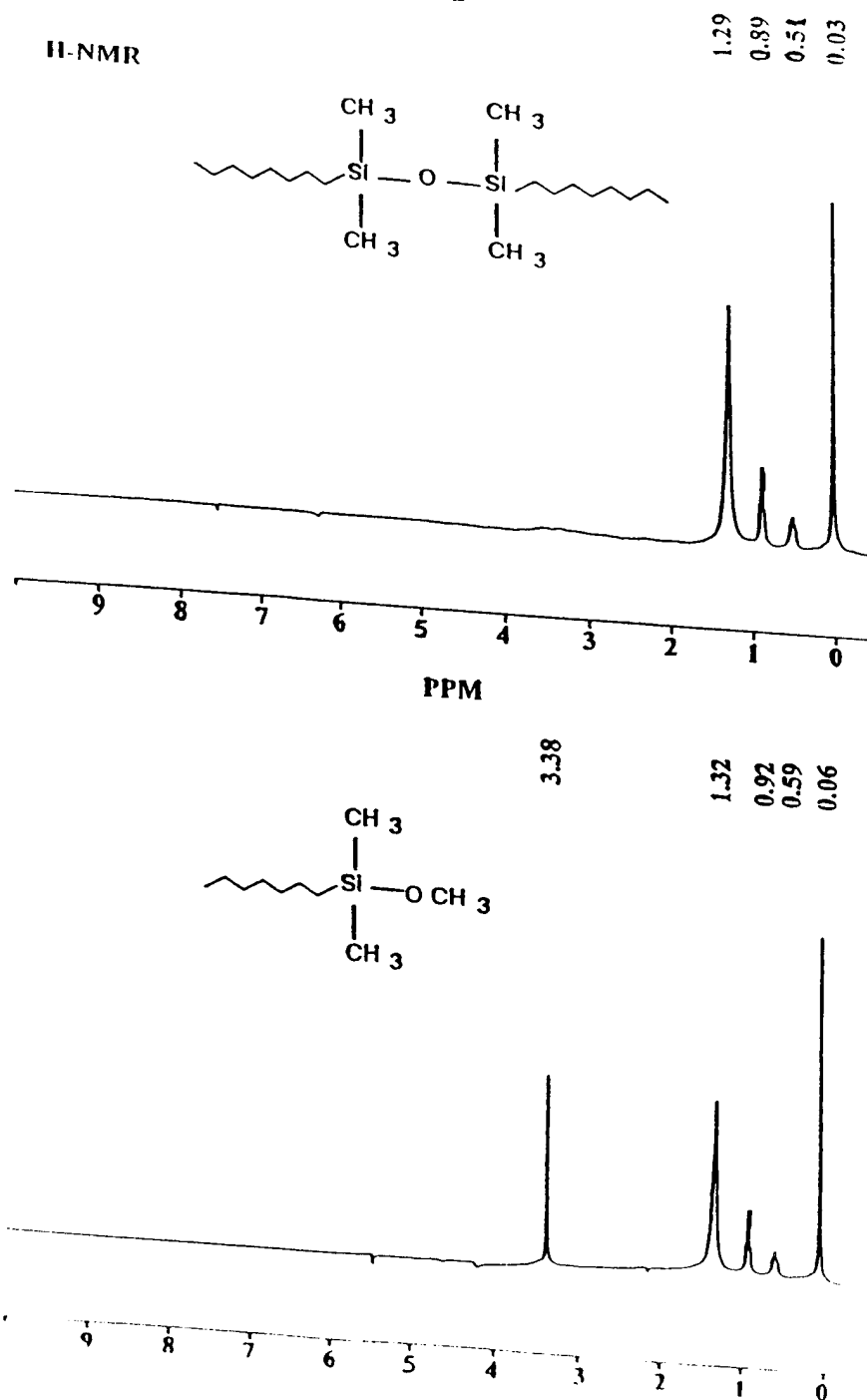


Figure 1 ¹H NMR spectra of 5/1 MDOS/Cu(NO₃)₂·2.5 H₂O mole ratio in methanol. Top: reaction product, Bottom: initial reaction mixture.

methoxy signal at 3.38 PPM as compared to MDOS. Secondly, all the chemical shifts for the product are upfield by 0.03 PPM respectively to MDOS. TMS was used as a standard reference at 0.0 PPM.

Attempts to follow the reaction by the changes in NMR signals failed in spite of deuterated methyl alcohol being used as a solvent to eliminate the methanol signals in the proton spectra. The reaction mixture of MDOS and copper nitrate hydrate resulted in extreme signal broadening for the $-OCH_3$, $-OH$, and H_2O characteristic signals, rendering a concentration-time dependence study uninterpretable.

The ^{29}Si NMR spectra, Figure 2, shows the chemical shift differences for the separated product as compared to the initial reaction mixture of 25 w/w % MDOS in methanol solution. The initial signal peak of MDOS relative to TMS was well defined at the start of the concentration-time reaction run. The final product signal was also well defined after reaction completion. However, the signal intensities of product, reactant, and any intermediates could not be distinguished once the reaction began. A partial explanation for the loss of these signals was due to the low concentration of silica species in the reaction mixture [6]. Further attempts to enhance the silica species signal in NMR experiments was the addition of 1 wt% chromium acetyl-acetonate (a paramagnetic relaxing agent) to the previously mentioned reaction mixture. Unfortunately, the signal intensities again could not be distinguished once the reaction proceeded and no useful data was obtained.

Figure 3 shows the FTIR of each separated phase of the reaction mixture after the

FIGURE 2

Si-NMR

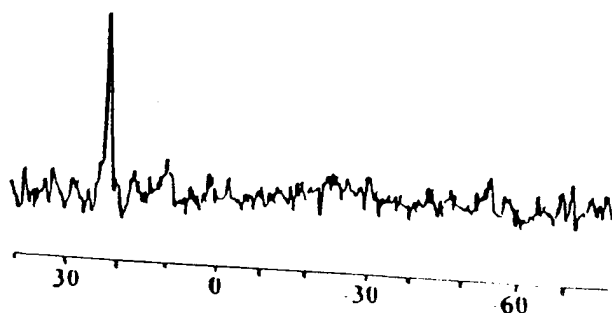
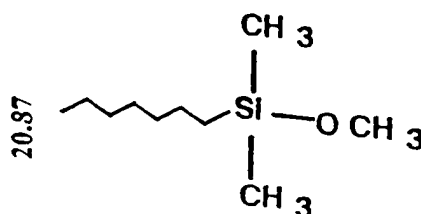
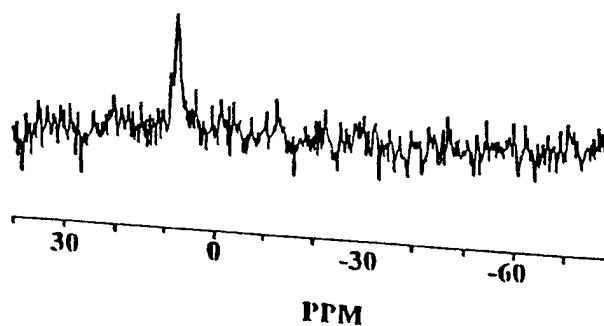
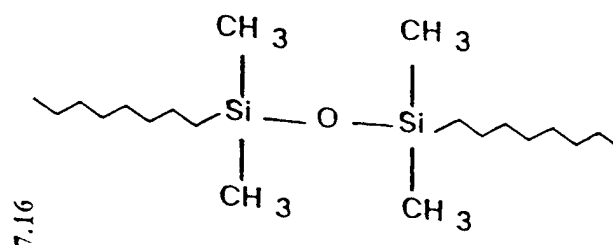


Figure 2 ^{29}Si NMR spectra of 5/1 MDOS/ $\text{Cu}(\text{NO}_3)_2 \cdot 2.5 \text{H}_2\text{O}$ mole ratio in methanol. Top: reaction product, Bottom: initial reaction mixture.

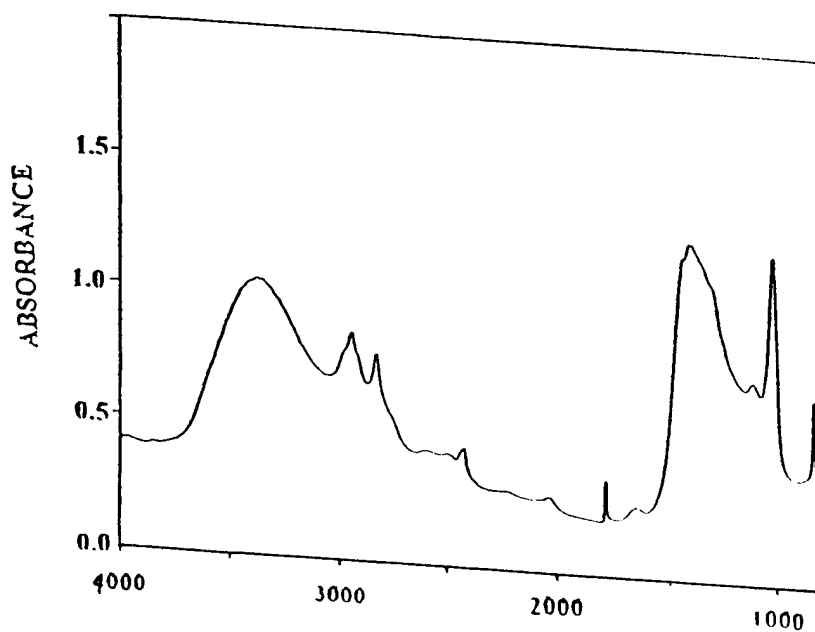
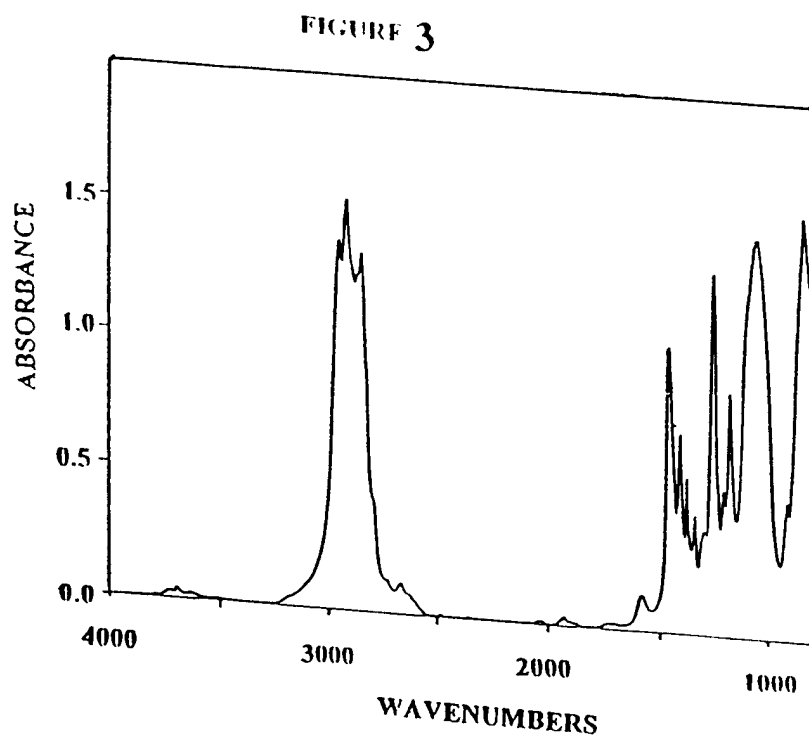


Figure 3 FTIR spectra of 5/1 MDOS/ $\text{Cu}(\text{NO}_3)_2 \cdot 2.5 \text{H}_2\text{O}$ mole ratio in methanol. Top: reaction product, Bottom: final reaction mixture.

reaction was complete. The top graph illustrates the product phase, which contains no hydroxyl group, -OH , with in the region of 3500 to 3200 cm^{-1} . The bottom graph represents the reaction mixture phase after completed reaction. Note the broad band at 3500 to 3200 cm^{-1} indicates -OH group of methyl alcohol. A very small band at 1252 cm^{-1} indicates NO_3 scissoring bend. The absence of characteristic Si bands, 1200 to 1000 cm^{-1} , associated with Si-CH_3 , Si-OCH_3 , $\text{Si-CH}_2\text{-}$, or Si-OH indicated no MDOS or reaction product to remain in the reaction solution.

The concentration-time dependence of the reaction product between $\text{Cu}(\text{NO}_3)_2$ 2.5 H_2O and MDOS is shown in Figure 4a. Figure 4b shows the concentration-time dependence of MDOS and H_2O reaction under the same conditions: temperature, pressure, pH 2.5, and MDOS: H_2O molar ratio 2:1. Both curves intersect x-axis at the turbidity point of 3.2 hours and are virtually identical.

The Karl Fischer titration of the reaction mixture gave results for the water concentration-time dependence shown in Figure 5. Neither MDOS nor the product reacted with the Karl Fischer reagent, thus rendering an accurate reading of water in the reaction mixture.

Figure 6 depicts the phase diagram of the MDOS (Q^0), methanol, and dimer (Q^1). The solubility regions of these three components illustrate several interesting characteristics. Region I represents the solubility region of the components, and region II represents the two phase region. Note the tie-lines along the two phase boundary result in complete separation to the pure Q^0 corner and its respective two component solubility.

Figure 4a

5/1 MDOS/Cu(NO₃)₂ * 2.5 H₂O molar ratio

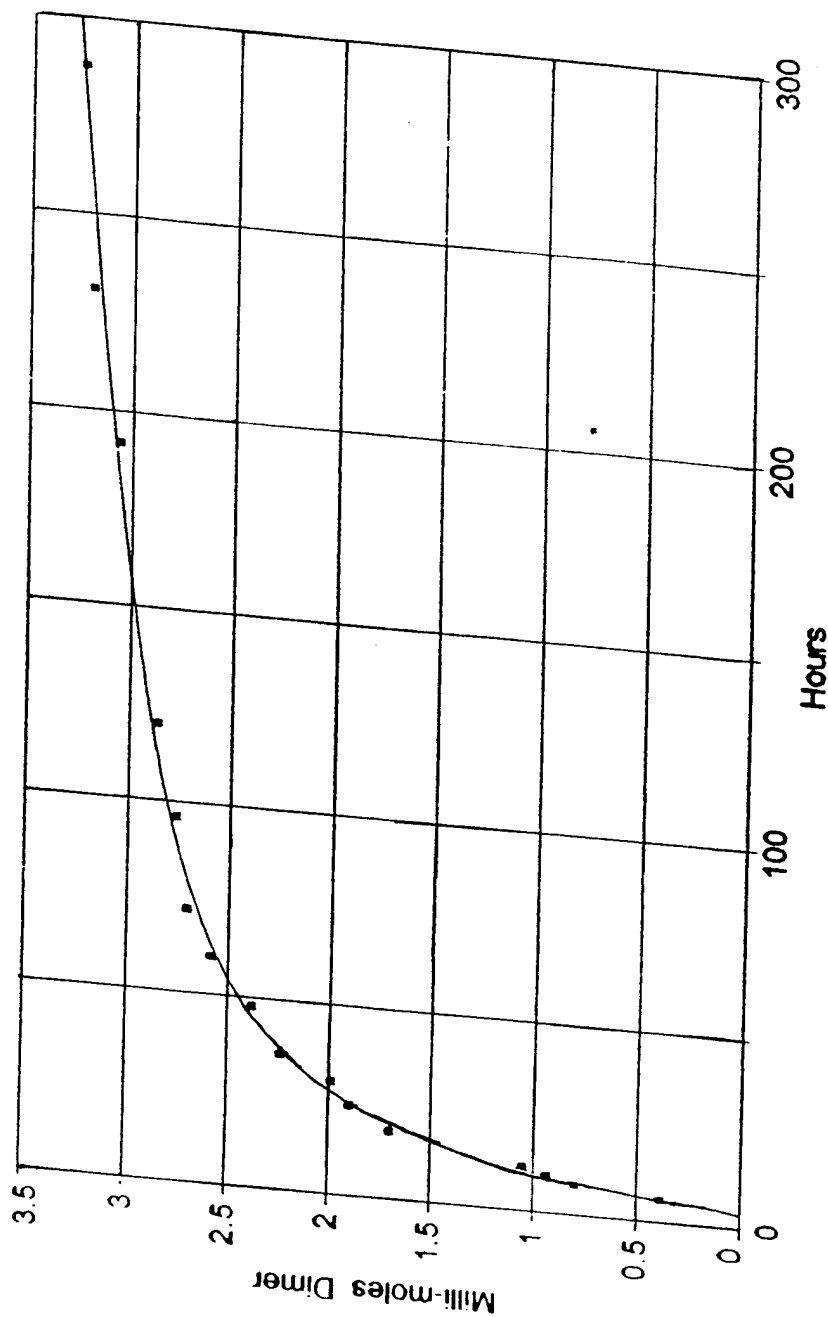


Figure 4a: Dimer Concentration versus Time for reaction 5/1 MDOS/Cu(NO₃)₂·2.5H₂O mole ratio in Methanol.

Figure 4b

2/1 MDOS/H₂O molar ratio

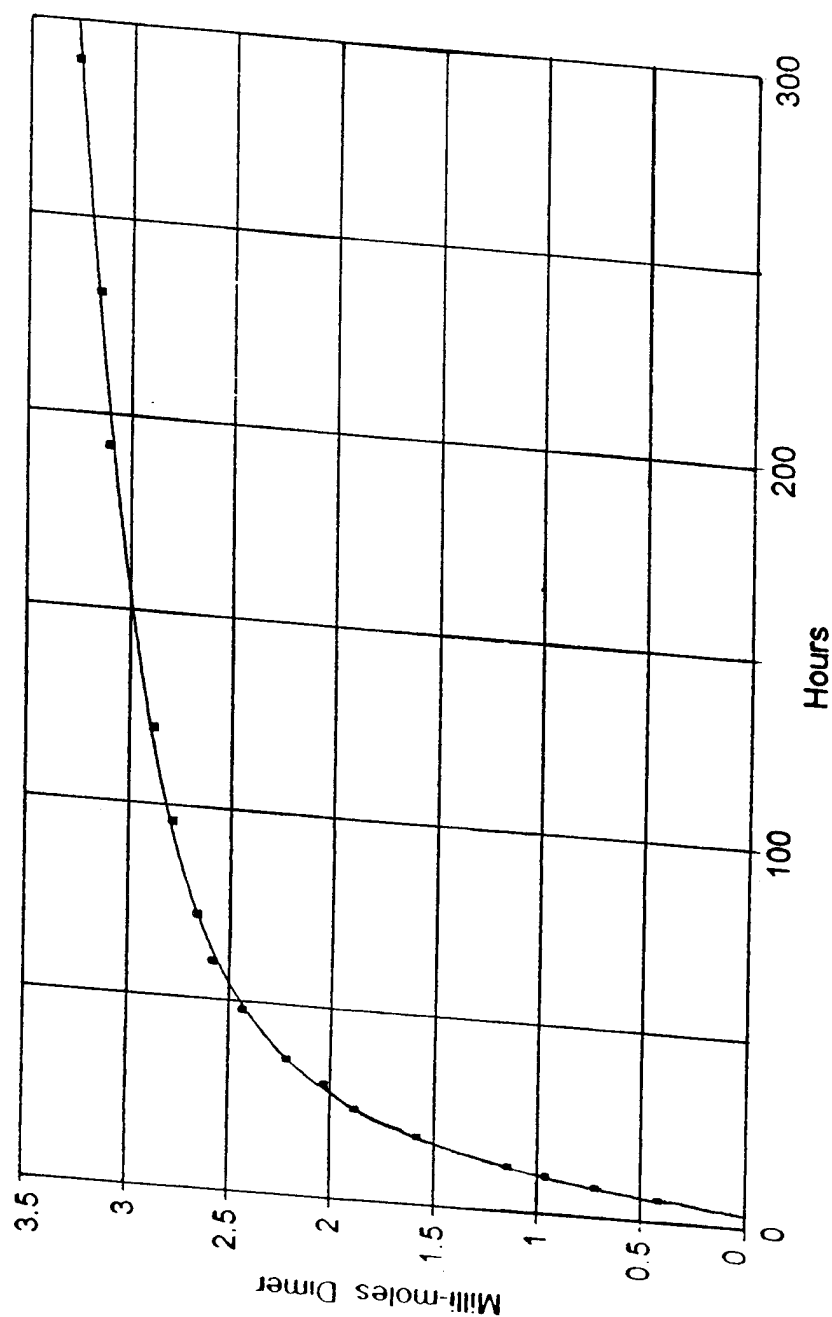


Figure 4b: Dimer Concentration versus Time for reaction 2/1 MDOS/H₂O mole ratio in Methanol.

Figure 5

5/1 MDOS/Cu(NO₃)₂ * 2.5 H₂O molar ratio

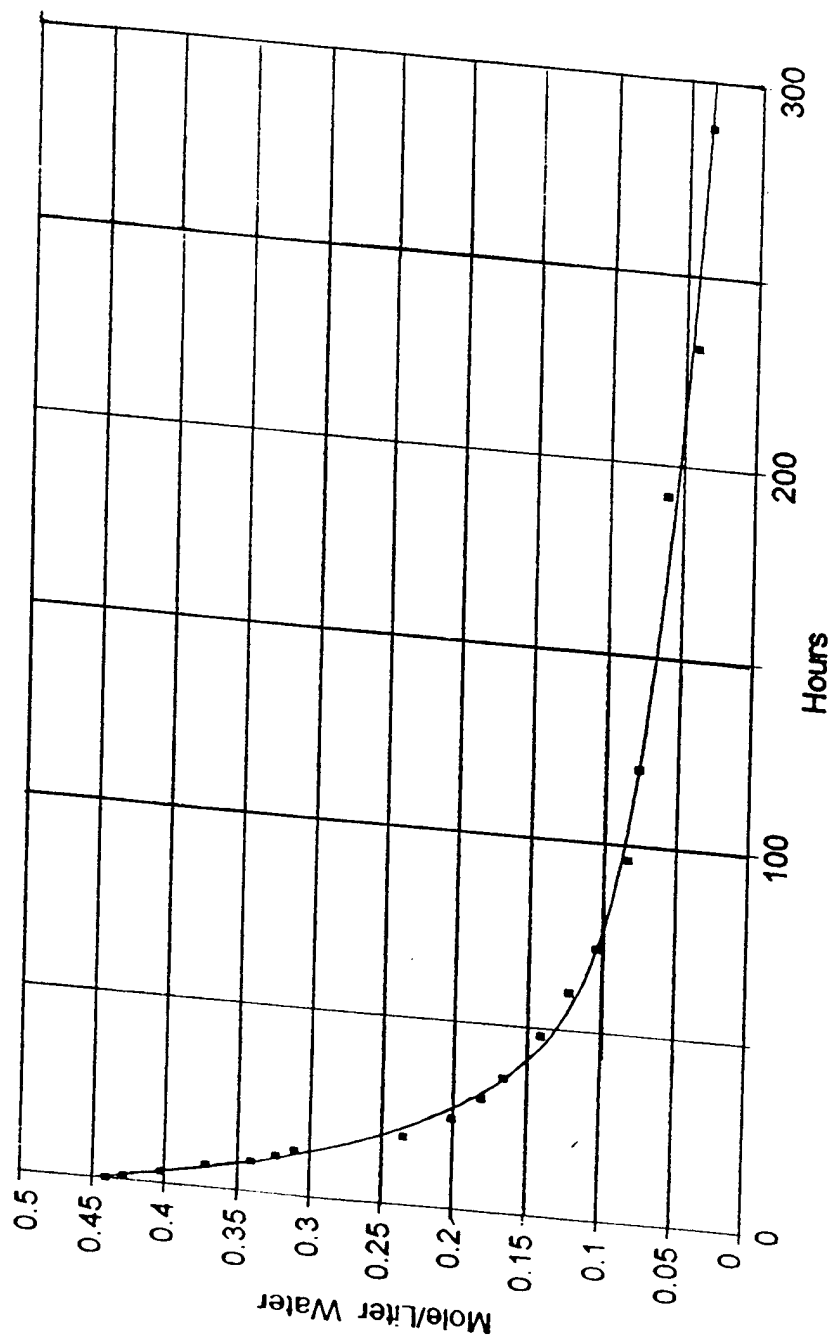


Figure 5: Water Concentration versus Time for reaction 5/1 MDOS/Cu(NO₃)₂*2.5H₂O mole ratio in Methanol determined by Karl Fischer titration.

FIGURE 6

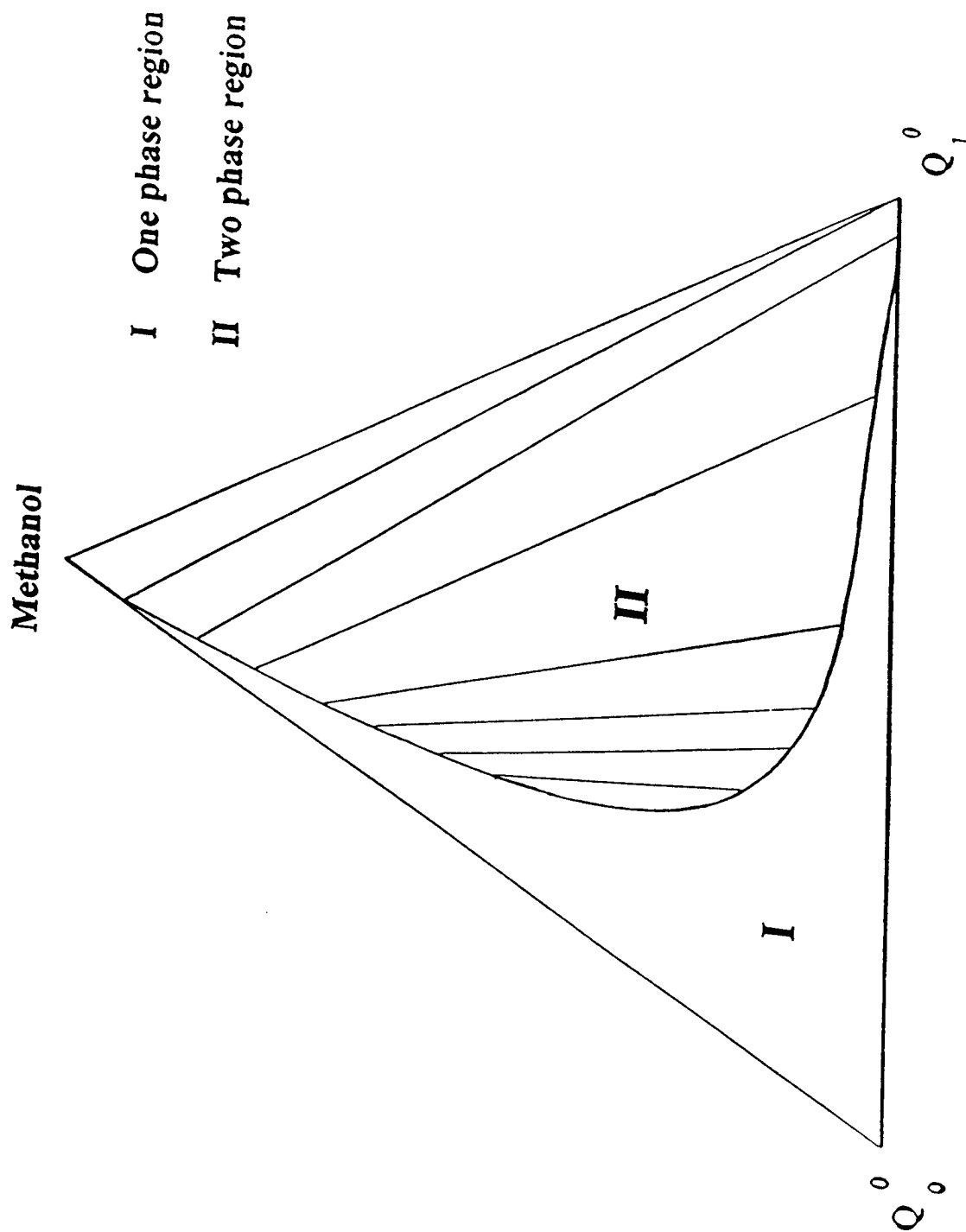


Figure 6: Phase Diagram of MDOS (Q_0^0), Methanol, Dimer(Q_0^1) w/w%.

Second, the two component line between Q^0 and methanol are completely soluble. This region is not depicted accurately in the methanol corner for MDOS concentrations below 7%. The dimer is insoluble in this region and separates out completely. This is a necessary feature for our experiment, working in the methanol corner of the phase region. Obviously, the separation of the reaction product was quantitative. A similar feature is also present in the dimer corner of the phase diagram. MDOS and the dimer are completely soluble along the two component line between them, which may not be apparent below 5% MDOS. In the dimer corner, methanol is insoluble below 5% MDOS and separates out completely.

Discussion

The results for the product and water concentrations change over time allows the balanced chemical equations for the hydrolysis, water producing and alcohol producing condensation, and overall reaction to be written as follows:

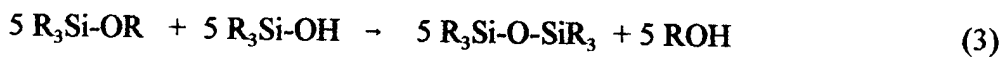
Hydrolysis



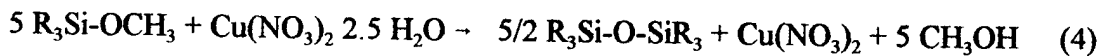
Water Condensation



Alcohol Condensation



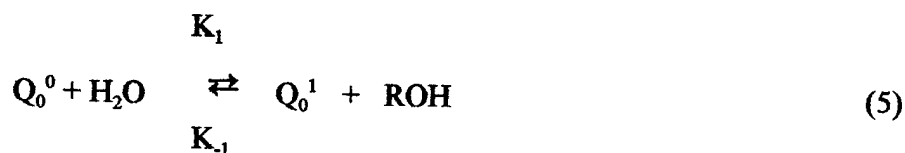
Overall Reaction



It is noteworthy to mention that with the correct stoichiometry, all the water and MDOS are reacted and removed from the reaction mixture regardless of the condensation path as noted in Equation (4).

The Q^x_y notation is utilized to simplify Equations (1-3), where the superscript x denotes the number of hydrolyzed sites and the subscript y denotes the number of condensed sites on the silicon atom. For the components of interest, MDOS is a monoalkoxy compound and therefore is restricted to one site of hydrolysis and one site of condensation. This convention reduces the amount of notation required to describe the reaction kinetics and thus clarifies the alkoxy precursor chemistry involved. Equations (1-3) now can be annotated to express the rate constants as follows:

Hydrolysis



Water Condensation



Alcohol Condensation



The initial step is the hydrolysis of MDOS with water of the hydrated copper salt by Equation (1). From the literature it has been observed that K_{-1} is one order of

magnitude smaller than K_1 [6]. This allows the neglect of the reverse reaction term for Equation (5). Initially $[Q_0^1] = [Q_1^0] = 0$ while $[Q_0^0]$ and $[H_2O]$ have fixed values. After three hours the reaction mixture became visibly turbid because more than trace amounts of dimer had formed. The dimer separated in accordance with the phase diagram in Figure 6. The fact that the dimer is not soluble means that the reverse reactions in Equations (2) and (3) do not proceed.

Accepting that for < 3 hours only hydrolysis occurs, the rate dependence governing the reaction can be written from Equation (5) as:

$$d[Q_0^0]/dt = d[H_2O]/dt = -K_1[Q_0^0][H_2O] \quad (8)$$

The continued treatment is based on the final reaction product, which is in its liquid standard state and, hence, the equilibrium reaction in Equation (4) is driven to the right as the product is removed from the reaction mixture. This ensures that all the MDOS and water react in solution and also allows us to establish the maximum yield of product from the initial concentration of the reactants.

The slope of the first 6 points of Figure 5 are linear, and are represented by a straight line from zero hours to 4.5 hours. The slope of this straight line section of the plot was used to calculate K_1 from initial concentrations of MDOS and water utilizing Equation (8) and Figure 5:

$$K_1 = 0.0305 \pm 0.0001 \text{ l mol}^{-1} \text{ hr}^{-1}$$

This value was compared to reaction constants obtained by Selle [16] for metal salt hydrates and McCormick [6] for the first hydrolysis rate of polyalkoxysilanes. As the

silicon concentration increased for TEOS/H₂O mole ratios of 1/4, 1/3, 1/2, their hydrolysis rate constants showed a decrease from 0.10, 0.08, 0.09 (L mol⁻¹ hr⁻¹) respectively for the reaction with water and similar valuations for the metal salt hydrate from McCormick [6] data. The present value is approximately 1/3 of the value of tetraethoxysilane, a reasonable value considering only one methoxy group being present instead of four.

However, a more recent ²⁹Si NMR study monitored at 15°C by McCormick [15], K₁ was calculated as 0.0233 (L mol⁻¹ hr⁻¹) for 1/5 TEOS/Water ratio and demonstrates a good approximation to our hydrolysis rate. This system utilized a sophisticated kinetics model and a supercomputer to calculate the integrated rate equations of over 15 possible reactions. These trends demonstrate the influence of subsequent alkoxy groups on the silicon site.

The treatment of condensation reaction requires a more complex examination. From Equation (6) and (7), we can express the rate dependence of the water producing and alcohol producing condensation of the dimer as:

$$d[Q_1^0]/dt = K_2[Q_0^1]^2 + K_3[Q_0^0][Q_0^1] \quad (9)$$

Equation (9) provides a basis to evaluate the relative contribution of each condensation step annotated in Equation (6) and (7). If $K_2 \gg K_3$, then the rate dependence of condensation will be proportional to $K_2[Q_0^1]^2$. If $K_3 \gg K_2$, then the rate dependence of condensation will be proportional to $K_3[Q_0^0][Q_0^1]$. When $K_2 \simeq K_3$, then the rate dependence can be expressed as annotated in Equation (9).

At > 3 hours condensation contributes to [H₂O] from Equation (5) and (7):

$$d[H_2O]/dt = -K_1[Q_0^0][H_2O] + K_2[Q_0^1]^2 \quad (10)$$

Equation (10) shows the concentration-time dependence of the water in the reaction mixture. The water producing condensation term in Equation (10) provides a useful tool to evaluate the previously mentioned analogy for the relative contributions of both condensation steps in the dimer formation.

The water which remains in solution, by Equation (5), after the hydrolysis step as a function of time is defined as:

$$[W1] = [W]_0 - [W]_H \quad (11)$$

where, $[W1]$ is the water content after hydrolysis, $[W]_0$ is the initial water in the reaction mixture, and $[W]_H$ is the water consumed in the hydrolysis or $K_1 \cdot t$. Equation (11) establishes the decrease in water content over time due to hydrolysis.

It follows that the difference in the measured water, $[W]_{KF}$, to that of the water consumed in hydrolysis, $[W1]$:

$$[W2] = [W]_{KF} - [W1] \quad (12)$$

should provide a reasonable correlation to the water producing condensation step in Equation (6). Figure 7 shows the plot of concentration versus time of $[W1]$, $[W2]$, $[W]_{KF}$, and dimer for the first 24 hours of the reaction. The plot shows that the $[W2]$ is nearly equal to that of the dimer concentration, thus the contribution of alcohol producing condensation is negligible in Equation (9).

Figure 7 allows the determination of the initial condensation rate. The $W2$ curve provides additional plotting points within a linear range of 0 to 18 hours. The first

Figure 7

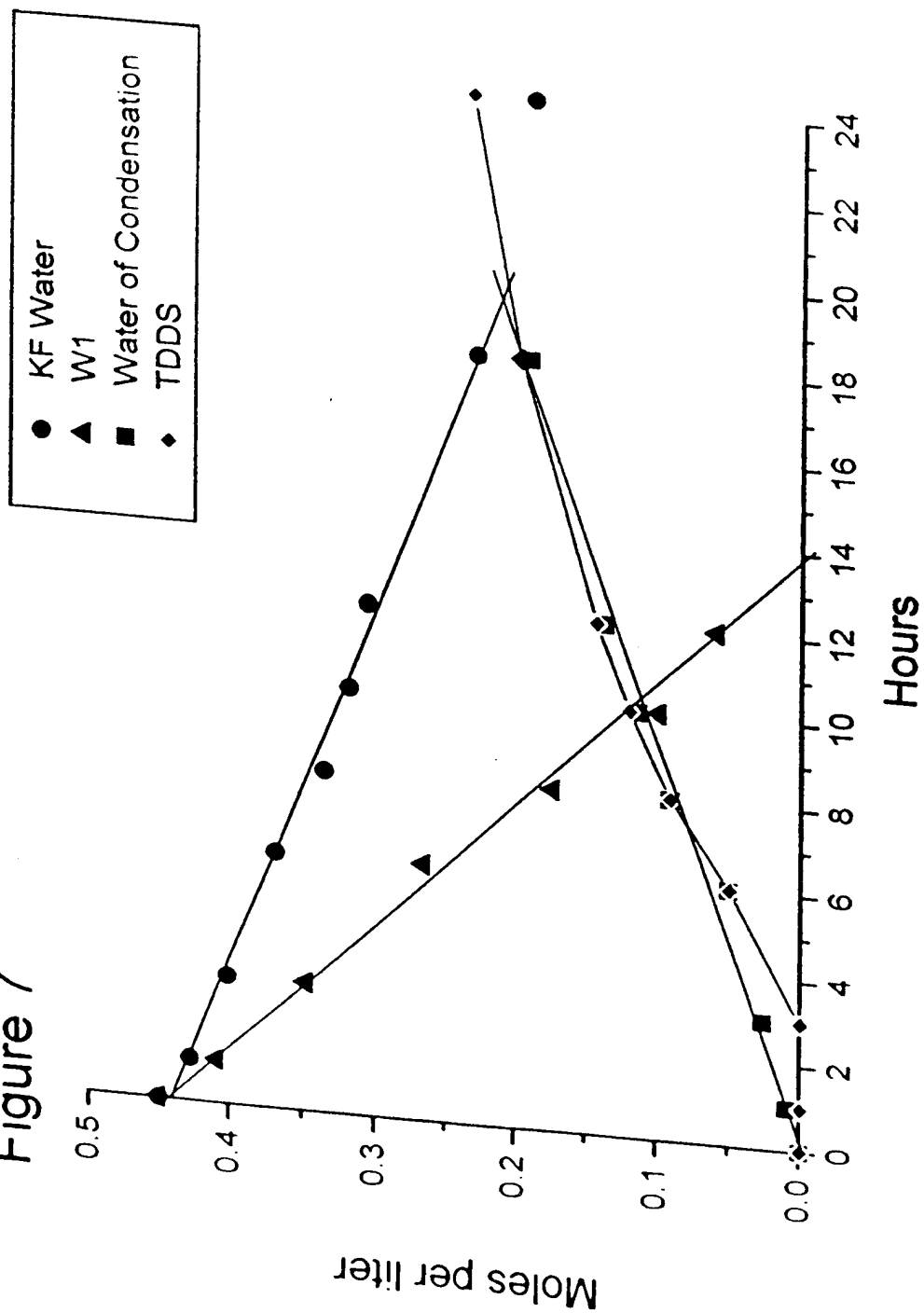


Figure 7: Concentration versus Time for Components: W1, W2, WKF, Dimer within first 24 Hours of reaction.

quantitative measurements of the dimer, in Figure 4, were restricted to the accurate extraction of the product from the reaction mixture. With the evidence presented from Figure 7, the dimer formation is proportionately equal to the W2 curve. This observation concurs with the turbidity point at 3.2 hours. Thus, the slope of the W2 curve can now be taken as the first derivative of the dimer content function. The concentration-time dependence of the dimer in Equation (9) reduces to:

$$d[Q_1^0]/dt = K_2[Q_0^1]^2 \quad (13)$$

Equation (13) dramatically simplifies the determination of the initial condensation rate constant. This equation allows the calculation of $[Q_0^0]$ from the available data of $[H_2O]$ and $[Q_1^0]$ and their respective derivatives.

The dependence of $[Q_0^0]$ is now only influenced by the hydrolysis as expressed from Equation (5) and (8). Likewise, the dependence of $[Q_0^1]$ is expressed from Equations (5) and (6):

$$[Q_0^1]_t = [Q_0^0]_0 - [Q_0^0]_t - 2[Q_1^0]_t \quad (14)$$

Figure 8 converts the data curve of Figure 4 from milli-moles to moles per liter of the reaction vehicle and shows the calculated values for $[Q_0^0]$ and $[Q_0^1]$ as a function of time from Equations (8) and (14) respectively.

All the necessary information to utilize Equation (13) and calculate K_2 is now available:

$$K_2 = \{d[Q_1^0]/dt\} / [Q_0^1]^2 \quad (15)$$

The calculated $K_2 = 0.0075 + 0.0005 \text{ L mol}^{-1} \text{ hr}^{-1}$, is valid for the initial condensation rate

Figure 8

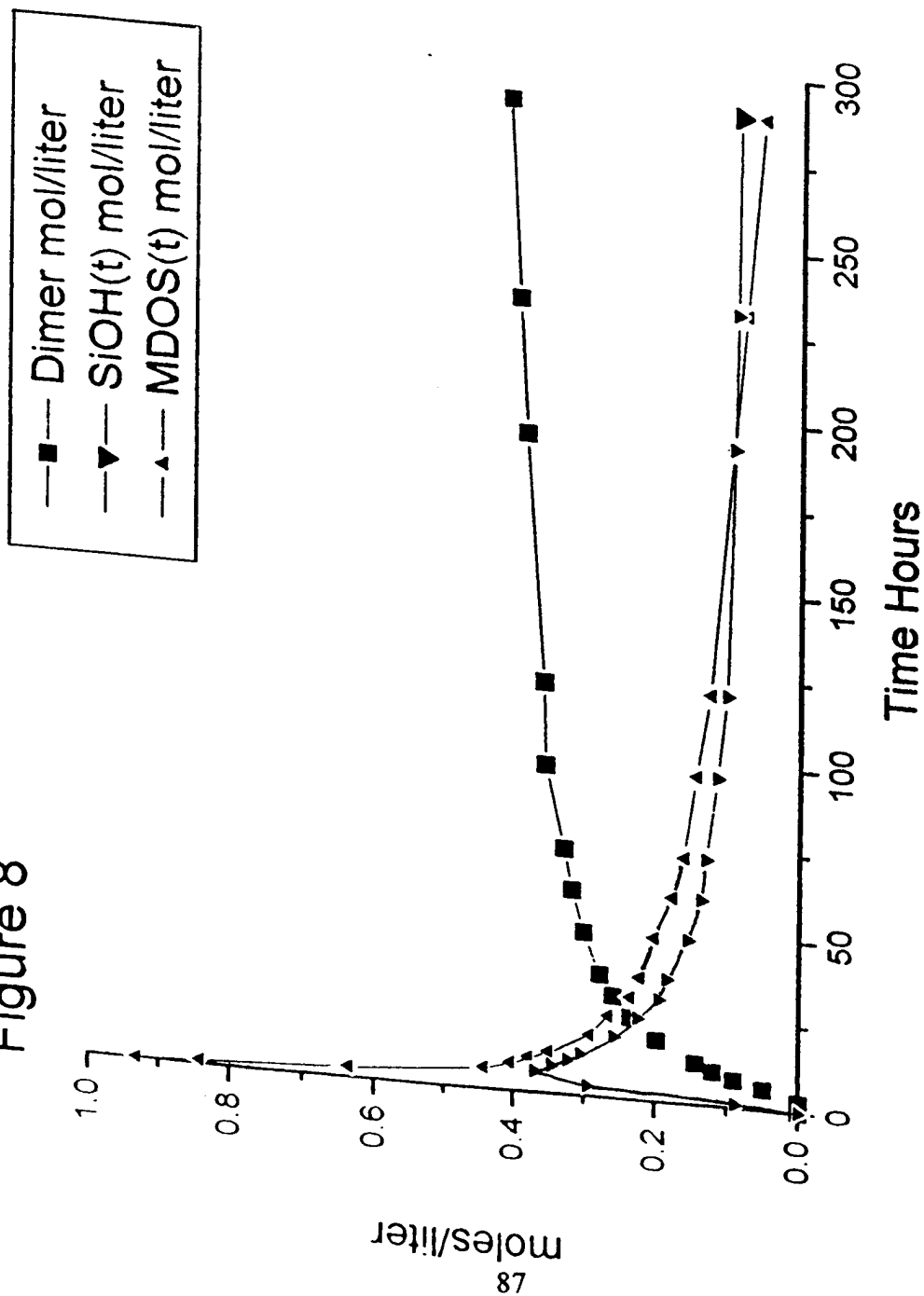


Figure 8: Si Concentration versus Time.

where the time is less than 24 hours. For times greater than 24 hours, the assumptions and evidence presented thus far may not be valid.

This water producing condensation rate constant is comparable to McCormick [15] reported rate constant of $0.00488 \text{ L mol}^{-1} \text{ hr}^{-1}$ for the condensation of two completely hydrolyzed species, $Q_0^4 + Q_0^4 \rightarrow Q_1^3 + Q_1^3$.

This conclusion implies that the established reaction kinetics for the tetraalkoxysilanes is valid for the trialkylmethoxysilane under investigation. Such a result is not unrealistic regardless of the difference in structure between partially hydrolyzed tetraethoxysilanes and trialkylhydroxysilane would be expected to cause a distinction of their reactivity. The strongly hydrophobic trialkylhydroxy compound is expected to be distinctly amphiphilic. For a normal acid catalyzed condensation to take place, the proton must activate the $R(\text{CH}_3)_2\text{SiOH}$ to $R(\text{CH}_3)_2\text{SiOH}_2^+$ after which the activated complex will condense with the iso-protonated hydroxysilane to form a dimer at low pH [17].

Conclusions

Significance of reaction with copper nitrate: when all H_2O is consumed in the reaction of 5/1 MDOS/ $\text{Cu}(\text{NO}_3)_2 \cdot 2.5 \text{ H}_2\text{O}$, an anhydrous solution of copper nitrate in methanol solution was obtained. The product dimer was insoluble in the continuous phase and thus separated out. The analysis of the reaction kinetics suggest that the alcohol producing condensation does not take place under these conditions.

Acknowledgment

This research was supported in part by the New York State Commission of Science and Technology at the Center for Advanced Materials Processing at Clarkson University, Potsdam, NY and the Department of the Army, United States Military Academy, West Point, NY.

References

- [1] "Sol-Gel Technology" (L.C Kleya, ed.) Noyes Publications, NJ 1988.
- [2] C.J. Brinker, G.W. Scherer "Sol Gel Science" Academic Press, NY 1990.
- [3] B.D. Kay, R.A. Assink, Mater. Res. Symp. Proc. 1988, 107, 35.
- [4] H Yang, Z Ding, Z Jiang, X Xu, J. Non-Cryst. Solids, 1988, 112, 449.
- [5] J. C. Pouxvil, J.P. Boilot, J. Non-Cryst. Solids, 1987, 94, 374.
- [6] J. Sanchez, A McCormick, J. Phys. Chem, 1992, 96, 8673.
- [7] S.E. Friberg, Z. Ma, J. Non-Cryst. Solids, 1992, 147, 30.
- [8] J. Sjöblom, T. Skodvin, M.H. Selle, S.E. Friberg, J. Phys. Chem, 1992, 96, 21.
- [9] B. Gestblom, J. Sjöblom, Chem Phys. Lett. 1985, 122, 553.
- [10] S.E. Friberg, Jun Yang, Ali Amran, J. Sjöblom, J. Phys. Chem, 1994, 98, 13528.
- [11] Ali Amran, S.E. Friberg, J. Sjöblom, J. Disp. Sci. Techn., 1994, 15, 621.
- [12] S.E. Friberg, C.C. Yang, "Silica Glass from W/O Microemulsions", Innovations in Material Processing Using Aqueous, Colloid and Surface Chemistry, Edited by F.M. Doyle, S. Raghaven, P. Somasundra and G.W. Warren, The Minerals, Metals & Materials Society, 1988.
- [13] M. Biscoglia, C. Brancewicz, S.E. Friberg, Ali Amran (in press)
- [14] J. Sjöblom, S.E. Friberg, Ali Amran, J. Disp. Sci. Techn., 1995, 16, 31.
- [15] J. Sanchez, A McCormick, J. Phys. Chem, 1993 (in press)
- [16] M. Selle, F. Fredricksen, J. Sjöblom, A. Christy, S.E. Friberg, Acta Chem. Scand. 1996, 50, 12
- [17] E. R. Pohl, F.D. Ostertraltz in "Molecular Characterization of Composite Interfaces" H. Ishidu and G. Kumer Eds Plenum Press, NY 1985 p.157.

7. Article 2: Phase Equilibria of Methoxydimethyloctylsilane,
Tetramethyldioctyldisiloxane in Organic Solvents

Daniel M. Heenan, Stig E. Friberg

Center for Advanced Materials Processing, Clarkson University,

Potsdam, New York 13699-5814

Johan Sjöblom

Department of Chemistry, University of Bergen,

N-5007 Bergen, Norway

Abstract

The phase diagrams and partial solubility parameters for methoxydimethyloctyl silane (MDOS), tetramethyldioctyldisiloxane (TDDS), and several organic components were determined. The solubility limits were established by quantitative analysis and compared to the refractive index of known single phase mixtures. The partial solubility parameters were used to provide a qualitative analysis of the phase equilibria. The results showed the phase equilibria depended on the polarity and hydrogen bonding characteristics of the solvents. The solubility of TDDS was reduced with increasing polarity/hydrogen bond character of the amphiphiles solvents.

Introduction

The interest in the sol/gel method has led to extensive research efforts for applications [1] and fundamental understanding of the reactions [2]. The reaction rates

for tetraalkoxysilanes have been described using different methods [3-5] as well as the subsequent steps in the process [6-12].

The mechanism and kinetics of polyalkoxysilanes requires an in-depth knowledge of the reaction media. The fundamental analysis of the structures and relationships [1,2] in this area have been expanded to include polymer/surfactant combinations, microemulsions, emulsions [13, 14], and liquid crystals [15, 16]. However, the predominate literature sources pertain to complex tetraalkoxysilanes reactions, their relationship between gelation and their phase equilibria in simple three component systems [17-20].

A knowledge of the solubilization limit of a monomer silane unit in an emulsion/microemulsion polymerization system is of considerable importance in interpreting the polymerization kinetics. The rate of polymerization is expected to depend on whether most of the monomer is in monomer-swollen micelles or in emulsion droplets. However, these efforts have been concerned with three component systems of tetraalkoxysilanes, water and alcohols [20]; interest in monovalent methoxysilanes has attracted little attention.

In a previous investigation, the analysis of MDOS, TDDS and methanol phase diagram was previously reported by Heenan *et al.* [21] on the sol-gel kinetics study of a monomethoxysilane compound. The phase separation was shown to be quantitative; hence, further investigation into the phase equilibria of similar systems is warranted. In this paper we report the solubility in a system of TDDS, MDOS with various organic solvents.

Solubility Parameter Theory

Hildebrand [24] was first to propose a fundamental thermodynamic relationship for component solubility in mixtures to the molar internal "cohesive" energy of individual components. The cohesive energy, ΔE , of a liquid is the energy required to separate its molecules into an infinitely dilute vapor at constant temperature. The theory considers the events in a mixing process: the molecules of each component in a mixture are separated by an infinite distance, comparable in many respects to the phase transition of a liquid to a gas in the vaporization process. Although ΔE is temperature dependent, at pressures below atmospheric pressure and temperatures below the normal boiling point of the liquid, the cohesive energy is routinely calculated from the molar heat of vaporization ΔH_{vap} as

$$\Delta E = \Delta H_{\text{vap}} - RT \quad (1)$$

where R is the gas constant, T is kelvin temperature and the term RT accounts for the volume work done during the isothermal expansion. Equation (1) is a good approximation when the saturated vapor is considered an ideal gas under low pressure. However this is not a valid argument when a component approaches the critical point, ΔH_{vap} becomes zero, leading to negative values in Equation (1) for the cohesive energy.

The cohesive energy density (CED) is defined as the ratio of the internal energy per molar volume $\Delta E/V_M$. By definition, the solubility parameter is the square root of the CED value

$$\delta = (\text{CED})^{1/2} = [\Delta E/V_M]^{1/2} = [(\Delta H_{\text{vap}} - RT)/V_M]^{1/2} \quad (2)$$

The δ values have the unit SI dimensions of $\text{MPa}^{1/2}$. Molar volume and enthalpy information is easily obtained in standard references [25-28]. However, for many materials, especially polymers, solids and surfaces it is necessary to use indirect empirical relationships to estimate the cohesion parameters. The group contribution theory is one such method which uses the chemical structure of a material to estimate the cohesion parameters according to Barton [25, 26].

The Hildebrand solubility parameter is often referred to as the "total" cohesion parameter, δ_t , due to the variety of "partial" cohesion parameters developed by other researchers. In a pioneering effort to characterize the total cohesion parameter into partial contributing terms, Hansen proposed an extension of the Hildebrand parameter to include polar and hydrogen bonding systems [29, 30]. The total cohesion parameter, δ_t , is a function of dispersion δ_d , polar δ_p , and hydrogen bonding δ_h partial parameters. The three partial parameters are related to the total cohesion parameter by

$$\delta_t^2 = \delta_d^2 + \delta_p^2 + \delta_h^2 \quad (3)$$

The Hansen total cohesion parameter, δ_t , corresponds to the Hildebrand parameter, although the two quantities are determined by different methods and should not be expected to be identical. The advantage of the partial parameters over the Hildebrand parameter for practical formulation efforts seems self-evident. The Hansen partial cohesion parameters for a material can be represented as a vector in three dimensional space. This feature allows both visual and numerical comparisons in the relative strength of each partial parameter coordinate.

The most exact determination of solubility behavior is in a series of solvent mixtures with varying degrees of hydrogen bonding ability and polarity. The distance of solvent coordinates $(\delta_d^i, \delta_p^i, \delta_h^i)$ from the center point $(\delta_d^j, \delta_p^j, \delta_h^j)$ of a solute determines the degree of interaction and solubility of the solvent i and the solute j is

$${}^jR = [4(\delta_d^i - \delta_d^j)^2 + (\delta_p^i - \delta_p^j)^2 + (\delta_h^i - \delta_h^j)^2]^{1/2} \quad (4)$$

where jR is the radius of interaction of the solute sphere. When this difference in jR is less than the radius of jR alone, the probability of the solvent to dissolve the solute is high.

The Hansen parameters were extended further by Teas [31] in the development of fractional cohesion parameters. These were defined as

$$f_d = \frac{\delta_d}{(\delta_d + \delta_p + \delta_h)} \quad f_p = \frac{\delta_p}{(\delta_d + \delta_p + \delta_h)} \quad f_h = \frac{\delta_h}{(\delta_d + \delta_p + \delta_h)} \quad (5)$$

The fraction parameters defined in Equation (5) are strictly an empirical relationship, but they have the advantage of spreading data points more uniformly over a triangular chart.

The determination of Hansen solubility parameters has gained considerable interest in solvent extraction and polymer miscibility systems [32,33].

Thermodynamic treatment

For mixing to be possible, the molar Gibbs free energy of mixing at constant pressure must be negative:

$$\Delta G_m = \Delta H_m - T\Delta S_m \leq 0 \quad (6)$$

The entropy change of a mixing process is usually positive, therefore it is necessary to evaluate the enthalpy term in Equation (6). When ΔH_m is negative, or positive and less

than $T\Delta S_m$, mixing can occur. The aim of cohesion parameters are to predict the magnitude of this enthalpy term. Spontaneous "unmixing" or phase separation may occur if the temperature of a mixture is decreased. This is due primarily to the temperature dependence of the entropy term; however, meta-stable homogeneous systems may also occur under these conditions.

For an ideal mixture there is no volume change during the formation, $\Delta V_m = 0$, no enthalpy change at constant pressure, $\Delta H_m = 0$, and an entropy change equal to that of an ideal gas mixture as a result in the extra degrees of freedom created by the mixing. The entropy change is

$$\Delta S_m = -R \sum_i X_i \ln X_i \quad (7)$$

where X_i is the mole fraction of component i .

The resulting molar Gibbs free energy change in the formation of an ideal mixture is therefore provided by the entropy increase of each component. Substitution of Equation (7) into Equation (6) yields

$$\Delta G_m = \Delta H_m - T\Delta S_m = RT \sum_i X_i \ln X_i \quad (8)$$

where the components forming an ideal mixture are completely miscible in all proportions.

In non-ideal systems, the Gibbs free energy change is not equal to the ideal value, and the excess Gibbs free energy change on mixing is

$$\Delta G_E = \Delta G_m - RT \sum_i X_i \ln X_i \quad (9)$$

Similarly the excess entropy of mixing is defined as

$$\Delta S_E = \Delta S_m + R \sum_i X_i \ln X_i \quad (10)$$

Hildebrand's regular solution theory [24] provides a basis for evaluating the excess energy terms of mixing under the conditions of constant pressure and temperature. The theory states that under constant temperature and pressure, the entropy excess of mixing vanishes and no volume change occurs. With $\Delta S_E = \Delta V_E = 0$ results in a binary mixture as

$$\Delta G_{E12} = \Delta H_{E12} = \Delta E_{E12} = \phi_1 \phi_2 (X_1 V_1 + X_2 V_2) (\delta_1 - \delta_2)^2 \quad (11)$$

where ϕ_1, X_1, V_1 are the volume fraction, mole fraction, molar volume of each component respectively. The expression in Equation (11) can be expanded to three component mixture

$$\begin{aligned} \Delta E_{E123} = & (X_1 V_1 + X_2 V_2 + X_3 V_3) [\phi_1 \phi_2 (\delta_1 - \delta_2)^2 + \phi_1 \phi_3 (\delta_1 - \delta_3)^2 \\ & + \phi_2 \phi_3 (\delta_2 - \delta_3)^2] \end{aligned} \quad (12)$$

By inspection of Equation (12), it follows that excess energy will not prevent mixing if $(\delta_1 - \delta_2)$ is small or equal to zero. Insolubility occurs when $(\delta_i - \delta_j)$ difference is considerably large for components i and j .

Experimental

Materials

The following chemicals were used as received: chloroform (JT Baker, 99+%), methanol (Fisher, certified), acetone (Fisher, certified), ethanol (Pharmco, absolute), ethylene glycol (JT Baker, 99+%), 1-propanol (Aldrich, 99+%), 1,2 propane diol (Aldrich, 99+%), 1,3 propane diol (Aldrich, 99+%), Brij 30 (ICI Surfactants), synperonic A-9 {SA9, non ionic surfactant $C_{13/15}EO_9$ } (ICI Surfactants), methoxydimethyloctylsilane (Aldrich, 98%), and water (doubly distilled).

The tetramethyldioctyldisiloxane was prepared by reacting a one to one mole ratio of methoxydimethyloctylsilane with water (pH 2.0, adjusted with HNO_3) in 75% w/w methanol. The TDDS is insoluble at high concentrations of methanol and easily separates out after 48 hours. The TDDS was washed in absolute methanol, separated, and placed in 60°C oven for two hours to evaporate any trace volatile components.

Phase Diagrams

The one and two phase regions of MDOS, TDDS, and solvent were established by titration. The composition of two components were fixed as the third component was added to the mixture. Combinations with the third component were added until a transparent system was visually observed.

The tie lines for the two phase regions were determined with Bausch & Lomb model ABBE-3L refractometer. A series of samples with different ratios of the three components in the one phase region were prepared close to the demixing line and measured for refractive index. Samples in the two phase region were allowed to separate and centrifuged at 5000 rpm for one minute. The two separated phases were then measured for refractive index and compared to those of known refractive index near the demixing line.

Results

The phase diagrams are presented in increasing order of carbon chain length and polarity. Figure 1 shows the solubility of MDOS - TDDS and chloroform. All three components are completely soluble in each other and a single phase isotropic solution is

FIGURE 1

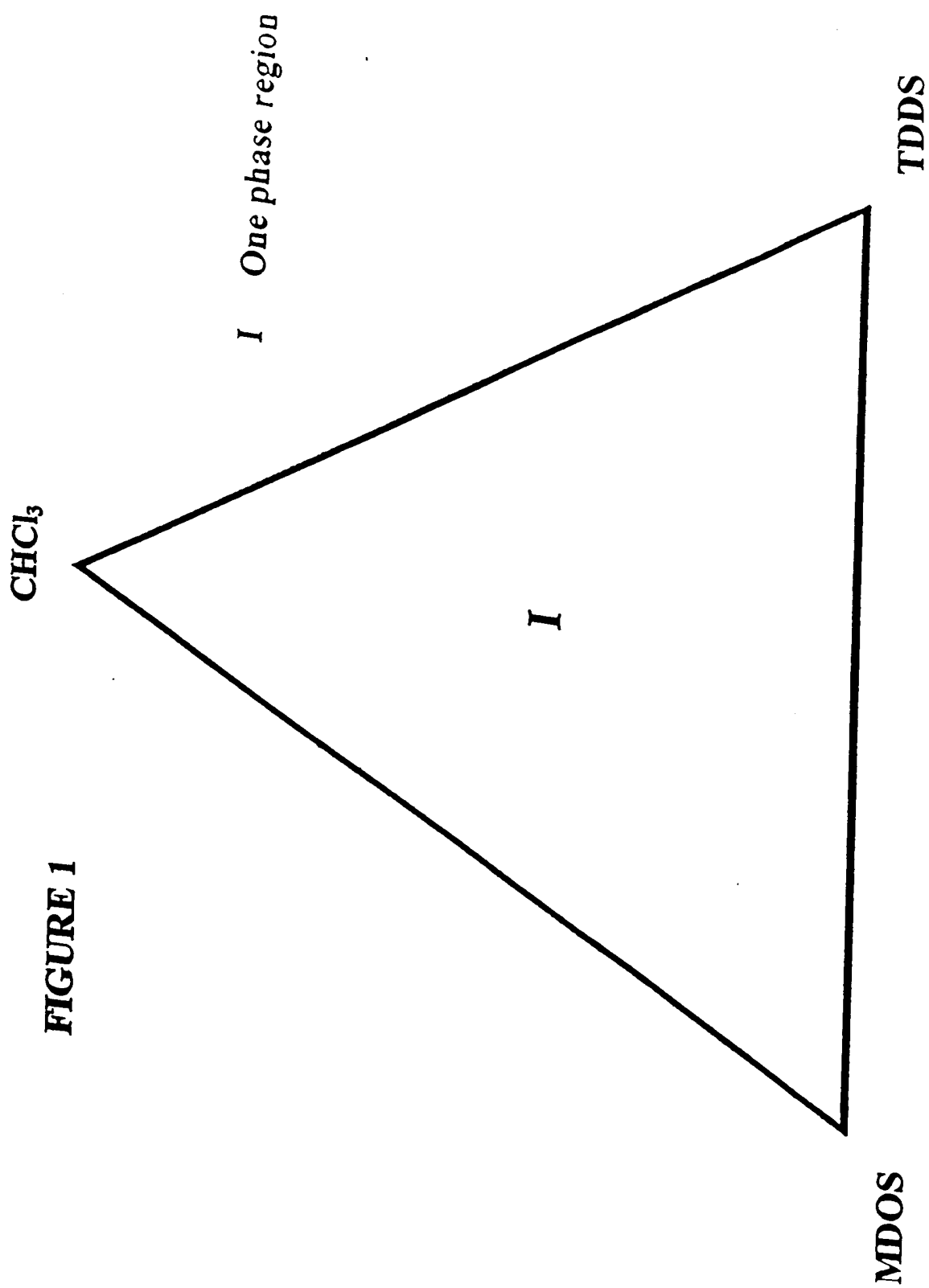


Figure 1: Phase Diagram of MDOS, TDDS, CHCl_3 w/w%.

obtained for all compositions.

Figure 2 depicts the phase diagram of the MDOS, TDDS, and methanol. The solubility regions of these three components illustrate several interesting characteristics. Region I represents the solubility region of the components, and region II represents the two phase region. Note the tie-lines along the two phase boundary result in complete separation to the pure TDDS corner and its respective two component solubility. TDDS and methanol are completely immiscible along the two component region. Second, the two component line between MDOS and methanol are completely soluble. This region is not depicted accurately in the methanol corner for MDOS concentrations below 7%. TDDS is insoluble in this region and completely separates out. A similar feature is also present in the TDDS corner of the phase diagram. MDOS and the TDDS are completely soluble along the two component line between them, which may not be apparent below 5% MDOS. In the TDDS corner, methanol is insoluble below 5% MDOS and separates out completely.

Figure 3 illustrates the solubility of MDOS, TDDS, and acetone. A single phase isotropic solution was observed, where all three components were completely soluble in each other.

Figure 4 shows the solubility of MDOS, TDDS, and ethanol. The solubility of both MDOS and TDDS has increased significantly with the extension of the carbon chain by one unit, as compared to methanol. The tie-line was established at the critical concentration of the two phase region.

FIGURE 2

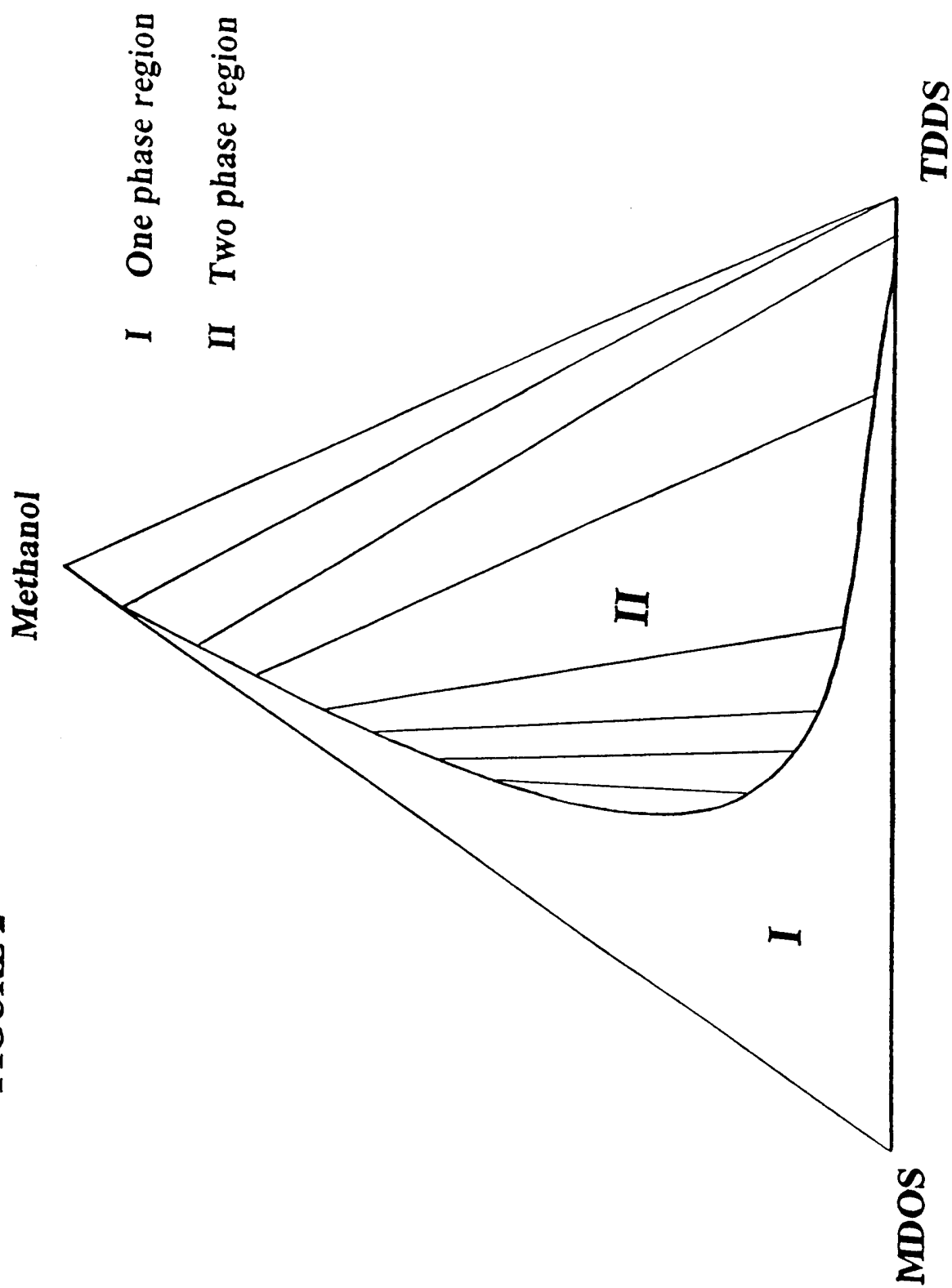


Figure 2: Phase Diagram of MDOS, TDDS, Methanol w/w%.

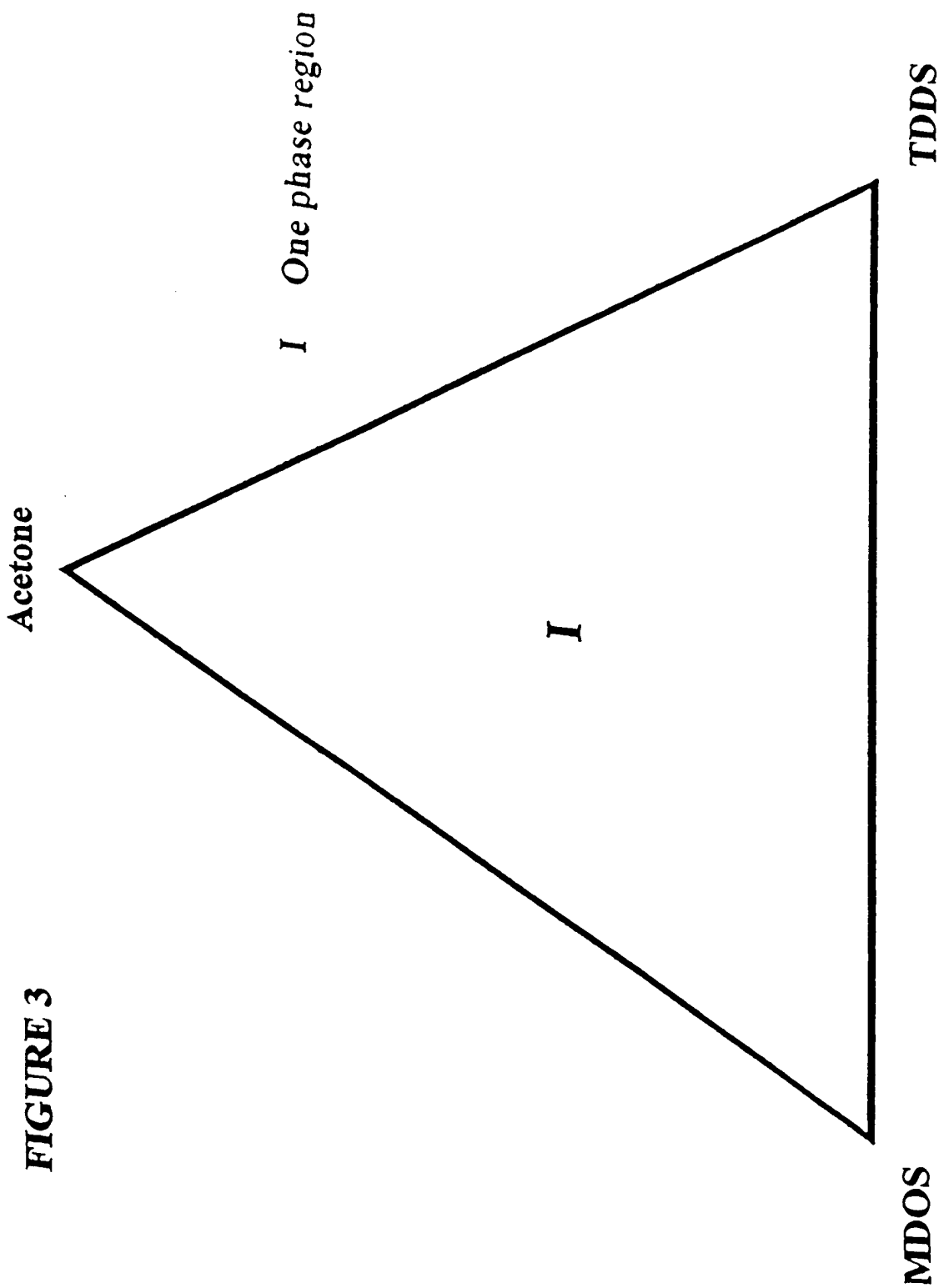


Figure 3: Phase Diagram of MDOS, TDDS, Acetone w/w%.

FIGURE 4

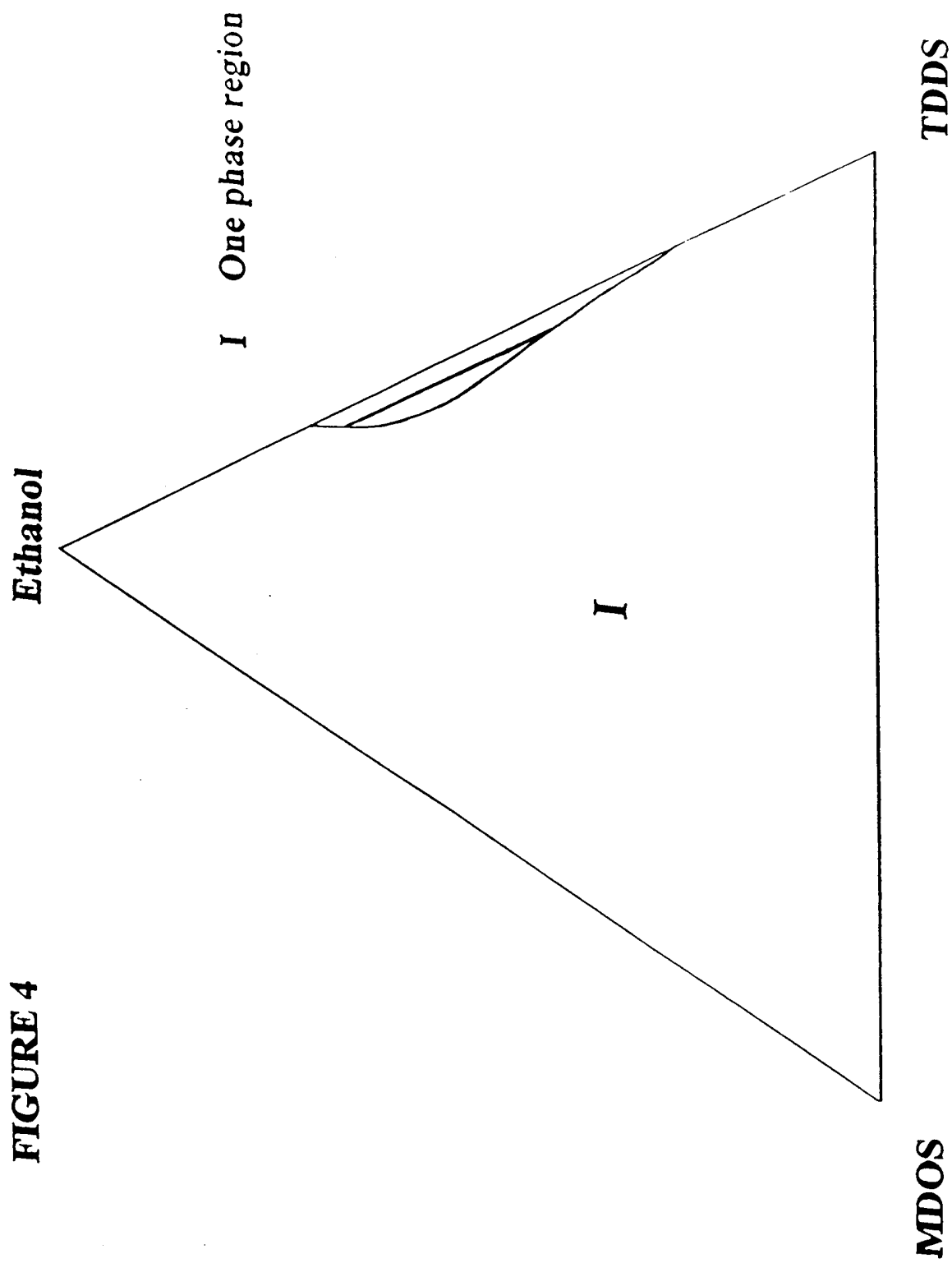


Figure 4: Phase Diagram of MDOS, TDDS, Ethanol w/w%.

Figure 5 displays the insolubility of MDOS, TDDS, and ethylene glycol. It is interesting to note that the phase separation occurs at all concentration of this polar component.

Figure 6 depicts the phase diagram of MDOS, TDDS, and propanol. In a similar comparison with Figures 2 and 4, we see the complete solubility of the three components with the addition of carbon chain length to the alcohol molecules.

Figures 7 and 8 show the phase diagrams of MDOS, TDDS, with 1,2 propane diol and 1,3 propane diol, respectively. Here we see the extent of additional polar groups added to the base alcohol unit, which results in complete phase separation.

Figure 9 illustrates the phase diagram of MDOS, TDDS, and Brij 30. There are several interesting aspects of this diagram. Note the tie-lines in the two phase region exhibit an associative phase separation [22]. It is apparent that there is sufficiently strong effective attraction between MDOS and TDDS, and/or the two silanes exhibit similar affinity towards Brij 30. Along the MDOS-Brij 30 line, the two phase region begins ~ 5% and continues to separate up to ~ 18% surfactant. Similarly along the TDDS-Brij 30 line, the separation begins immediately and continues until the concentration of Brij 30 reaches ~ 14%. In both cases, the miscibility gap occurs at low Brij 30 concentration and results in a narrow 14% band across the phase diagram. The composition of MDOS/TDDS to Brij 30 are relatively constant across the two phase band.

Figure 10 shows the phase diagram of MDOS, TDDS, and SA9. Here we see that along the MDOS-SA9 line, the two phase region begins at ~ 7% and continues to

FIGURE 5 ***C*₂ Glycol**

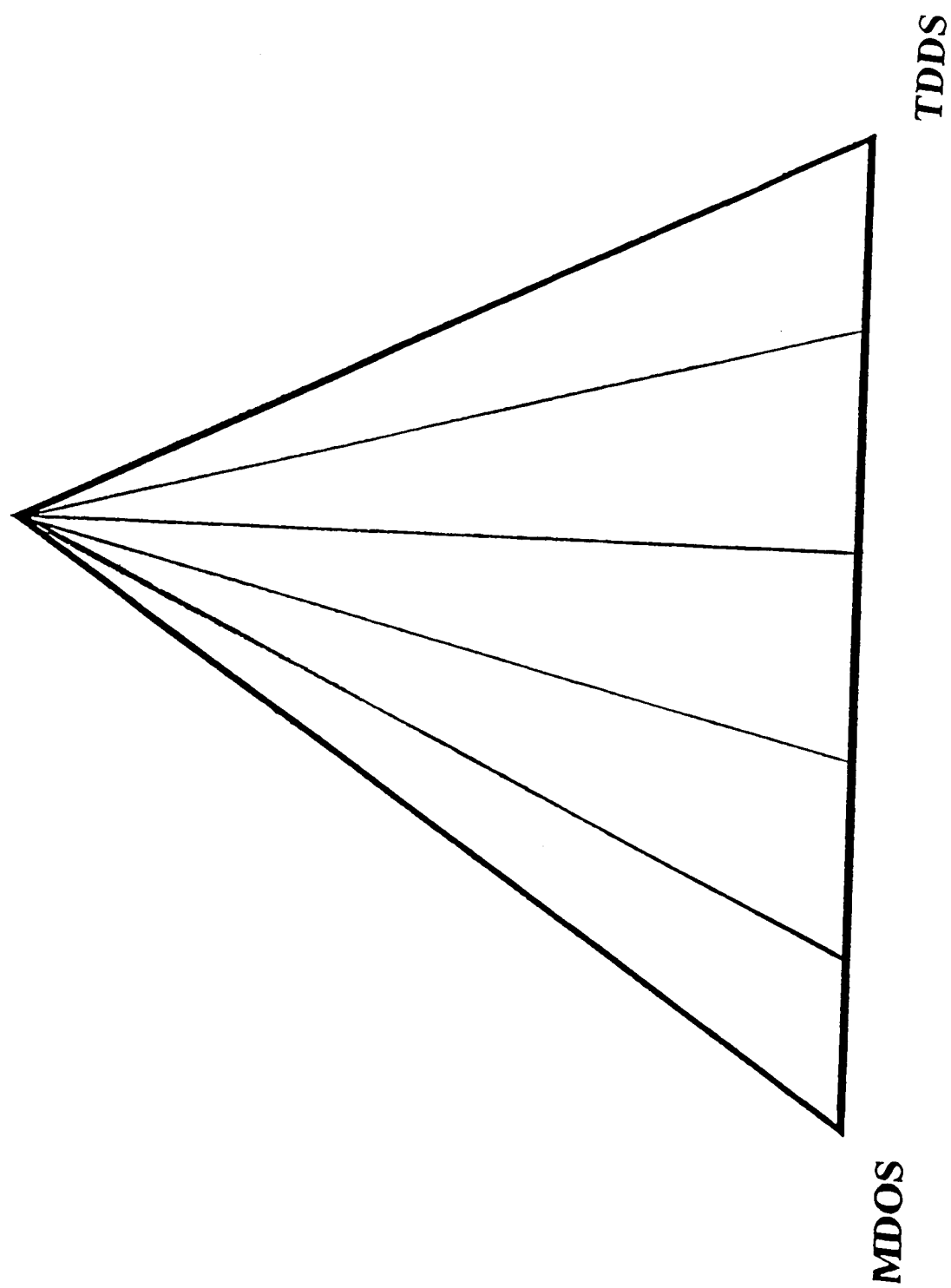


Figure 5: Phase Diagram of MDOS, TDDS, Ethylene glycol w/w%.

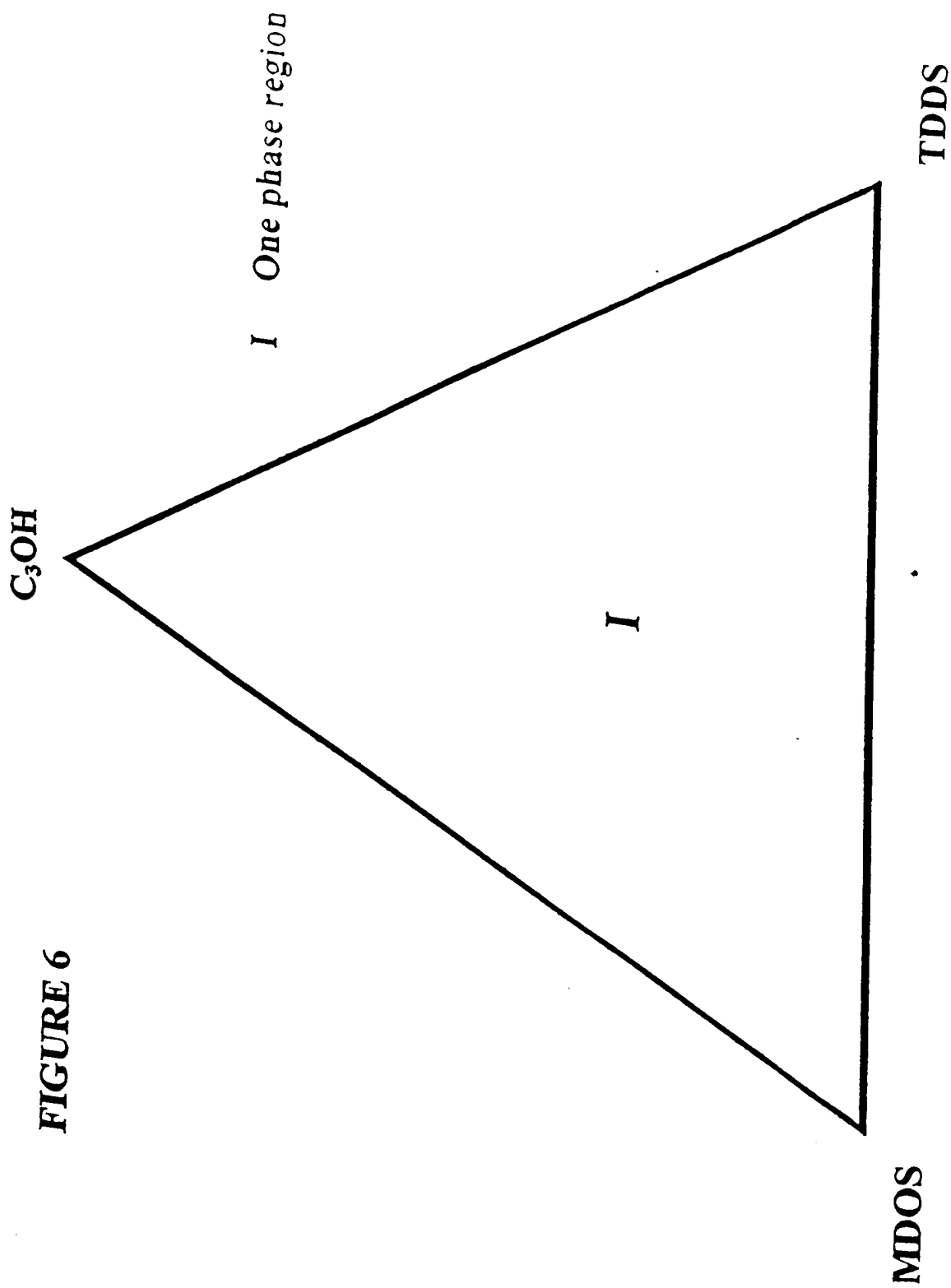


Figure 6: Phase Diagram of MDOS, TDDS, Propanol w/w%.

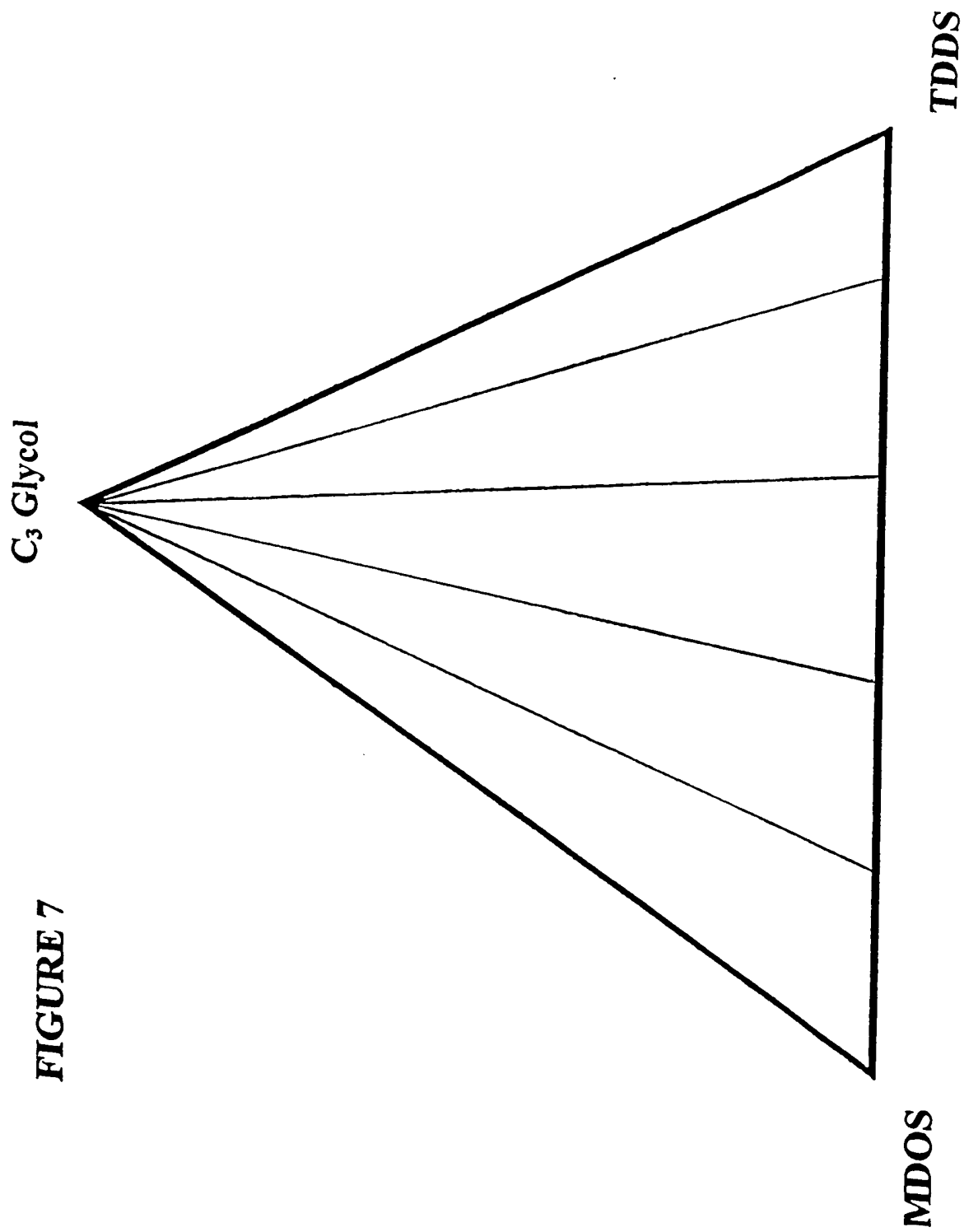


Figure 7: Phase Diagram of MDOS, TDDS, 1,2 Propane diol w/w%.

1,3 C₃ DIOL

FIGURE 8

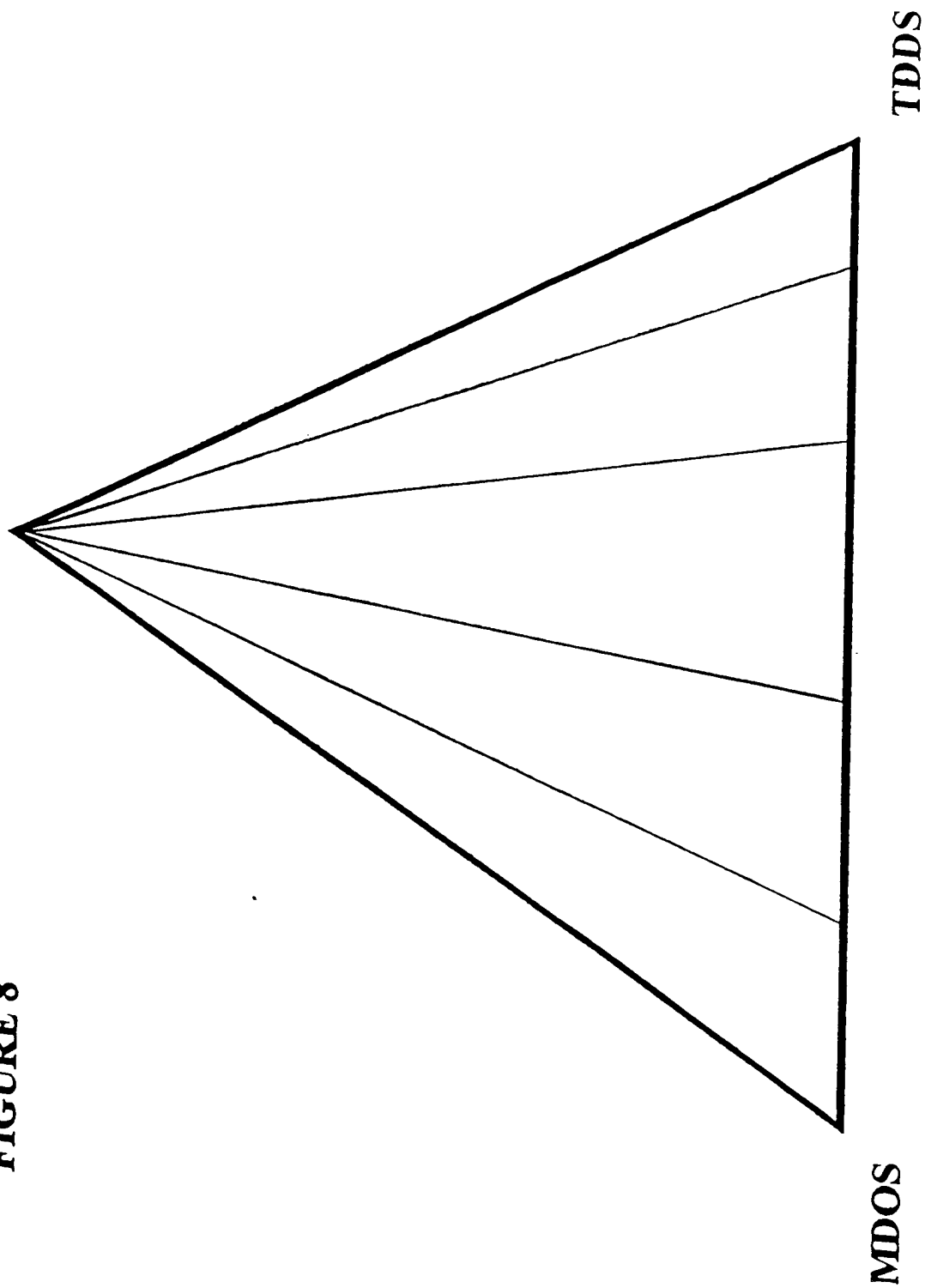


Figure 8: Phase Diagram of MDOS, TDDS, 1,3 Propane diol w/w%.

FIGURE 9

Brij 30

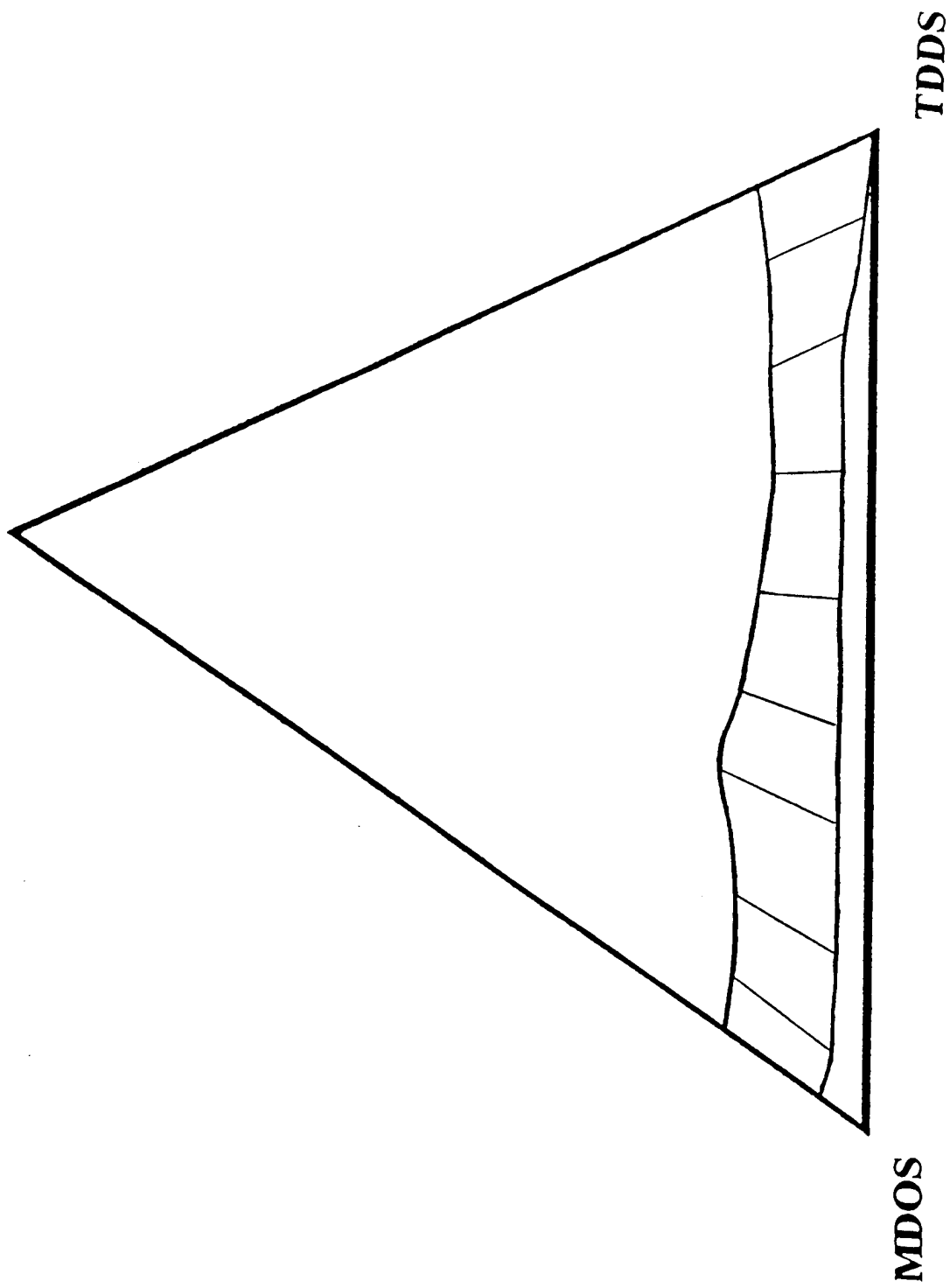


Figure 9: Phase Diagram of MDOS, TDDS, Brij 30 w/w%.

SA-9

FIGURE 10

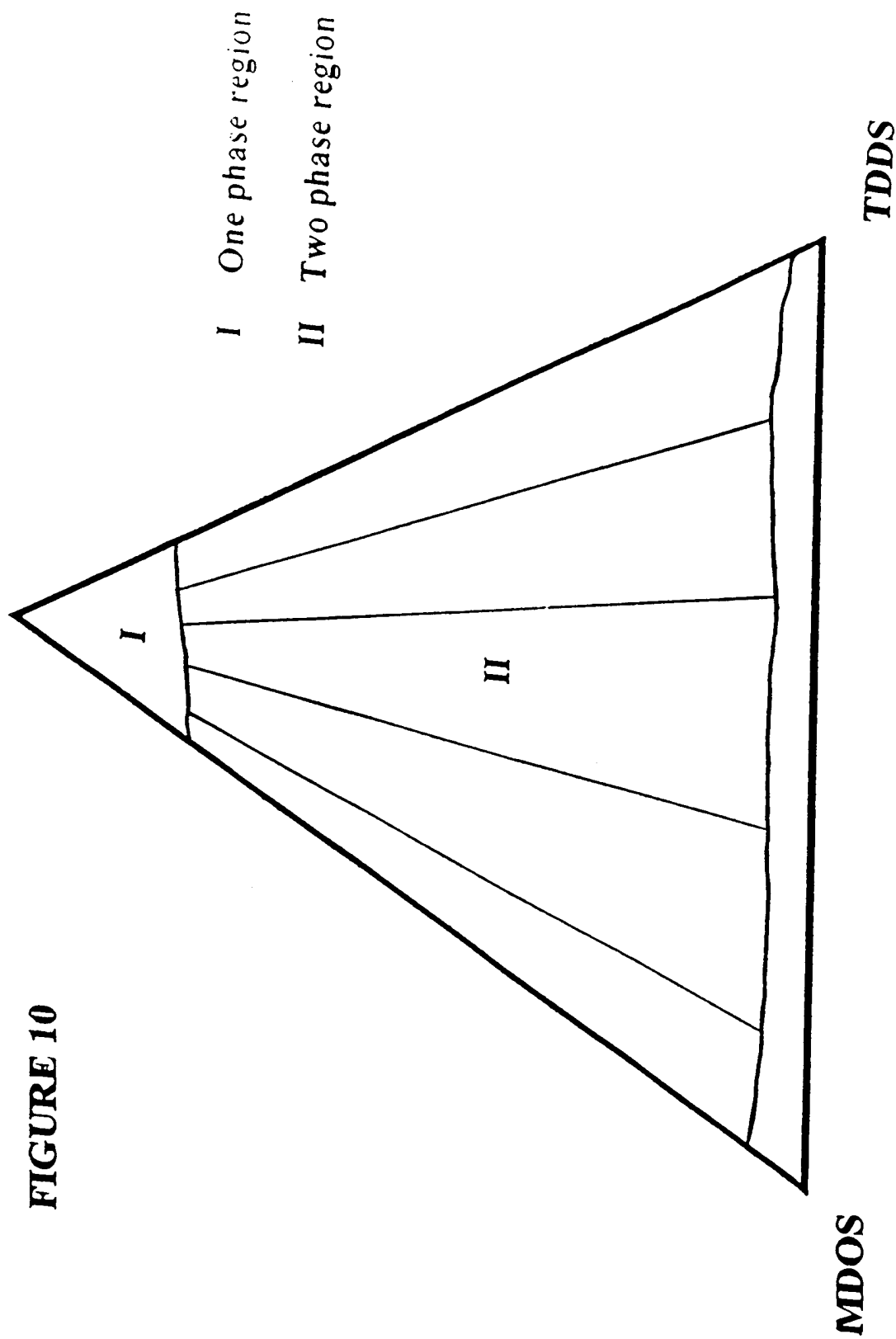


Figure 10: Phase Diagram of MDOS, TDDS, SA9 w/w%.

separate until ~ 78% SA9 concentration. The TDDS- SA9 line shows the phase separation at ~ 4% and continues until ~ 80% SA9 concentration. The miscibility gap in this case spans over a 70% range. As with Figure 9, the phase separation is associative, resulting in a surfactant rich solution and a silicate rich solution. Noteworthy is the increase in the two phase region as compared to Figure 9. The increase in the polar ethoxy groups from four to nine is considerable.

Discussion

The partial solubility parameters for the chemicals used in this study are listed in Table I. These compounds, with varying solubility parameters, were used to determine the solubility profile of TDDS. Hansen parameters were collected from the CRC Handbook of Solubility Parameters [25,26]. Estimates for the partial parameters for MDOS, TDDS, Brij 30, and SA9 were calculated by the molar group contribution method as described by Barton [25].

The results demonstrate the importance of polarity and hydrogen bonding character on the solubility of MDOS and TDDS. Low polar/H-bonding solvents, acetone and chloroform, formed an isotropic clear solution with the two silanes as indicated by Figures 1 and 3 respectively. For chloroform, there is a considerable difference in the polar parameters of these compounds in Table I, this however does not induce phase separation. For acetone, the difference in the polar and H-bonding values of Table I are still considerably large, but apparently not large enough to cause instability in the system.

High H-bonding/polarity solvents, alcohols and diols, displayed characteristic

| TABLE I - Hildebrand & Hansen Parameter @ 298 K, 1 atm | | | | | | | |
|--|-------------------------------|--------------------------------------|------|------------|------------|------------|------------|
| Liquid | Mol Wt g mol ⁻¹ | density ρ g cm ⁻³ | Bp.C | δ_d | δ_p | δ_h | δ_t |
| Chloroform | 119.4 | 1.477 | 61.7 | 11.0 | 13.7 | 6.3 | 18.7 |
| Acetone | 58.1 | 0.785 | 56.1 | 13.0 | 9.8 | 11.0 | 19.7 |
| Propanol | 60.1 | 0.799 | 97.2 | 14.1 | 10.5 | 17.7 | 24.9 |
| Ethanol | 46.1 | 0.785 | 78.3 | 12.6 | 11.2 | 20.0 | 26.1 |
| MEOH | 32.0 | 0.786 | 64.5 | 11.6 | 13.0 | 24.0 | 29.7 |
| 1,2 propanediol | 76.1 | 1.033 | 187 | 11.8 | 13.3 | 25.0 | 30.7 |
| 1,3 propanediol | 76.1 | 1.050 | 214 | 12.4 | 14.1 | 27.1 | 33.0 |
| Et glycol | 62.1 | 1.110 | 198 | 10.1 | 15.1 | 29.8 | 34.9 |
| Water | 18.0 | 0.997 | 100 | 12.2 | 22.8 | 40.4 | 48.0 |
| Dodecane | 170.3 | 0.744 | 216 | 16.2 | 0 | 0 | 16.2 |
| Octane | 114.2 | 0.698 | 126 | 15.4 | 0 | 0 | 15.4 |
| Decane | 142.3 | 0.725 | 174 | 15.8 | 0 | 0 | 15.8 |
| Brij 30 * | 362.6 | 0.950 | -- | 16.1 | 3.8 | 9.2 | 18.9 |
| SA-9 * | 610 | 0.976 | -- | 15.8 | 3.2 | 8.7 | 18.2 |
| MDOS * | 202.4 | 0.813 | 221 | 14.7 | 1.8 | 3.5 | 15.2 |
| TDDS * | 358.9 | 0.820 | -- | 14.8 | 0.7 | 2.6 | 15.7 |

d-dispersion interactions, p-polar interactions, h-hydrogen bonding, t-total cohesive parameter;
Hansen parameters collected from pp 94-109 CRC Handbook Solubility Parameters, Barton, 1983.
* Parameters calculated by molar group contribution method pp 82-86 CRC handbook

Table I: Hansen Solubility Parameters

phase separation. We see from Figure 2 that methanol exhibits segregative phase separation. The methanol's polar and hydrogen bonding parameters listed in Table I are extremely large when compared to the two silanes. The solubility dramatically increased as the carbon chain length extended to C2 and C3, as illustrated in Figures 4 and 6, respectively.

The partial solubility of ethanol in TDDS reveals an interesting aspect of the Hansen parameters in Table I. The ethanol polar value is comparable to that of acetone and chloroform, yet the hydrogen bonding value is extremely large when compared to the previously mentioned materials, as well as the two silanes. From Table I, propanol slightly increases in dispersion and polar interaction as compared to acetone with a significant decrease in H-bonding as compared to other alcohols.

However, when the number of hydroxyl groups is increased with respect to the carbon chain length (Figures 5, 7, and 8), it resulted in complete insolubility of the silane compounds in the system. At first glance, one may deduce the hydrophilic/hydrophobic ratio of the alcohol to cause segregative separation should be one to one as in Figure 2. If this were the case, one would expect ethylene glycol to exhibit similar behavior. The tie lines in Figure 5 illustrate the glycol to be completely insoluble toward the two silanes in all proportions. For ethylene glycol, the comparison of Hansen parameters is similar to ethanol with a distinction. The polar parameter again is comparable to chloroform, but the H-bonding is substantially larger than ethanol and methanol. The high H-bonding character of the propane diols are also comparable to that of ethylene glycol. The small

differences in the partial parameters are illustrated in Figure 11.

Figure 9 and 10 illustrate the extent of hydrophilic/hydrophobic interactions between the two silanes and the non ionic surfactants of similar carbon chain length. The Brij 30 is slightly soluble in the silicate solution up to 5%. In this one phase region, we expect the association of the three components to be comparable, following the 'like dissolves like' rule. Above 5% surfactant, the affinity of the silanes changes towards Brij 30. The solubility of the ethoxy chain reaches unfavorable interactions at its maximum, therefore it is reasonable to expect the ethoxy groups can no longer freely associate in the solution. Above 18% surfactant, a single phase reappears. At this concentration there is enough ethoxy chains to associate with themselves, forming tightly bound small premicellar aggregates [23]. These aggregates are not micelles, but it is reasonable to see the carbon chain of the surfactant interacting with the similar carbon chains of the silanes.

In Figure 10, we see the increase in associative phase separation. The same reasoning for the Brij 30 diagram still applies here with one additional distinction pertaining to the longer ethoxy chain of SA9. The SA9 carbon chain length is similar to Brij 30; hence, we expect favorable interactions between surfactant hydrocarbons and silane hydrocarbons chains. The polarity of the two surfactants are distinctively different. Brij 30 contains four ethoxy group chain length while SA9 has nine ethoxy group chain. It is easy to identify the effect of the longer polar chain length by comparison of Figure 9 and 10, where a five fold increase in the miscibility gap resulted.

Figure 11 plots the polar interaction parameters versus the hydrogen bonding

FIGURE 11

Partial Solubility Parameters

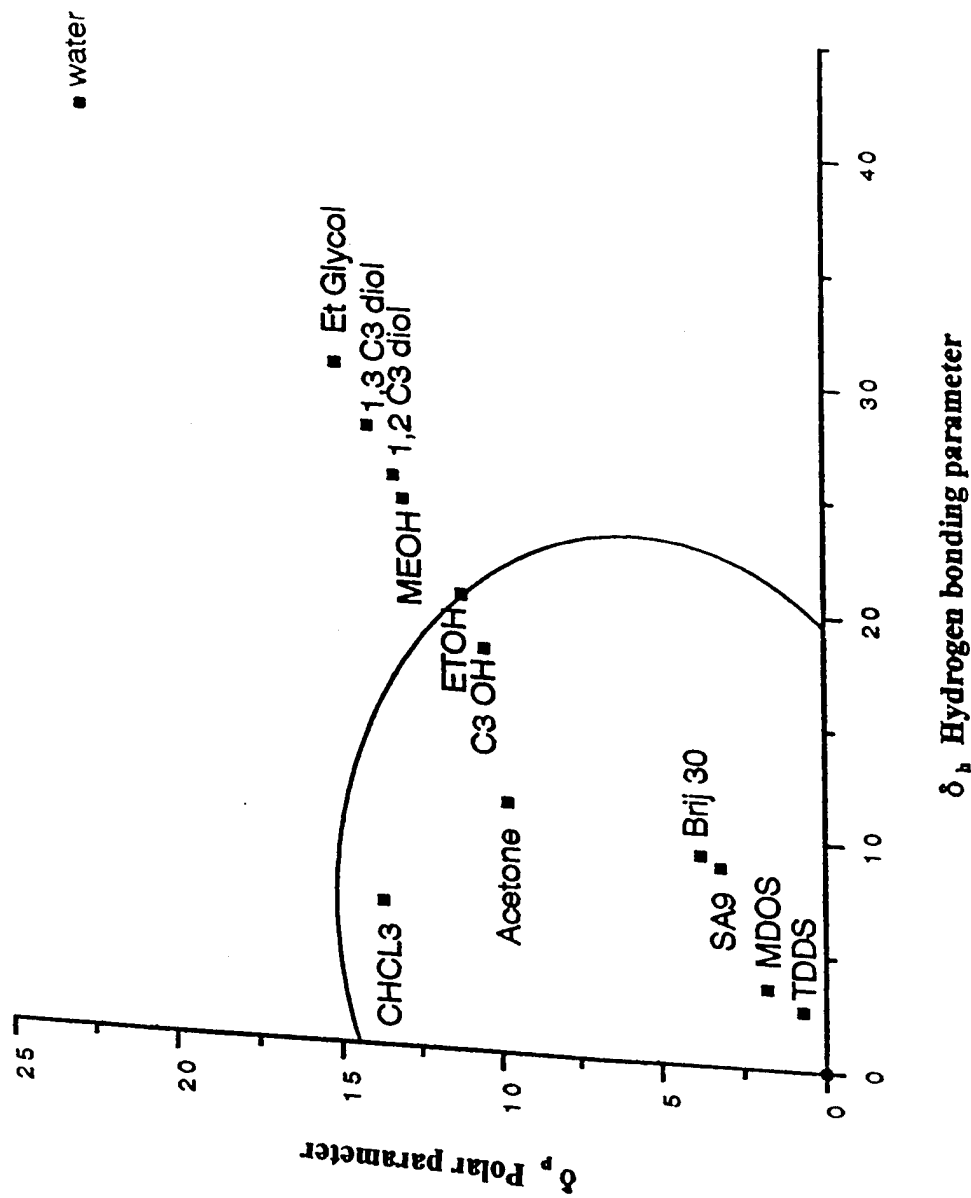


Figure 11: Polar versus H-bonding Parameters of Table 7.1.

parameters listed in Table I. The solubility region is represented by an arc across the diagram with a limiting value which intersect the ethanol point. It is reasonable to assume that values above that of ethanol will result in complete insolubility of TDDS.

Figure 12 utilizes the data in Table I to plot the Hansen parameters in accordance with Equation (5). The representative equilateral triangle spaces the data considerably more than that of Figure 11 and does not neglect the dispersion force parameter.

The calculated parameters for the non ionic surfactants listed on Table I require an additional note. Barton points out in his books [25, 26] that the partial parameters do not accurately characterize surfactant molecules. In particular, the polar character of surfactants contribute substantially larger values than those presently available. Figures 9 and 10 illustrate how calculated values for determining the solubility of a particular system can go awry. According to the differences in Table I, as illustrated in Figure 11 & 12, one would expect the two silanes to be completely soluble in either surfactant; however, the phase equilibria shows a significant miscibility gap. The comparison of surfactant solubility parameters with those of the silanes in these systems are used with extreme caution. The difficiencies in the polar contribution to the solubility parameters for amphiphilic molecules require additional attention and possible modifications to the present method.

Conclusion

The polarity and hydrogen bonding characteristics of a solvent plays a significant role in the solubility behavior of monomeric silane units. As the hydrogen bonding/

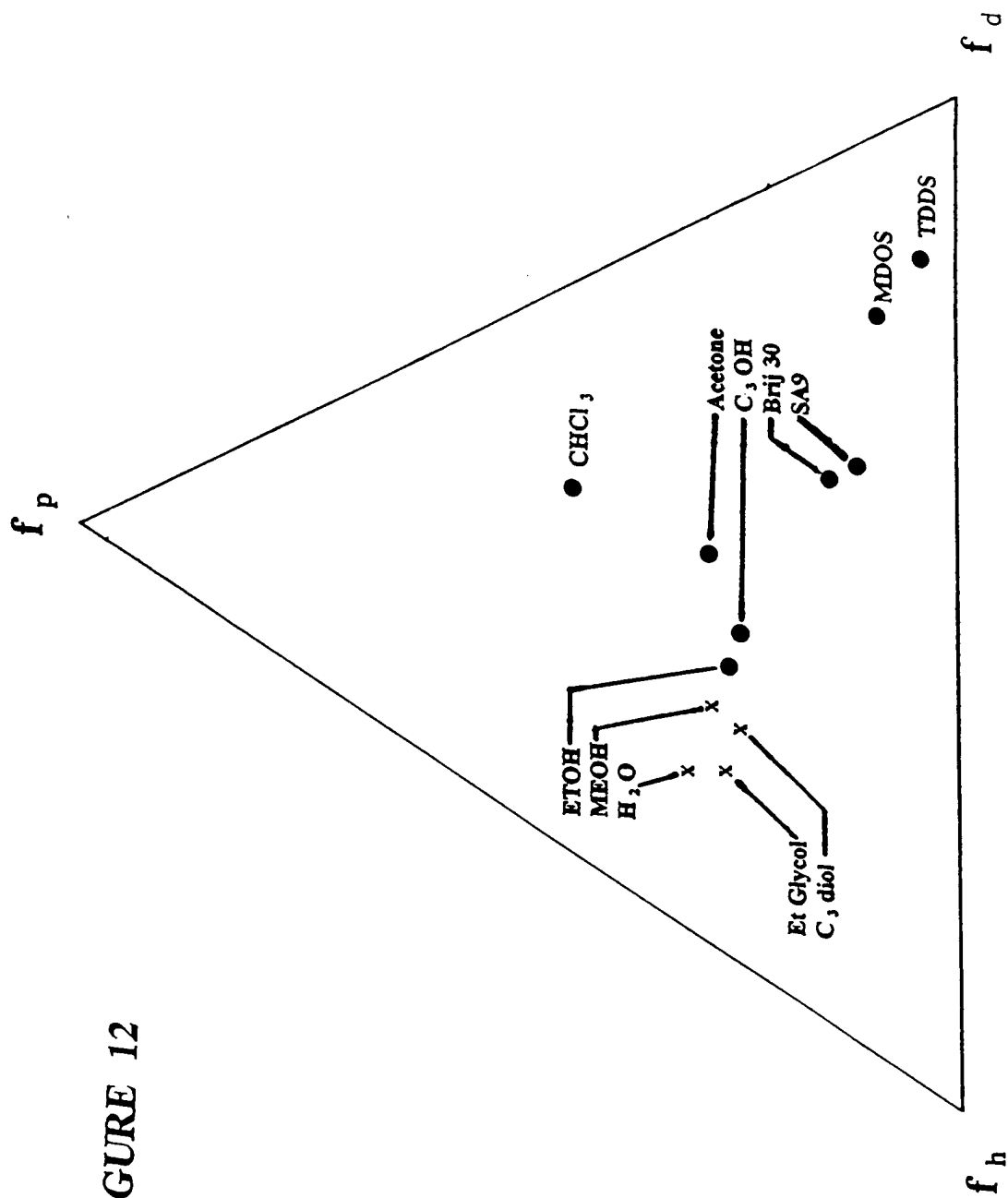


Figure 12: Triangle Plot of Table 7.1, Hansen Solubility Parameters.

polarity increased, characteristic phase separation predominated the equilibria of the system. The Hansen solubility parameters are a useful tool in determining the miscibility of a system if used with discretion. The results illustrate the dependence of phase equilibria on solvent polarity.

Acknowledgment

This research was supported in part by the CAMP program at Clarkson University, Potsdam, New York and the Department of the Army, United States Military Academy, West Point, New York.

References

- [1] "Sol-Gel Technology" (L.C. Klein, ed.) Noyes Publications, NJ 1988
- [2] C.J. Brinker, G.W. Scherer "Sol Gel Science" Academic Press, NY 1990
- [3] Mehrotra, R.C., J. Non-Cryst. Solids 100, 1, 1988
- [4] Guglielmi, M., and Cartman, G., J. Non-Cryst. Solids 100, 16, 1988
- [5] Sanchez, C. Livage, J., Henry, M., J. Non-Cryst. Solids 100, 65, 1988
- [6] Pouxviel, J.C. Boilot J.P., J. Non-Cryst. Solids 89, 345, 1987
- [7] Brinker, C.J., J. Non-Cryst. Solids 100, 31, 1988
- [8] Pouxviel, J.C. Boilot J.P., J. Non-Cryst. Solids 103, 331, 1988
- [9] Sakka, S., Kozuka, H., Adachi, T., J. Non-Cryst. Solids 102, 263, 1988
- [10] Scherer, G.W., J. Non-Cryst. Solids 107, 135, 1989
- [11] Orcel, G., Hench, L.L. Araki, I., J. Non-Cryst. Solids 105, 223, 1988
- [12] Orcel, G., Phalippou, J, Hench, L.L., J. Non-Cryst. Solids 105, 223, 1988
- [13] Friberg, S.E., Yang, CC, Sjoblom, J., Langmuir, 8, 372, 1992
- [14] Friberg, S.E., Yang, J, Amran, A, J Phys Chem 98, 13528, 1994
- [15] Sjoblom, J., Selle, M.H., Friberg, S.E., Moaddel, T., Colloids and Surf. 88, 235, 1994
- [16] Friberg, S.E., Ma, Z, J. Non-Cryst. Solids, 147 & 148, 30, 1992
- [17] Mukhejee, S.P., J. Non-Cryst. Solids 63, 35, 1984
- [18] Yoldsa, B.E., J. Non-Cryst. Solids 82, 11, 1986
- [19] Sakka, S., Tanaka, Y., Kokubo, T., J. Non-Cryst. Solids 82, 24, 1986

- [20] Friberg, S.E., Jones, S.M., Yang, CC, J. Disp Sci Tech 13, 1, 65, 1992
- [21] Heenan, DM, Friberg, SE, Sjoblom, J, Farrington G. (in press)
- [22] Piculell, L., Lindman, B., Adv Colloid Int. Sci, 41,149, 1992
- [23] Friberg S.E., Progr Colloid & Polymer Sci, 68,41, 1983
- [24] Hildebrand J.H., Scott, R.L., *Regular and Related Solutions*; Van Nostrand Reinhold Company, NY, NY 1970
- [25] Barton, A.F. M. *Handbook of Solubility Parameters and Other Cohesion Parameters*; CRC Press; Boca Raton, FL, 1983.
- [26] Barton, A.F. M. *Handbook of Polymer-Liquid Interaction Parameters and Solubility Parameters*; CRC Press; Boca Raton, FL, 1983.
- [27] CRC Handbook of Chem and Physics; CRC Press, Boca Raton, FL, 1982
- [28] Perry's Chemical Engineers Handbook; McGraw Hill Pub. NY, 1984
- [29] Hansen, C.M. J. Paint Technol., 39, 505, 104-117, 1967
- [30] Hansen, C.M., Ind Eng Chem Prod Res Dev., 8, 1, 2-11, 1969
- [31] Teas, J.P., J. Paint Technol., 40, 516, 19, 1968
- [32] Hansen, C.M., Anderson, B.H., Am Hyg. Assoc J., 49, 6, 1988
- [33] Archer, W. L., Ind Eng Chem Prod Res., 30, 2292, 1991

8. Article 3: Phase Equilibria of Tetramethyldioctyldisiloxane, Water and Organic Solvents

Daniel M. Heenan, Stig E. Friberg

Center for Advanced Materials Processing, Clarkson University,

Potsdam, New York 13699-5814

Johan Sjöblom

Department of Chemistry, University of Bergen,

N-5007 Bergen, Norway

Abstract

The phase diagrams for tetramethyldioctyldisiloxane (TDDS), water and several organic components were determined using refractive index, polarizing microscopy and low angle x-ray diffraction. The solubility limits of the alcohols were established by quantitative analysis and compared to the refractive index of known single phase mixtures. The non-ionic surfactants systems contained isotropic liquids of varying concentrations. Two lyotropic liquid crystal regions were discovered, one of lamellar structure and one consisting of a hexagonal array of closed packed cylinders. The character of the amphiphiles components to solubilize the TDDS is reflected in the phase equilibria.

Introduction

The interest in phase equilibria of water and different amphiphiles has generated considerable attention following Ekwall's pioneering contribution [1]. This has led to

extensive research efforts into the fundamental analysis of the structures and their relationships [2-7, 21], which has recently expanded to include phase equilibria of silane polymers with surfactant combinations to form: microemulsions, emulsions, and liquid crystals [13-16]; and to link their use as reaction medium in the sol-gel process [8-12]. Thus far, the predominate literature sources on sol-gel processing pertain to gelation and reaction kinetics of complex tetraalkoxysilanes species and their phase equilibria in the for mentioned amphiphilic association structures [17-19].

The solubility limitations of organo-silanes in amphiphilic association structures is of considerable importance to the system polymerization kinetics. However, these efforts have been concerned with three component systems which form gel and/or glassy silicates [19]; interest in phase equilibria of liquid organo-silanes products formed by the sol-gel process has received little attention.

The analysis of phase diagrams of Methoxydimethyloctylsilane (MDOS), tetramethyldioctyldisiloxane (TDDS) and methanol was previously reported by Heenan *et al.* [22] on the sol-gel kinetics in a organized system. The phase equilibria was then expanded for MDOS, TDDS and various organic solvents, which were characterized for miscibility behavior and solubility parameters [23] through the thermodynamic treatment of mixing . These results prompted further investigation into the phase equilibria of TDDS, water and organic solvent systems. In this publication we report the solubility of TDDS and water with various organic solvents.

Experimental

Materials

The following chemicals were used as received: methanol (Fisher, certified), ethanol (Pharmco, absolute), 1-propanol (Aldrich, 99+%), 1-butanol (Aldrich, 99+%), n-decanol (Aldrich, 99+%), Brij 30 (ICI Surfactants), synperonic A-9 {SA9, non-ionic surfactant $C_{13/15}EO_9$ } (ICI Surfactants), tetramethyldioctyldisiloxane (prepared as described below), methoxydimethyloctylsilane (Aldrich, 98%), and water (doubly distilled).

The tetramethyldioctyldisiloxane was prepared by reacting a one to one mole ratio of methoxydimethyloctylsilane with water (pH 2.0, adjusted with HNO_3) in 75% w/w methanol. The TDDS is insoluble at high concentrations of methanol and easily separates out after 48 hours. The TDDS was washed in absolute methanol, separated, and placed in 60 C oven for two hours to evaporate any trace volatile components.

Phase Diagrams

The one and two phase regions were established by titration. The composition of two components were fixed as the third component was added to the mixture. Combinations with the third component were added until a transparent system was visually observed. The solubility areas were marked for clarification and turbidity point during the titration. The extent of the solubility regions were confirmed by centrifugation at 5000 rpm for 45 minutes for samples with composition close to the solubility limit and also by storage at room temperature for several weeks.

The tie-lines for the two phase regions were determined with Bausch & Lomb model ABBE-3L refractometer. A series of samples with different ratios of the three components in the one phase region were prepared close to the demixing line and measured for refractive index. Samples in the two phase region were allowed to separate and centrifuged at 5000 rpm for one minute. The two separated phases were then measured for refractive index and compared to those of known refractive index near the demixing line.

The liquid crystalline phases were determined by analysis of composition of each phase in equilibrium. The phases were separated using the following procedure. The phases were heated to 65°C, vigorously mixed and cooled to room temperature. Each phase was analyzed for its content of water and TDDS. The water was titrated by the Karl Fisher method whereas the combined amount of water and TDDS was measured from the weight loss after complete evaporation. Finally the three phase areas were verified by the weight ratio of each phase in equilibrium.

The exact tie-lines between solution and liquid crystal were not determined for the two phase regions. The limit of the two phase region of the isotropic liquid phases were determined in the following manner. A series of samples with different ratios in the one phase region were prepared close to the demixing line of the corresponding phase in equilibrium, and other components were then titrated in. The samples were observed under cross-polarizer microscope, and the limit of the two phase area was detected from the appearance of a liquid crystalline phase.

The three phase region tie-lines were established in a similar way. Liquid crystal was mixed with high concentrations of TDDS, water was then titrated in varied amounts to the three phase sample. Under the microscope, the liquid crystal was observed to be in a continuous phase of TDDS; when water is titrated in, small droplets begin to appear in the continuous phase with the liquid crystal. As the water content was increased, the size and number of droplets present increased. This technique was repeated for water as the continuous phase and TDDS titrated in, which constructed the tie lines to be approached from two different composition directions in the phase diagram.

Results

The phase diagrams are presented in increasing order of carbon chain length. Figure 1 shows the solubility of TDDS, water and methanol. Note the tie-lines along the two phase boundary result in complete separation to the pure TDDS corner and its respective two component solubility. TDDS and methanol are completely immiscible along the two component region as well as TDDS and water. Second, the two component line between water and methanol are completely soluble in all proportions.

Figure 2 illustrated the solubility of TDDS, water and ethanol. A single isotropic solution was observed in the ethanol corner. The two component line of water-ethanol are completely soluble, while TDDS is completely insoluble along the TDDS-water composition line. Two solubility regions were observed along the TDDS-ethanol composition line. At high TDDS concentration, a solution consisting of 75% to 83% TDDS and a maximum of 1% water content was present. Reduction in the TDDS content

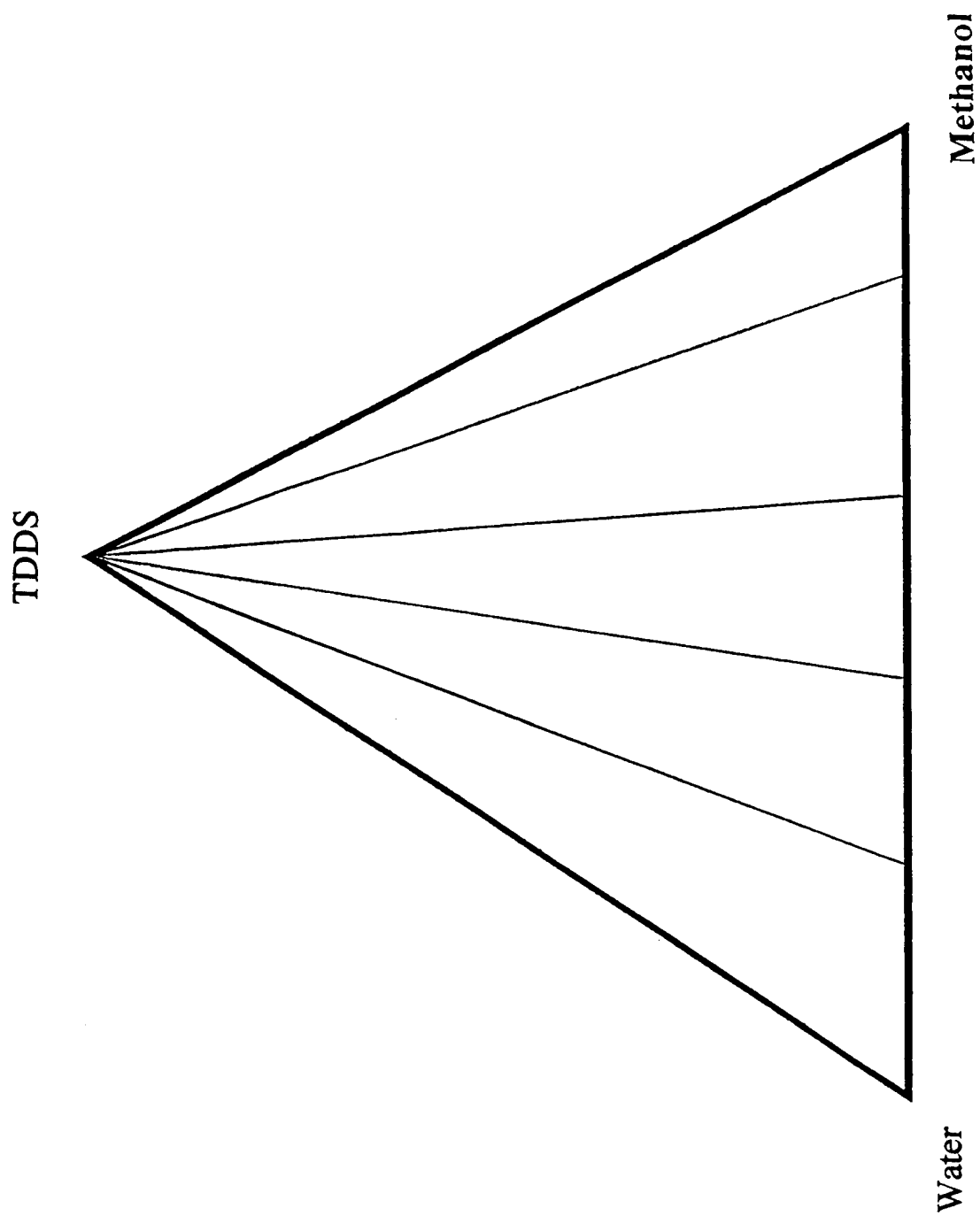
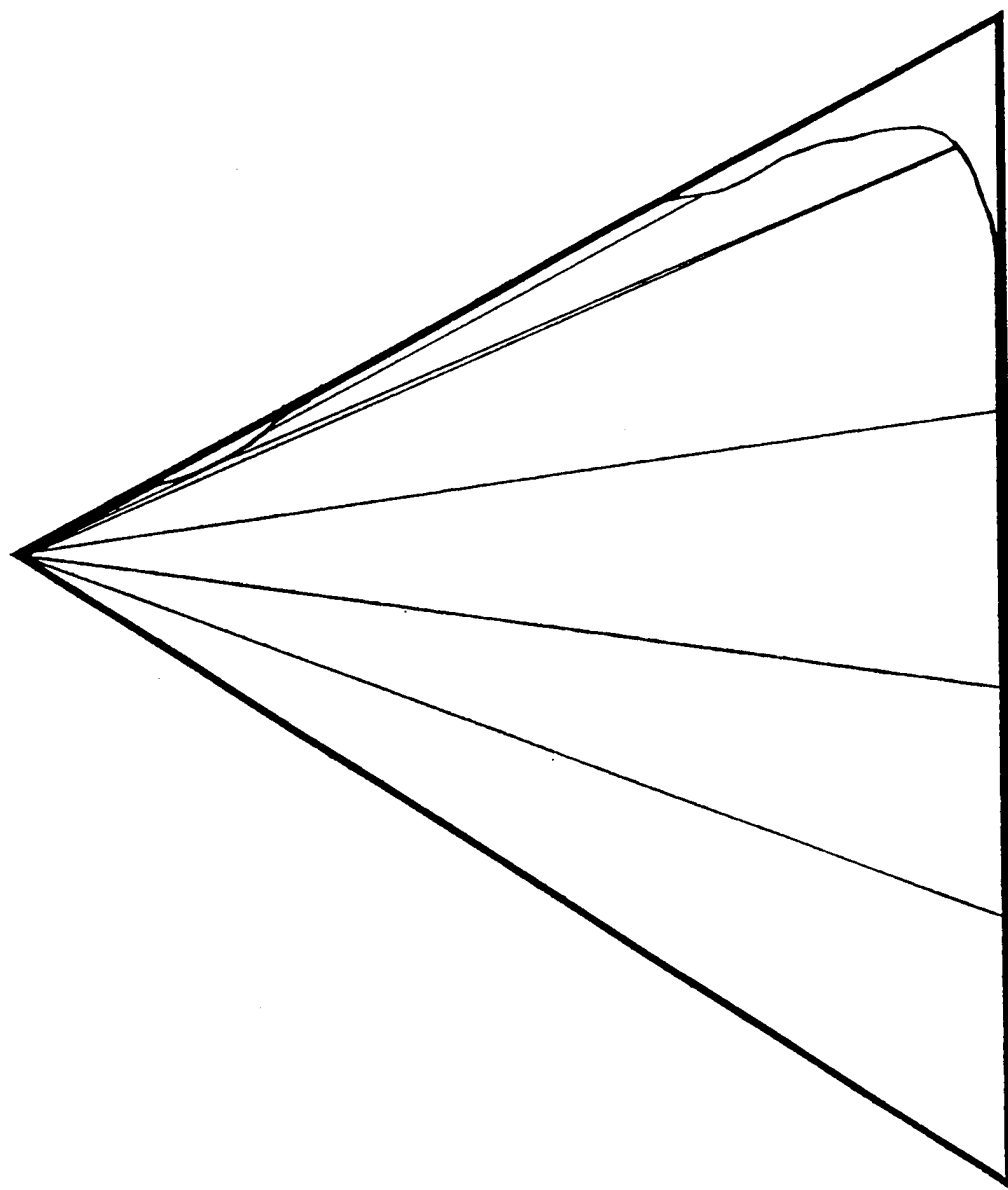


Figure 1: Phase Diagram of Water, TDDS, Methanol w/w%.

TDDS



Ethanol

Water

Figure 2: Phase Diagram of Water, TDDS, Ethanol w/w%.

resulted in a miscibility gap at 75% TDDS and continued till 30% TDDS, where the second isotropic single phase appeared. The two phase region spanning the two isotropic single phase region are connected by a tie-line as noted. The maximum water content of 5% was solubilized in 90% ethanol, resulting in a one to one weight ratio of water to TDDS.

Figure 3 shows the solubility of TDDS, water and propanol. The isotropic single phase has increased considerably with the extension of the carbon chain by one unit, as compared to ethanol. Along the water-propanol composition line, again both components are completely soluble, where TDDS is immiscible in this mixture until 70% propanol. The two component line between TDDS-propanol are completely soluble in all proportions, where water solubility begins at 85% TDDS. Note the tie-lines of the two phase region, TDDS separates out completely when the water exceeds the solubility limit.

Figure 4 displays the solubility of TDDS, water and butanol. The maximum solubility along the water-butanol composition line is 20% water, where increases in the water concentration result in the separation of water for the isotropic solution. TDDS and butanol are completely soluble along its two component line.

Figure 5 depicts the phase diagram of TDDS, water and decanol. In a similar analogy to Figures 3 and 4, we see the complete solubility of TDDS in the alcohol. The maximum water content has been reduced to 5% along the water-decanol line. The tie-lines show that water completely separates for the single phase.

Figure 6 illustrates the phase diagram of TDDS , water and Brij 30. There are

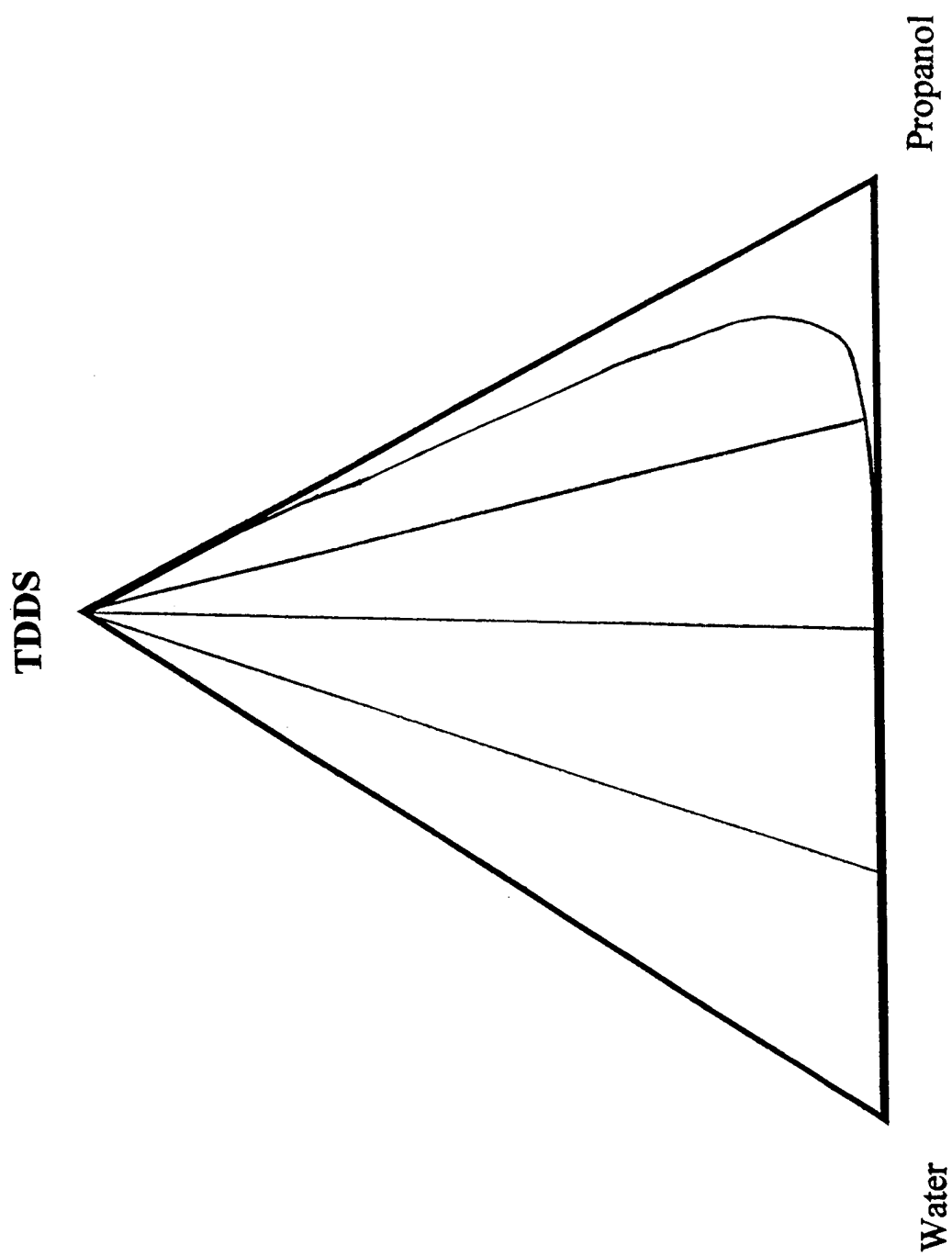


Figure 3: Phase Diagram of Water, TDDS, Propanol w/w%.

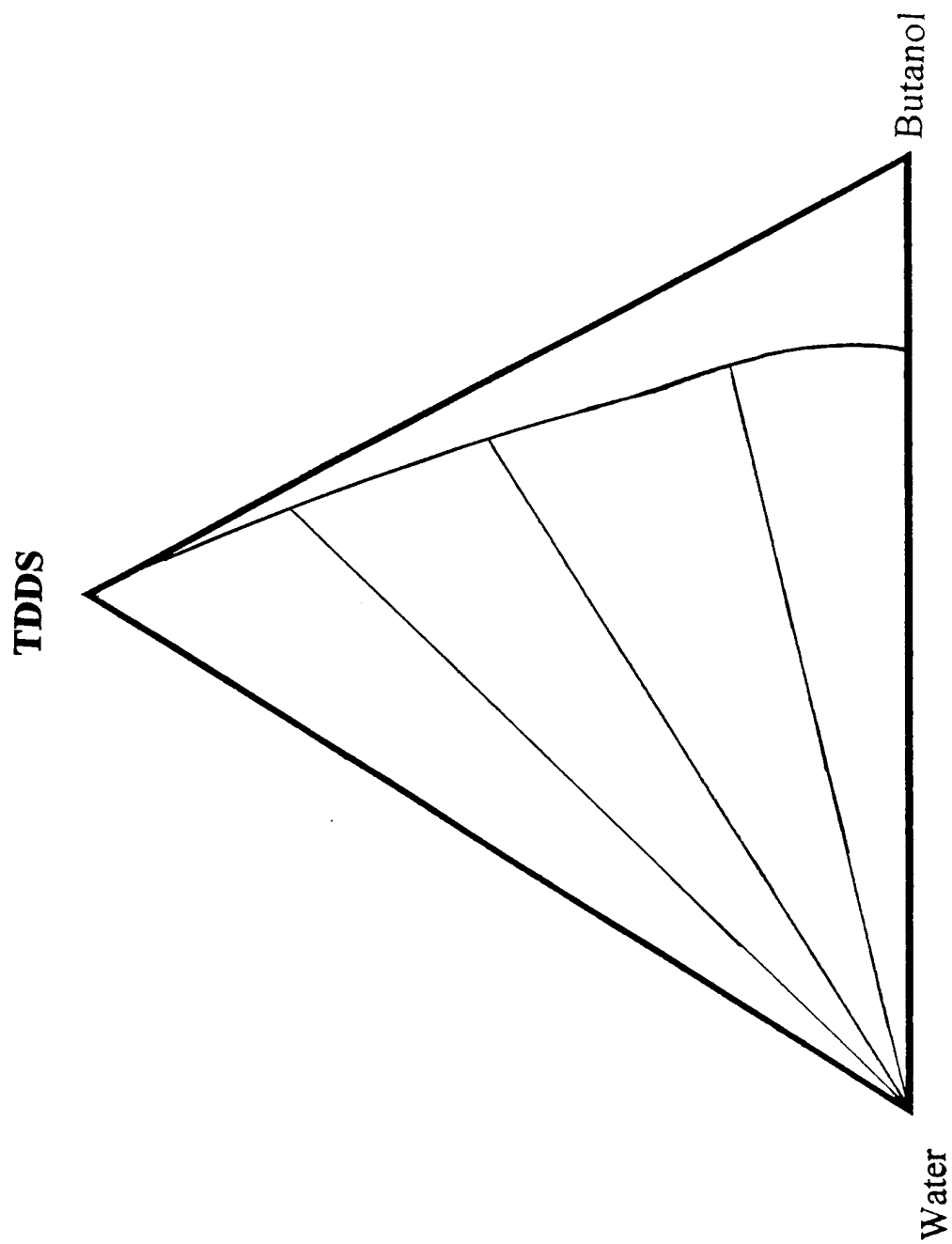


Figure 4: Phase Diagram of Water, TDDS, Butanol w/w%.

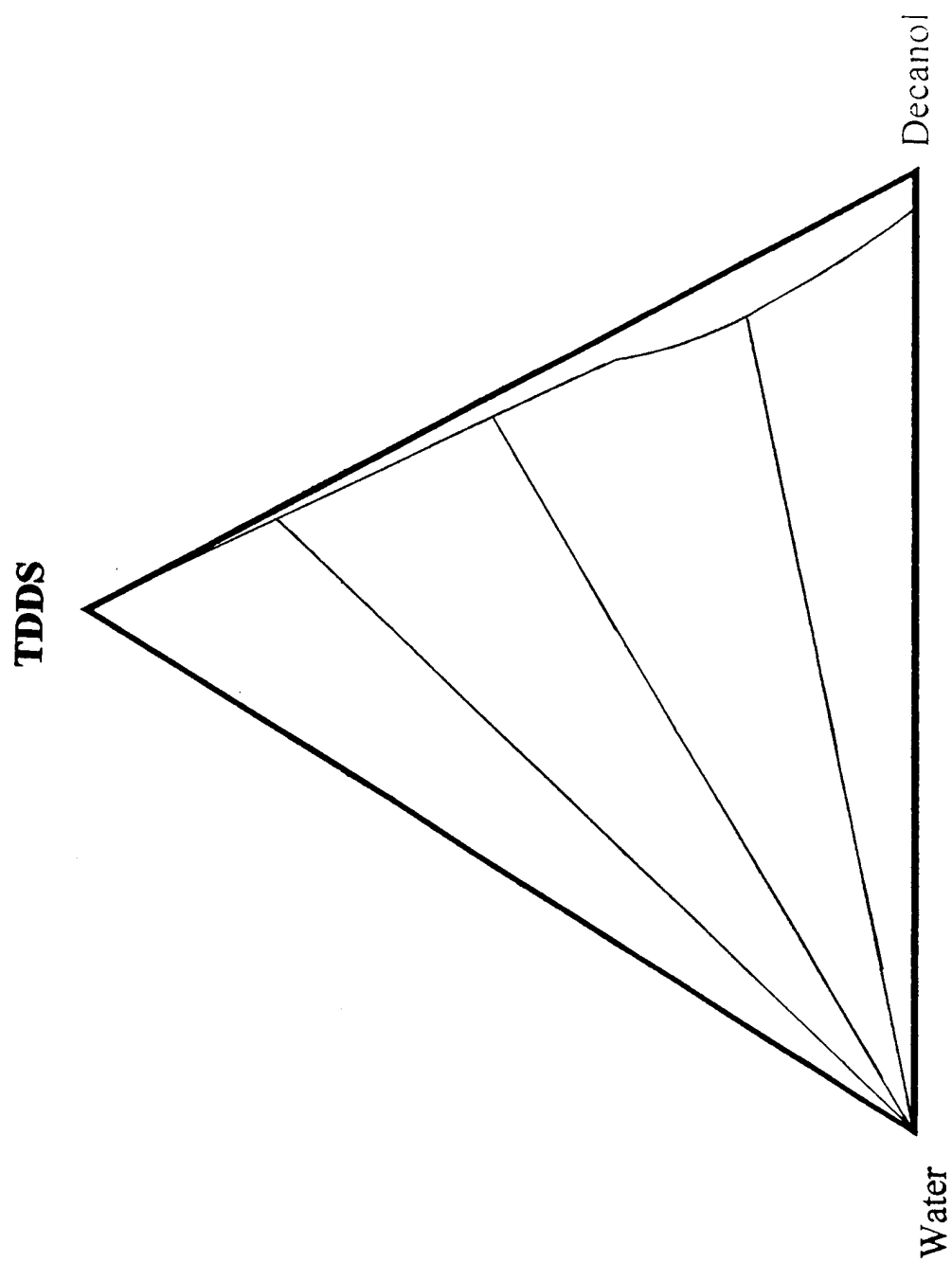


Figure 5: Phase Diagram of Water, TDDS, Decanol w/w%.

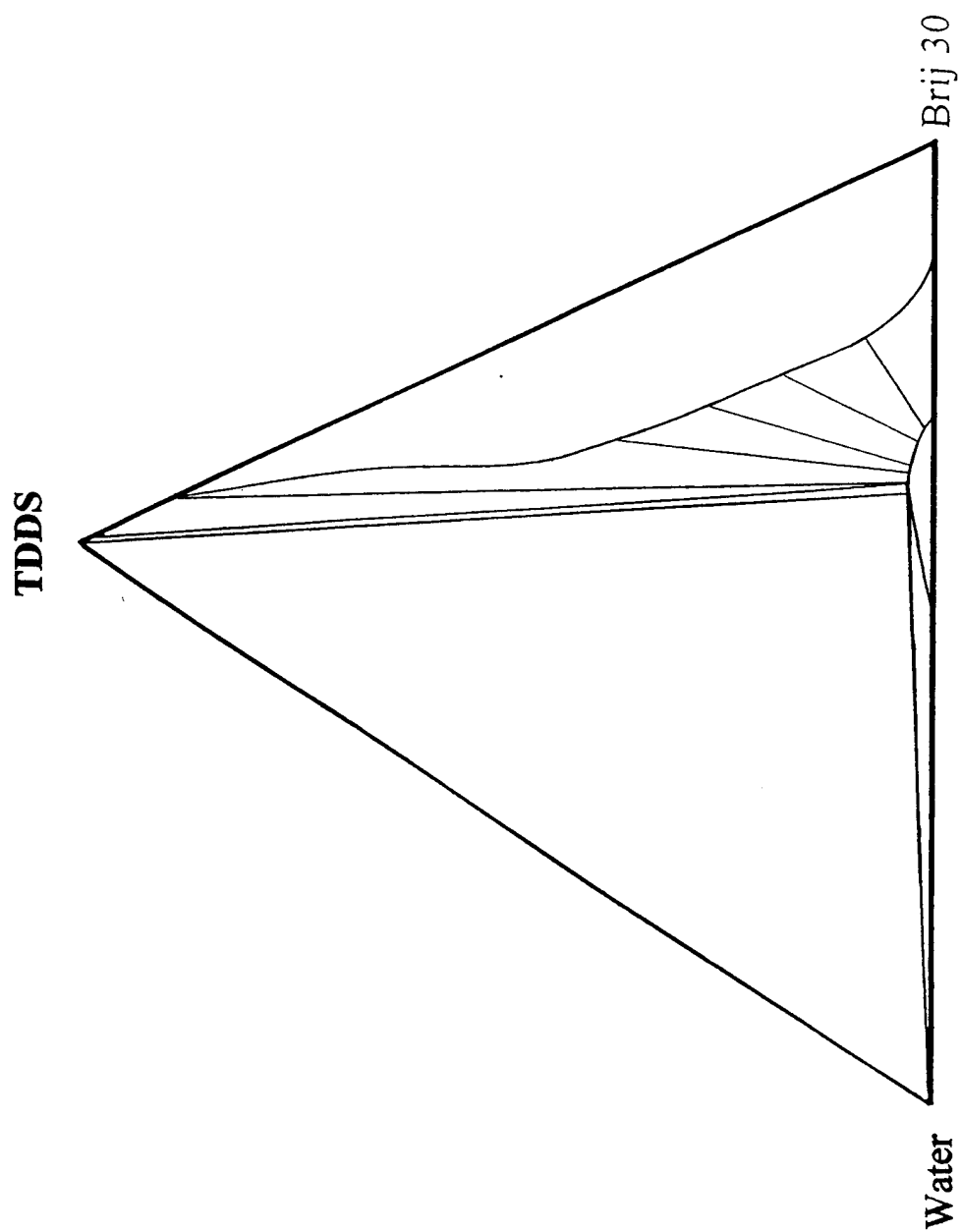


Figure 6: Phase Diagram of Water, TDDS, Brij 30 w/w%.

several interesting aspects of this diagram. Along the TDDS-Brij 30 composition line, a single phase solution (bottom right) was formed to a maximum of 85% TDDS, above 85% TDDS separations out. This one phase region can also solubilize ~15% water. A lamellar liquid crystalline region, LLC (bottom center), forms between 70% and 50% Brij 30 concentration along the Brij 30-water composition line. This phase can solubilize a maximum of ~6% TDDS. Above this maximum, the LLC no longer incorporate any additional water or TDDS and results in a large three phase region as denoted on the diagram.

Figure 7 shows the phase diagram of TDDS, water and SA9. The phase diagram shows three single phase regions. At high water concentration, a single isotropic solution, L1, has a maximum solubility of 30% SA9 and ~5% TDDS. The second isotropic single phase, L2, begins at ~80% SA9 concentration, which is in equilibrium with the third solution phase of TDDS-SA9. The third solution phase ranges from 100% to 96% TDDS, which can not solubilize water at any concentration. Two lyotropic liquid crystalline regions are also present. Along the SA9-water composition line a lamellar liquid crystal, LLC, is formed between 85% and 70% SA9 concentration (bottom right), which can solubilize a maximum of ~6% TDDS. A normal hexagonal liquid crystal phase, HLC, is also formed (bottom center) from 61% to 45% SA9 concentration along the SA9-water line, which can solubilize a maximum of ~5% TDDS.

Discussion

The results demonstrate the importance of carbon chain length on the solubility of

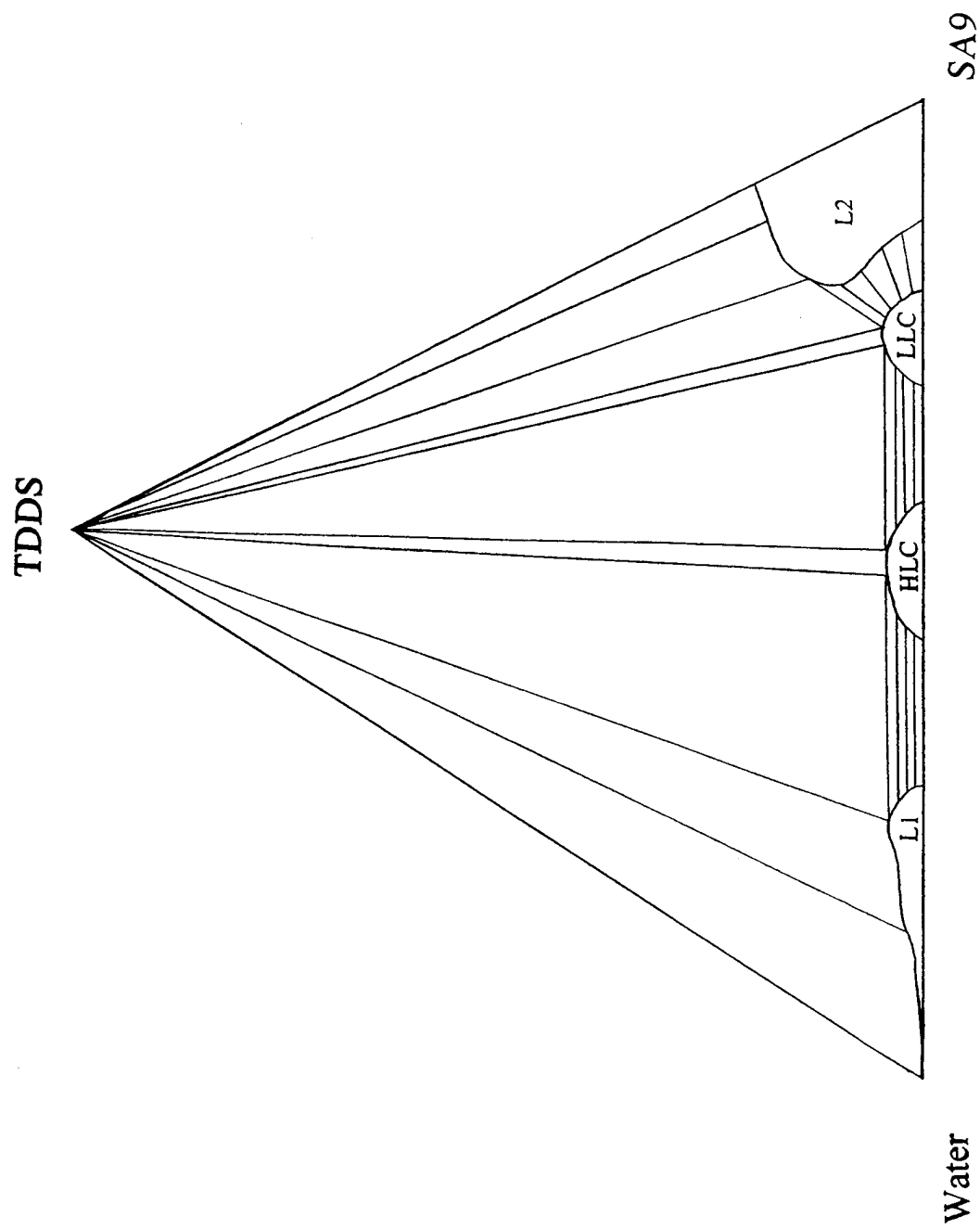


Figure 7: Phase Diagram of Water, TDDS, SA9 w/w%.

TDDS and water. The solubility dramatically increased as the carbon chain length extended to C2 and C4, as illustrated in Figures 1, 2, 3 and 4, respectively. However, this trend does not continue when a long chain alcohol is introduced into the system. The solubility of decanol with TDDS is maximized, Figure 5, while the solubility of water in the system is reduced substantially. Thus with respect to the carbon chain length, the hydrophilic/hydrophobic ratio of the alcohol to water must be balanced to maximize the solubility of all three components.

In comparison of Figure 2 to Figure 3, propanol produced an isotropic single phase along the entire length of the TDDS-propanol line, where as ethanol-TDDS results in two separate single phases.

It is interesting to note that the one phase region of Figure 4 is substantially larger than that of ethanol or propanol, where the tie-lines show the water separates out when its solubility limit is exceeded rather than the TDDS separates out in Figures 2 and 3.

Figure 6 illustrates the extent of hydrophilic/hydrophobic interactions between the TDDS, water and Brij 30. The TDDS is soluble in the surfactant solution up to 85% TDDS. In the single isotropic phase region, we expect the association of the three components to be complementary. The maximum water solubility in this single phase is ~15%, which must certainly associate with the ethoxy chain groups of Brij 30. Increasing the water concentration beyond this limit results in the associative structural changes to the LLC phase. Above 85% TDDS, the associative properties of Brij 30 changes towards TDDS, which results in equilibrium between a lamellar liquid crystalline phase and TDDS.

Here the surfactant solution reaches its maximum solubility, where the ethoxy groups can no longer freely associate in the solution and order into a parallel packing arrangement to reduce the surface free energy. Similarly at low surfactant concentrations and 15% water, the surfactant phase disappears and results in an equilibrium with the LLC and single isotropic solution.

In Figure 7, we see the increase in associative phase equilibria. Similar reasoning for the surfactant behavior apply here with the addition of a new liquid crystalline region and one additional single isotropic solution phase. The SA9 carbon chain length is similar to Brij 30, hence we expect favorable interactions between surfactant hydrocarbons and silane hydrocarbons chains. The polarity of the two surfactants are distinctively different. Brij 30 contains four ethoxy group chain length while SA9 has nine ethoxy group chain. The surfactant solution of Brij 30, Figure 6, is considerably larger than that of the SA9 surfactant solution, L2; thus the reduction in the L2 phase, in Figure 7, is due primarily to the increase in the ethoxy group chain length. Figure 7 also shows the presence of HLC phase, which is not present in the Brij 30 system. Here, the conformational changes in the SA9 ethoxy group chain length in the LLC phase results in the formation of a HLC phase when the water content is increased to 39%. With the water as the continuous phase, the SA9 molecules form cylindrical micelles. As the water is increased to 70% a micellar aqueous solution appears which can solubilize a maximum of 5% TDDS in the SA9 system. The Brij 30 system does not form an aqueous solution phase beyond the LLC phase.

Conclusion

The polarity and carbon chain length characteristics of the alcohols plays a significant role in the solubility behavior of TDDS. The results illustrate the dependence of phase equilibria on solvent mixture behavior and the preferred association structures with the non-ionic surfactant systems.

Acknowledgment

This research was supported in part by the CAMP program at Clarkson University, Potsdam, New York and the Department of the Army, United States Military Academy, West Point, New York.

References

- [1] Ekwall, Brown, GH, Eds. *Advances in Liquid Crystals*; Academic Press, NY 1975
- [2] Tiddy, GJ, T *Phys. Rep* 57, 1, 1980.
- [3] Fontell, K; Ceglie, A.; Lindman, B. Ninham, B; *Acta Chem Sci* A40, 1986.
- [4] Safran, S.A.; Turkevich, LA; *Am Phys. Soc* 50, 24, 1983.
- [5] Lu, CF; Spielman, LA; *J Colloid Interface Sci.* 103, 1, 1985.
- [6] Benton, WJ; Miller, CA, *Progr Colloid Polym. Sci.* 50, 24, 1983.
- [7] Bellocq, AM; Biais, J; Clin. B.; Gelat, A; Lalme, P; Lemanceau, B., *J Colloid Interface Sci.* 74, 2, 1980.
- [8] Sakka, S., Kozuka, H., Adachi, T., *J. Non-Cryst. Solids* 102, 263, 1988
- [9] Scherer, G.W., *J. Non-Cryst. Solids* 107, 135, 1989
- [10] Orcel, G., Hench, L.L. Araki, I., *J. Non-Cryst. Solids* 105, 223, 1988
- [11] Orcel, G., Phalippou, J, Hench, L.L., *J. Non-Cryst. Solids* 105,223,1988
- [12] Friberg, S.E., Yang, CC, Sjöblom, J., *Langmuir*, 8,372, 1992
- [13] Friberg, S.E., Yang, J, Amran, A, *J Phys Chem* 98, 13528, 1994
- [14] Sjöblom, J., Selle, M.H., Friberg, S.E., Moaddel, T., *Colloids and Surf.* 88, 235, 1994
- [15] Friberg, S.E., Ma, Z, *J. Non-Cryst. Solids* 147&148, 30, 1992
- [16] Mukhejee, S.P., *J. Non-Cryst. Solids* 63, 35, 1984
- [17] Yoldsa, B.E., *J. Non-Cryst. Solids* 82, 11, 1986

- [18] Sakka, S., Tanaka, Y., Kokubo, T., J. Non-Cryst. Solids 82, 24, 1986
- [19] Friberg, S.E., Jones, S.M., Yang, CC, J. Disp Sci Tech 13, 1, 65, 1992
- [20] Friberg S.E., Progr Colloid & Polymer Sci, 68,41, 1983
- [21] Piculell, L., Lindman, B., Adv Colloid Int. Sci, 41,149, 1992
- [22] Heenan, D.M., Friberg, S.E., Sjöblom, J., Farrington G. (in press)
- [23] Heenan, D.M., Friberg, S.E., Sjöblom, J. (in preparation).